UNIVERSITA' DEGLI STUDI DI PAVIA

FACOLTA' DI INGEGNERIA
DIPARTIMENTO DI INGEGNERIA INDUSTRIALE E DELL'INFORMAZIONE

DOTTORATO DI RICERCA IN BIOINGEGNERIA E BIOINFORMATICA
XXVI CICLO - 2014

VESTIBULO-OCULAR REFLEX: INSIGHTS ON PLASTICITY AND DEVELOPMENT OF A NEW DIAGNOSTIC APPROACH

PhD Thesis by

PAOLO COLAGIORGIO

Advisor:
Prof. Stefano Ramat

PhD Program Chair:
Prof. Riccardo Bellazzi

Sintesi

Il sistema vestibolare nei mammiferi consente la percezione dell'orientamento nello spazio, l'equilibrio e più in generale il movimento. Esso invia segnali alle strutture neurali che controllano sia i muscoli scheletrici per mantenere la postura sia i movimenti oculari per stabilizzare la visione. In particolare il riflesso vestibulo-oculomotore (VOR) stabilizza l'immagine sulla retina durante i movimenti della testa producendo un movimento oculare compensatorio opposto.

La tesi è incentrata sullo studio del comportamento del sistema vestibolare umano attraverso la registrazione e l'analisi delle risposte del VOR a seguito sia di perturbazioni indotte sperimentalmente per la comprensione dei processi di plasticità, sia di patologie, per fini diagnostici. In particolare il VOR è stato utilizzato come modello neurale su cui testare l'applicazione di principi generali della funzione cerebellare basati sulle risposte di sistemi motori più complessi. La conoscenza e le tecniche acquisite sono state quindi utilizzate nello sviluppo di un approccio diagnostico di potenziale utilizzo clinico.

Il VOR ci permette di avere una visione chiara durante le attività quotidiane anche per movimenti che comportano perturbazioni del capo ad alta frequenza come il cammino o la corsa. Tali movimenti possono essere compensati grazie ad un circuito neurale relativamente semplice consistente in 3-4 neuroni che permettono una latenza di 7-15 millisecondi. L'implementazione neurale di questo circuito è stata studiata approfonditamente negli anni passati, rendendo il VOR un sistema particolarmente adatto allo studio del controllo del movimento. Altre ragioni che hanno spinto allo studio di questo sistema sono dovute al fatto che si può esattamente quantificare lo stimolo (il movimento della testa) e misurare la risposta motoria degli occhi (che hanno solo tre gradi di libertà). Questo ha permesso negli anni '60 e '70 di descrivere tutta la generazione del riflesso, dai canali semicircolari, alle risposte neuronali, fino al movimento degli occhi, attraverso la teoria dei sistemi dinamici e le funzioni di trasferimento. Partendo anche da questi lavori sono state sviluppate le teorie più moderne sul controllo motorio dei movimenti volontari, in particolare il concetto di "modelli interni" per cui intendiamo dei processi neurali che simulano la risposta di un sistema motorio. I modelli interni servono sia a calcolare il comando motorio necessario a produrre un movimento desiderato ("modello inverso") che per predire l'esito di un movimento partendo da una copia efferente del comando motorio ("modello forward"). La nostra percezione è il risultato dell'integrazione tra l'informazione sensoriale e le predizioni del cervello; i

modelli forward permettono quindi di predire l'esito delle azioni prima dell'arrivo del feedback sensoriale in modo da risolvere il problema del controllo motorio in presenza di ritardo e rendere la percezione più accurata rispetto alle sole misure sensoriali. Le predizioni vengono poi confrontate con il feedback sensoriale reale, per verificare se il sistema motorio lavora correttamente; la discrepanza (errore di predizione) viene usata per aggiornare i modelli forward (cioè i circuiti che producono le predizioni) tramite processi di apprendimento, per mantenere una calibrazione robusta del sistema di controllo anche quando cambiano le dinamiche del sistema motorio (invecchiamento, danneggiamento, fatica). Gli attuali modelli teorici indicano il cervelletto come responsabile dell'aggiornamento di questi modelli sulla base dell'errore di predizione. L'adattamento motorio dei movimenti volontari (ad es. movimenti del braccio e saccadi) è stato oggetto di numerosi studi negli anni recenti che hanno mostrato come almeno due processi intervengano durante l'apprendimento: uno poco sensibile all'errore che ritiene molto l'informazione appresa ed uno molto sensibile all'errore ma che dimentica velocemente. Tali processi permettono di trovare un equilibrio tra la plasticità nell'integrazione di nuove informazioni e la stabilità nel conservare la precedente conoscenza. Questo ha portato alla formulazione di modelli lineari tempo-invarianti che predicono molto bene a livello comportamentale i fenomeni tipici dell'adattamento osservati per i movimenti volontari. Noi ci siamo chiesti se anche la plasticità di un riflesso sensorimotorio come il VOR sia regolata da processi a più scale temporali. Inoltre per descrivere tali comportamenti abbiamo applicato l'architettura dei modelli interni al controllo riflesso. I nostri risultati mostrano la presenza di un processo noto come recupero spontaneo della memoria, che testimonia la presenza di più scale temporali. Nell'esperimento, una prima fase di adattamento che diminuisce la risposta motoria è seguita da una fase più breve, con una perturbazione in senso opposto, che riporta la risposta vicino alle condizioni iniziali (de-adattamento); quando in una terza fase viene tolto il feedback visivo, la risposta motoria ritorna spontaneamente verso la prima condizione appresa. Anche se la risposta motoria è tornata nelle condizioni iniziali, alla fine della fase di de-adattamento, in assenza di feedback recupera il comportamento appreso nella prima fase poiché la memoria non è stata completamente cancellata dal de-adattamento. Questo comportamento è spiegato solo se l'apprendimento è il risultato di almeno due processi a diverse scale temporali. I dati sono stati interpretati usando un modello ispirato a quelli in grado di spiegare i movimenti volontari, secondo cui il comando motorio viene calcolato da un modello inverso e l'adattamento aggiorna un modello forward dell'apparato oculomotore implementato nel cervelletto. I modelli interni rappresentano concetti teorici che, nell'ambito dei movimenti scheletrici, ancora devono trovare riscontro nell'attività elettrofisiologica dei neuroni. Il VOR, vista la conoscenza molto approfondita del circuito neurale che genera il movimento e delle connessioni con il cervelletto, è un sistema eccellente sul quale studiare

l'implementazione neurale di tali processi, la codifica dell'informazione nei neuroni e i siti di plasticità.

Un corretto funzionamento del VOR permette di stabilizzare lo sguardo durante i movimenti della testa. Vista la relazione diretta tra la funzione dei recettori vestibolari nell'orecchio interno e la risposta oculare prodotta dal VOR, quantificare la risposta del riflesso ed individuarne i malfunzionamenti ha una grande importanza nella diagnosi delle patologie vestibolari. Gli individui affetti da danni al sistema vestibolare sono soggetti a vertigini, nausea, disequilibrio, instabilità posturale e del cammino e oscillopsia, e questi sintomi hanno spesso importanti ricadute sulla psiche dei pazienti. La maggior parte dei casi clinici è dovuta a patologie vestibolari benigne, ma circa un terzo possono essere infarti cerebellari o del tronco encefalico. La gestione dei pazienti prevede l'analisi della storia clinica, gli esami clinici del medico e i test di laboratorio. Un test clinico molto efficace è lo "head impulse test" (HIT): il clinico impone, in modo imprevedibile nel tempo e nella direzione, delle rotazioni impulsive (piccola ampiezza ma alta accelerazione) alla testa del paziente che, seduto di fronte a lui, fissa un punto (di solito il naso del medico). Se il sistema vestibolare funziona correttamente il paziente riesce a mantenere lo sguardo sul punto di fissazione durante la rotazione, altrimenti, una saccade correttiva che riporta lo sguardo sul punto di fissazione dopo la fine della rotazione è un segno clinico di un deficit. Una versione quantitativa dello HIT si può ottenere misurando contemporaneamente il movimento degli occhi e della testa e calcolando un rapporto tra le due velocità (guadagno) per avere una misura dell'entità del deficit. Misurare i movimenti oculari richiede esperienza e una strumentazione costosa, quindi di fatto tali misure quantitative possono esse fatte solo in pochi laboratori specializzati. Il VOR può anche essere testato in termini di efficacia della stabilizzazione della scena visiva sulla retina durante le rotazioni della testa. Infatti, pochi gradi al secondo di slittamento dell'immagine sulla retina peggiorano drammaticamente l'acuità visiva (approccio funzionale). Il nostro gruppo ha sviluppato e brevettato un dispositivo (Head Impulse Test Device, HITD) che valuta la capacità di leggere un ottotipo presentato brevemente su uno schermo durante rotazioni impulsive della testa del soggetto. L'hardware necessario comprende un pc, un monitor per la presentazione degli stimoli e un sensore inerziale per misurare la velocità della testa e presentare l'ottotipo al superamento di una soglia di accelerazione. Se il VOR funziona correttamente, lo sguardo rimane fisso nello spazio durante il movimento ed il soggetto è in grado di leggere; in caso contrario gli occhi si muovono con la testa e l'immagine della lettera slitta sulla retina impedendo la lettura. Il risultato del test in termini di percentuali di lettura alle varie accelerazioni del capo indica la presenza e il grado del deficit senza misurare il movimento degli occhi. Il test HITD richiede uno strumentario molto limitato poiché non prevede la registrazione dei movimenti oculari, inoltre visti i costi contenuti e la facilità di utilizzo potrebbe avere un utilizzo ambulatoriale di complemento alla valutazione clinica.

Per avere una validazione del test e per vedere la relazione tra la misura funzionale della percentuale di lettura e la misura quantitativa del guadagno ho realizzato uno strumento (videoHITD) che permette di acquisire contemporaneamente i movimenti degli occhi (tramite un sistema di video-ocoulografia commerciale), i movimenti della testa (tramite un sensore inerziale) e un feedback della comparsa dell'ottotipo. Lo strumento permette quindi di calcolare posizione e velocità dello sguardo durante la presentazione dell'ottotipo. Abbiamo somministrato il test su pazienti affetti da deficit vestibolare unilaterale confrontandone i risultati con i test di laboratorio più comuni.

La tesi si divide in quattro capitoli:

- il Capitolo 1 è una sintesi sull'anatomia, fisiologia e patologia del sistema vestibolare;
- nel Capitolo 2 si fa riferimento all'organizzazione sensori-motoria del VOR analizzando le principali teorie computazionali del controllo motorio e le teorie sull'apprendimento;
- nel Capitolo 3 è descritto lo studio sulla plasticità del VOR e l'implicazione di due processi di adattamento che intervengono su scale temporali diverse;
- nel Capitolo 4 partendo da una breve descrizione delle tecniche diagnostiche di laboratorio si descrive il test HITD e la sua funzionalità nella diagnosi delle patologie vestibolari.

Abstract

The vestibular system, in mammals, allows spatial orientation, balance and movement. It sends signals to the neural structures that control both the muscles that help maintaining balance and eye movements that allow clear vision. In particular, the vestibulo-ocular reflex (VOR) allows maintaining stable vision during head motion compensating head movements with eye rotations.

My thesis is focused on studying the behavior of the human vestibular system through the recording and the analysis of VOR responses following both artificially induced perturbations, with the purpose of studying plasticity mechanisms, and pathologies, for diagnostic approaches. In particular, the VOR has been considered as a simple neural model for testing general principles of cerebellar function arising from more complex motor systems. The same techniques have been used for the development of a new diagnostic approach of prospective clinical use.

VOR allows a clear vision during daily activities and during movements producing high frequency head perturbations as walking or running. A short latency (7-15 ms) neural pathway of 3-4 neurons allows compensating these movements up to frequencies of 5 Hz. The deep understanding of the neural implementation of this pathway made the VOR a good model for the studying of movement control. Moreover, in experimental conditions, the stimulus (head movements) and the motor response (eye movements) are easily quantifiable. This framework, in the 60s-70s, allowed to describe the generation of the reflex (semicircular canals, neuronal response and eye movements) using a control systems approach based on transfer functions and frequency domain analysis. Recently, new theories on motor control of voluntary movements (e.g. hand movements) introduced the concept of "internal model" i.e. a neural process that simulates the response of a motor system. Internal models map the desired movement into the appropriate motor command ("inverse models") or convert an efference copy of the motor command into an internal estimate of the current movement ("forward models") in terms of its sensory consequences. Our perception (i.e. the ability to estimate the state of our body and of the external world) is a combination of how the brain predicts what we should sense and how the sensory system reports what has been sensed. Forward models overcome the delay in sensory measurements that can cause instability during the execution of movements and improve our perception. Comparing prediction of the executed movement with sensed movement, also helps verifying if the motor effector

(i.e. the plant in control systems' terms) is working properly, and maintaining calibration to obtain a robust motor control even when the dynamics of the plant change (e.g. development, injury, aging, fatigue) by updating the parameters of the forward models (i.e. calibrating the predictions). Theoretical models of learning indicate the cerebellum as the locus responsible for the implementation and updating of forward models. Behavioral studies on short term motor learning in volitional movements (i.e., saccades and reaching) suggested that motor adaptation depends on at least two distinct neural systems that have different sensitivity to error and retain information at different timescales: one is highly sensitive to error but has poor retention and another is poorly responsive to error but has strong retention. These processes allow the brain to find an equilibrium between plasticity for the integration of new knowledge and stability in order to prevent the forgetting of previous knowledge. Our hypothesis is that also a reflex movement such as the rotational rVOR may be based on a similar architecture exploiting internal models and multiple adaptive processes having different timescales. Our results show the existence of the spontaneous recovery phenomenon, which is considered as the hallmark of multiple timescales in motor learning. In our experiment, a first phase of gain down adaptation was followed by a shorter gain up training that brought back the motor response near its baseline (de-adaptation); after de-adaptation, when the visual feedback was removed, the gain of the response returned toward that learned in the first condition. Despite the motor response returned to baseline, it then recovered the behavior of the first adaptation because motor memory was not completely erased by de-adaptation. We thus developed a mathematical model of rVOR adaptation based on two hidden state processes, which adapts the cerebellar forward model of the ocular motor plant, and showed that it accurately simulates our experimental data on rVOR gain adaptation, while a single timescale learning process fails to do so. Thus, VOR adaptation can be a good model for studying cerebellum-dependent learning in order to understand the neural implementation of internal models, the encoding of the information in the neurons and the sites of plasticity.

A normal VOR allows stabilizing gaze during head movements. Quantifying the response and the malfunctioning of the VOR has great importance in the diagnosis of vestibular diseases because of the close relationship between peripheral vestibular receptors in the inner ear and the ocular-motor response of the reflex. Vestibular disorders occur frequently and can affect people of all ages. The main symptoms are dizziness, vertigo, imbalance and oscillopsia, and these symptoms often have important psychological implications. Despite peripheral causes are more common, dangerous central causes, in particular ischemic stroke in the brainstem or cerebellum, can mimic benign peripheral vestibular causes closely; therefore, accurate diagnosis of dizzy patients at an early stage is important and can avoid potentially fatal complication and improve patients' outcome. Management of dizzy patients consists in clinical history inspection, bedside examination and laboratory testing. A widely accepted clinical test is the Head Impulse Test (HIT). Head impulses are

brief, rapid and unpredictable rotations of the head on the trunk. The rotations are unpredictable in both timing and direction, of low amplitude and high acceleration. If the rVOR is healthy, the compensatory vestibular eye rotation has exactly the same velocity as the head impulse but in the opposite direction. In case of vestibular loss, the patient's gaze is dragged in the direction of the head impulse and the patient must make corrective saccades to bring back the eyes on the target. Usually the head impulse test is a bedside test, but it can also be assessed quantitatively by recording simultaneously eye and head movements in order to quantify the degree of loss. The quantitative approach allows showing the pattern of slow phase and saccade response and computing the gain of the rVOR (eye velocity/head velocity). Eye movement recording is a relatively complicated laboratory procedure requiring specific technical knowledge and relatively expensive equipment, both aspects that limit the use of such approach to only a few laboratories. Functional testing of the rVOR is an alternative diagnostic tool for identifying peripheral vestibular deficits while avoiding the need to measure the movement of the eyes. The basic idea of functional testing is that even a few degrees/second of image slippage on the retina seriously deteriorate vision, so that during a head rotation that unveils a vestibular deficit, vision is impaired. Our group has recently patented and tested a functional head impulse testing device (HITD) to assess vestibular function based on the ability of a subject to read an optotype flashed on the screen during impulsive head rotations. The hardware includes only a pc, a monitor and an inertial sensor to measure head acceleration and trigger the optotype display. If the rVOR works properly, the gaze remains fixed in space during the head movement and the subject can read the optotype; otherwise the eyes move with the head and the optotype image slips on the retina so that the subject cannot read it. The outcome of the test is the percentage of reading at different head accelerations. In order to validate the test and find the relation between the functional (percentage of reading) and quantitative (gain) measure, I developed a new research tool (videoHITD) allowing the synchronized recording of eye and head movements, together with a feedback on visual display timing. We administered the test on patients affected by unilateral vestibular neuritis and compared the results with traditional laboratory tests. The HITD appears to be a promising tool for detecting abnormal rVOR performance and can provide a valuable assistance to the clinical evaluation of patients with vestibular disorders.

This thesis work is composed of four chapters:

- Chapter 1 is a synthesis of the anatomy, physiology and pathology of the vestibular system;
- in Chapter 2 the sensory-motor organization of the VOR is described starting from the main theories of the computational approach on motor control and motor learning;

- in Chapter 3 the study on VOR plasticity and the implications of learning based on two processes at different timescale is presented;
- in Chapter 4, starting from a short description of the common laboratory diagnostic techniques, I describe the HITD test and its functionality in vestibular disorders diagnosis.

Contents

Chapter 1

The Vestibular System: anatomy, physiology and pathology

The vestibular system detects head movements, especially involuntary ones, and generates reflexes that are crucial during daily activities such as body posture adjustments to keep us from falling and stabilizing gaze to keep the visual word stable. The human vestibular system comprises three components: a peripheral apparatus, a central processor and a system for motor output. A set of motion sensors (of head angular velocity and linear acceleration) in the peripheral apparatus sends information to the central nervous system (CNS), and specifically to the vestibular nuclei complex in the brainstem and the cerebellum. The CNS processes and combines these signals with visual and proprioceptive information to estimate head and body orientation. The output of the CNS goes to the ocular muscles and to the spinal cord to generate the *vestibulo-ocular reflex* (VOR), the *vestibulo-collic reflex* (VCR) *and the vestibulo-spinal* reflex (VSR). The VOR generates corrective eye movements stabilizing gaze and aiming at permitting clear vision; the VCR stabilizes the head controlling neck musculature; the VSR generates compensatory body movements to maintain posture and prevents falls. The performance of these reflexes is recalibrated by the CNS in response to injuries, diseases and aging, mainly by the cerebellum and is supplemented by slower but more capable higher cortical process. This chapter is a short overview about the vestibular system and vestibule-ocular reflex in particular; the majority of literature information are taken from references [1]–[5].

1.1. Anatomy of the peripheral vestibular system

The peripheral vestibular system lies within the inner ear, is composed of the membranous and the bony labyrinth. The sensory source are the hair

cells placed in the membranous labyrinth. In the human, there are two labyrinths, one for each inner ear, symmetrically arranged with respect to the sagittal plane of the head.

1.1.1. The Labyrinth

The bony labyrinth consists of three semicircular canals, the cochlea and a central chamber called vestibule. The bony labyrinth is filled with perilymphatic fluid. The membranous labyrinth is suspended within the bony labyrinth, supported by the perilymphatic fluid and connective tissues (Figure 1.1 B). It is composed by the membranous part of the semicircular canals, which sense head rotation, and the two otolith organs, the utricle and the saccule, which sense linear acceleration and static tilt of the head (Figure 1.1 A). Each semicircular canal presents a widening called the ampulla. The specialized hair cells contained in each ampulla (on the crista) and otolith organ (on the macula) transduce mechanical shearing forces into neural impulses. The membranous labyrinth is filled with endolymphatic fluid.

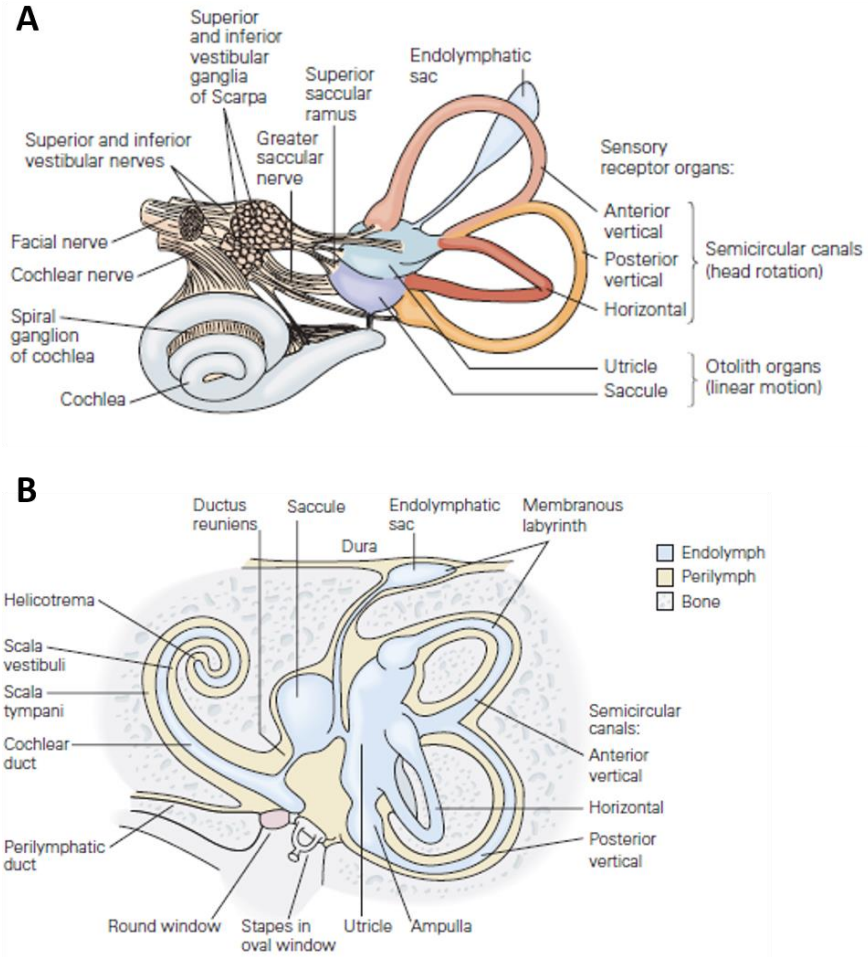

Figure1.1: A) orientation of vestibular and cochlear divisions in the inner ear. B) Bony and membranous labyrinth division. (Taken from [3]).

1.1.2. The Hair Cells

The hair cells transduce mechanical stimuli in electrical stimuli carried by the nerves. The hair cell is innervated by an afferent neuron located in the vestibular ganglion, and consist of many *stereocilia* and one *kinocilium* (Figure 1.2 A): deflection of the stereocilia toward the kinocilium causes depolarization (stimulation) of the hair cell; deflection in the opposite direction causes hyper-polarization (inhibition). There are two types of hair cells (type I and type II), which have specific cellular properties depending on potassium channel densities that contribute to sensitivity to frequency stimulation.

1.1.3. The Semicircular Canals

The three semicircular canals in each labyrinth are arranged in orthogonal planes [6] and are sensitive to angular (rotational) acceleration. Each canal is composed of a circular 'tube' filled with endolymph and interrupted at the ampulla by a gelatinous, sail-like structure, called *cupula* in which are embedded hair cells of the crista (Figure 1.2 B). The cupula is displaced because inertial forces produce a flow of the endolymph within the canals when the head rotates, causing the bending of the hair cells. The internal diameter of the semicircular canal is small relative to the radius of curvature, thus the motion of the endolymph and deflection of the cupula caused by head rotation is proportional to head velocity (in the range of frequencies in which the head commonly moves 0.5-7 Hz). Despite the input signal is angular acceleration, the mathematical integration due to the mechanics of the canals and the viscous properties of the fluid, allow them to provide the brain with a head velocity signal [7], [8]. A consequence of these mechanical properties is that only a small amount of endolymph displacements occurs, even with high acceleration turns. Moreover during the response to prolonged rotation at constant velocity (velocity step) the elastic properties of the cupula become important and cause a return to its resting position with an exponentially decaying time course (time constant of about 6 seconds [9]), resulting in a high-pass behavior of the semicircular canals in response to a head angular velocity input. The return of the cupula to its resting position can be related to the decline in nystagmus (Figure 1.4 B, C) during velocity step rotation (Figure 1.4 A). Moreover, if the subject is suddenly stopped post-rotational nystagmus will be produced indicating a displacement of the cupula in the opposite direction (Figure 1.4 A). However, the per-rotational nystagmus lasts considerably longer than the time required for the cupula to drift back suggesting that the brain manipulates the canal signal to prolong the time that motion of the head can be perceived (velocity storage see Chapter 1.2.2).

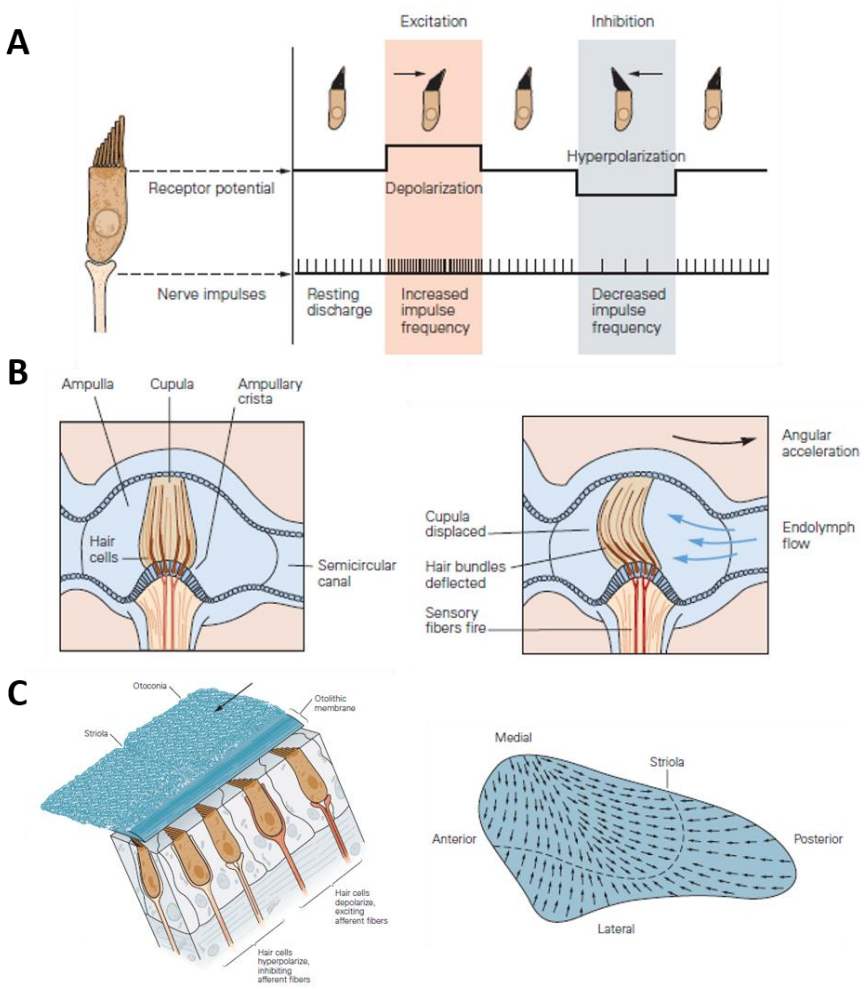

Figure 1.2: A) Hair cells in the vestibular system transduce mechanical stimulations. A cell is composed by one kinocilium (the long one), and many stereocilia. Deflection toward the kinocilium causes depolarization, deflection away from the kinocilium hyperpolarization. B) The ampulla: the hair cells body lies in the ampullary crista and the cilia extend into a gelatinous diaphragm, the cupula. The cupula is displaced by the flow of the endolymph when the head moves. C) The utricle: hair cells, oriented in different directions project into the otolithic membrane, that moving bands the hair cells. The striola separates the direction of hair cell polarization. (Taken from [3]).

Endolymph flowing within the canal, in one direction produces excitation and in the other inhibition. For the lateral (horizontal) canal, flow toward the ampulla (ampullopetal) is excitatory, conversely for vertical canals (ampullofugal). Canals can be thought as working in pairs: each semicircular canal is paired with another in the opposite side, both lying in the same plane; however, canals on opposite side of the skull may be not precisely aligned thus the brain makes adjustments for such individual variation. This arrangement is called "push-pull arrangement of coplanar pairing": right and left lateral, left anterior and right posterior, left posterior and right anterior (Figure 1.3 B). Thus, for example, an ampullofugal flow within the right anterior canal will be accompanied by

an ampullopetal in the left posterior canal. There are three advantages to the push-pull arrangement: (1) if a disease destroys one labyrinth the brain can use the decrease of activity of the other paired canal to detect ipsilesional velocity; (2) the brain can ignore changes in neural firing occurring in both canals in a pair (due to temperature or chemistry, common mode rejection); (3) this configuration assists in compensation of sensory overload.

1.1.4. The Otoliths

The utricle and the saccule are sensitive to linear acceleration, responding to linear head motion and static tilt with respect to the gravitational axes. The hair cells are embedded in a gelatinous matrix containing a layer of solid CaCO3 crystals (the otoconia layer) parallel to the sensory epithelium (Figure 1.2 C). The mechanism sensing acceleration is due to the inertia-generated movement of the otoconia that bands the cilia and causes excitation or inhibition. Linear acceleration can come from two sources, gravitational field and linear motion, thus there is a sensory ambiguity problem solved by the CNS through higher level processing (see Chapter 2.1.3).

Like the canals, the otoliths are arranged to respond to motion in all directions: despite the utricle best senses linear horizontal accelerations while saccule senses vertical linear accelerations both of them are curved structures, ellipsoid-like (Figure 1.2 C), and can thus respond to linear acceleration in any direction [10], [11].

Like in the canals, the geometry of each of the otolithic membrane allows a push-pull organization. Within each otolithic macula there is a curving zone, the *striola*, which separates the direction of hair cell polarization on each side (Figure 1.2 C), so that when a shear force causes an excitation in of the cells of one side of the striola, those of the other side are inhibited an vice versa [12].

1.1.5. The Vestibular Nerve

Vestibular nerve afferents innervate vestibular receptors and carry the signal to the vestibular nuclei (VN) in the brainstem. Vestibular nerve fibers have been classified as *regular afferents* and *irregular afferents* on the basis of regularity of their resting discharge. Regular afferents have tonic response dynamics showing low variability in inter-spike activity of the resting discharge. The caliber of their axon is medium to small and they provide bouton endings to type II haircells located at the periphery of the vestibular neuro-epithelium. The irregular afferents have phasic-tonic response dynamics and have higher variability in resting discharge. Their axons are medium to large and can be divided into two groups some provide calyx endings to type I haircells and the rest provide a mixed

innervation of calyx endings to type I haircells and bouton endings to type II haircells [13].

The regular and irregular afferents use different coding strategies depending on the resting discharge variability [14]. The higher variability of the irregular afferents lead to a low signal to noise ratio (and little information in the spike times) at lower frequency of rotation [14]. However, the response of the irregular units can be quantified by a rate code with increases in gain and phase lead of the response as a function of rotation frequency [15]. In contrast, regular afferents have a higher signal to noise ratio and higher information in spike times. Thus, while regular afferents give detailed information using temporal codes, irregular afferents use mostly rate codes and act as event detectors at high frequencies of movement.

1.2. Physiology of the VOR

Angular and linear motion of the head are sensed by the semicircular canals and the otoliths, providing the input to the vestibulo-ocular reflex (VOR). The VOR normally allows maintaining stable vision during head motion by compensating head movements with eye rotations. The response to the rotational component is called rVOR (rotational), and the response to linear head motion is called tVOR (translational). A third type called ocular counter-rolling that is a small change in static torsion of the eyes in the opposite direction of the head tilt. The rVOR in response to the three possible head rotations (roll, pitch, and yaw) produces horizontal, vertical and torsional eye movements, respectively. The tVOR responds to the three possible directions of head translation (sway, surge, and heave) producing horizontal, vertical and vergence eye movements.

Since the eyes are horizontally separated, rotational head movements produce also linear translation of the eyeballs. The compensation of the translational component during both rotation and pure translation depends on the viewing distance: the closer is the object higher is the translational component. Thus, depending on the location of the rotational axes relative to the eyes and target distance, the brain must adjust the movement of each eye independently.

The most ecological rotational head perturbations are of high frequency (0.5 to 5 Hz), e.g. vibration transmitted from the body to the head during walking. These movements are compensated by a neural pathway consisting of three or four neurons [16] producing a latency in rVOR eye movements of 7 to 15 ms [17]. Indeed, the visual-following reflex cannot substitute the VOR during brisk head movements because the latency of visual-mediated eye movements is greater than 100 ms [18].

1.2.1. VOR neural circuitry

Vestibular input from primary afferents is sent to the vestibular nuclear complex in the brainstem and to the cerebellum. The vestibular nuclear complex is the primary processor of vestibular information and implements a fast connection between afferent information and motor output neurons. The cerebellum is an adaptive processor; it evaluates vestibular performance and recalibrates the processing if necessary.

Motor command generation

The vestibular nerves project from *Scarpa's vestibular ganglion* to the vestibular nuclear complex. The *vestibular nuclei* integrate signals from the vestibular organs, the spinal cord, the cerebellum and the visual system. From these nuclei fibers cross to the *contralateral abducens nucleus*. From the abducens nucleus one pathway projects directly to the lateral rectus muscle of the ipsilateral eye via the abducens nerve, while another pathway projects to the contralateral *oculomotor nuclei* which contain motor neurons that drive the medial rectus activity through the *oculomotor nerve* (Figure 1.3 A). This short latency neural pathway is called *three-neuron-arc* and allows short eye movements latencies of about 7-15 ms.

The three pairs of canals are organized in three mutually perpendicular planes (push-pull organization, Figure 1.3 B). Each of these planes lies approximately in the pulling direction of each of two pairs of extraocular muscles (e.g. the left and the right horizontal canal in the plane of the medial and the lateral rectus). The projections of the vestibular nerves mirrors the geometric arrangement: each canal projects to the motor nuclei to excite the pair of muscles that move the eyes in the opposite direction of head rotation and to inhibit the pair which acts in the same direction. For example when a rightward horizontal head rotation occurs: (1) the right horizontal canal hair cells depolarize and the left hyperpolarize; (2) the right vestibular afferent activity therefore increases while the left decreases; (3) the right vestibular nuclei activity increases while the left decreases; (4) neurons of the left abducens nucleus and the right oculomotor nucleus begin firing at higher rate, while in the left oculomotor nucleus and the right abducens nucleus they fire at a lower rate; (5) the left lateral rectus muscle and the right medial rectus contract while the left medial rectus and the right lateral rectus relax, therefore the eyes rotate leftward (Figure 1.3 A).

The ocular motor command has two components: a velocity signal and a position signal. If only the motor signal from the vestibular nuclei (velocity signal) would drive the eye muscles (in response to head rotation), the eyes would drift back to the start position because no new position signal would be generated to hold the eyes in an eccentricity. As for the saccadic system, the necessary position command is calculated from the velocity signal by a brainstem structure called *neural integrator* (neural equivalent of a mathematical integration), which is common to all ocular motor

subsystems. The *nucleus prepositus hypoglossi* and the *medial vestibular nucleus* provide this function for the horizontal oculomotor system.

Cerebellum

Cerebellum is not directly involved in the vestibular reflexes but its impairment makes the reflexes uncalibrated. The *flocculus* and the ventral *paraflocculus* (FL/FVPL) of the cerebellum receive afferent connections from the vestibular system (through *mossy fibers*) and the Purkinje cells in FL/FVP inhibit *floccular target neurons* in the vestibular nuclei [19]. The role of cerebellum in VOR adaptation is explained in depth in Chapter 2.

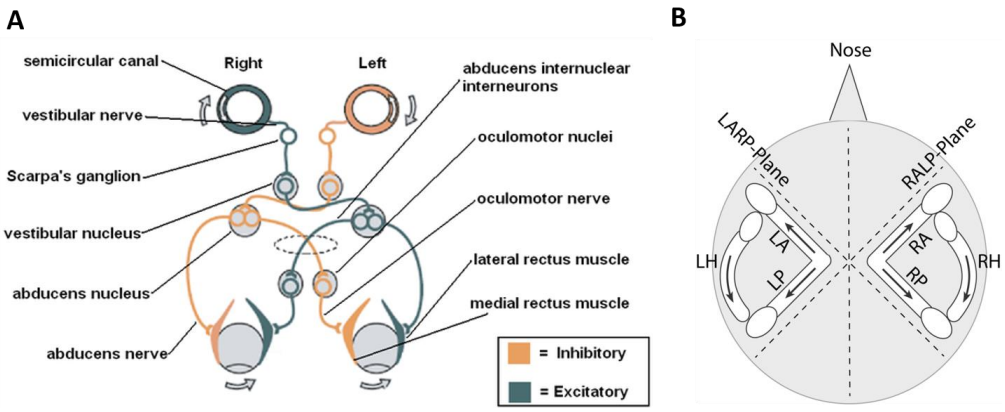

Figure1.3: A) Schematic of the horizontal rVOR neural pathways, from the canal stimulation to the eye muscles contraction. B) orientation of the semicircular canals. L/R: Left/Right, H/A/P: horizontal/anterior and posterior. The arrows indicate the direction of head movement that stimulates the respective pair of canals (Taken from [5]).

1.2.2. The Velocity Storage Mechanism

Vestibular nuclei neurons respond to sustained head rotation in darkness showing an initial increment that decays exponentially with a time constant around 15-35 seconds, while the semicircular canal response is characterized by a time constant of 6 seconds, due to the cupula mechanical properties. Therefore, the performance of the VOR is improved early in the processing of the vestibular nuclei improving the ability of the system to transduce the low frequency component of head rotation, while still behaving as a high-pass filter. This central processing stage is known as velocity storage mechanism (VSM).

The VSM integrates vestibular signals from the rVOR and visual signals from the *optokinetic nystagmus* (OKN) [9], i.e. the compensatory eye movement induced by a full field movement of the visual scene, characterized by a low-pass behavior. To reconstruct a reliable signal of estimated head velocity across all frequencies [20] the VSM processes also visual information (the processing of the retina is slower than the canals' one). Moreover, VSM is involved in estimation of the orientation relative to gravity and in distinguishing tilt of the head from translation separating

gravity and inertial acceleration. VSM is also probably involved in the implementation of an internal model of self-motion [21].

1.2.3. The Oculomotor Plant

To a good approximation the eye is a sphere standing in the orbit, and eye movements rotate the eye in the orbit about the three axes of rotation (horizontal, vertical and torsional). Horizontal rotation away from nose is called abduction, toward the nose adduction. Vertical movements are elevation (upward) and depression (downward). Finally, torsional movements are intorsion (toward the nose) and extorsion (away from the nose). Within the orbit, the eye is surrounded by orbital tissues and by the *six extraocular muscles* (EOMs). The four recti muscles (lateral, medial, superior and inferior) start from the annulus of Zinn, at the appendix of the orbit, and insert on the surface of the eye (sclera), anterior to the eye's equator. The oblique muscles insert into the posterior globe. The origin of the inferior oblique muscle is on the medial wall of the orbit; the superior oblique passes through the trochlea, or pulley, before inserting in the globe.

EOMs are arranged in three agonist-antagonist pairs and their action is ruled by *Sherrington's law* of reciprocal innervation, stating that whenever an agonist muscle is contracted, the antagonist is relaxed. Pointing the gaze toward one object, means moving the fovea in the retinal space (two dimensional problem). Eye plant has three degrees of freedom and therefore allows an infinite number of eye positions for each desired gaze direction. However it has been found that, when the head is stationary and upright, for any gaze direction, the eyes always assume the same unique orientation (Donders' law). The trajectory is determined by the *Listing's law*, stating that all eye orientations can be reached from one primary reference orientation with a single rotation about an axis that lies within the plane orthogonal to the primary eye position. This plane is called Listing's plane. For any gaze direction the eye's 3D spatial orientation is unique and independent of how the eye reached that gaze direction, thus there is a binary relationship between muscles contractions and gaze orientations. An important implication is in the control of eye movements because the brain does not need to know the history of the movement. During rVOR, however, Listing's law is not obeyed and eye movements are governed by a similar rule, called *quarter angle rule*, stating that the rotation axes have to rotate of a quarter of the angle of the eye. The difference is not completely clear, but is probably due to the fact the rVOR is involved in stabilizing the whole visual scene, while Listing's law is defined for gaze movements towards a target, such as saccades, which are fovea-oriented movements.

1.2.4. The systems approach to rVOR

The VOR system has been extensively described using control systems approach and frequency domain analysis [22]. This approach allows to describe how sensory input and motor output are related using transfer functions, but also to understand the neural processing performed at the different nuclei involved. Indeed the systems approach has led to great advances in our understanding of the neural processing of the oculomotor function. This analytic description can be easily illustrated for the rotational vestibular-ocular reflex.

During rotation at constant velocity in darkness, slow phase eye velocity ($\dot{E}$) decreases slowly (Figure 1.4 A):

$$\dot{E}(t) = g * \dot{H}_0 * e^{-\frac{t}{T_{VOR}}}; \quad (1)$$

where g is the gain of the VOR, $\dot{H}_0$ the velocity of the step, and T_{VOR} the major VOR time constant, about 20 sec for humans. The transfer function in Laplace notation results:

$$\frac{\dot{E}(s)}{\dot{H}(s)} = g * \frac{s\,T_{VOR}}{1 + s\,T_{VOR}}. \quad (2)$$

Equation 2 predicts eye velocity response elicited by head angular velocity. Now we describe, in terms of transfer function, how the various parts (semicircular canals, eye muscles) participate in the VOR. The dynamics of the canals can be described by a first order dynamic system with the following transfer function:

$$\frac{\dot{H}_c(s)}{\dot{H}(s)} = \frac{s\,T_c}{1 + s\,T_c}; \quad (3)$$

where T_c is the cupula time-constant (6 sec) and $\dot{H}_c$ is the modulation of the discharge rate of primary vestibular afferents (the canal estimate of head velocity) [7]. The time constant of the eye movements is therefore longer than that of the canal afferent signal, this lengthening means that the signal remains accurate for a longer period of time during low frequency stimulation. This phenomenon is called velocity storage. Two models were proposed for the velocity storage, one using a low pass filter and positive feedback [20] and the other using a combination of direct and low pass filter pathways [23]. In terms of transfer function in the Robinson's model [20] the relation between head velocity and the response of the secondary vestibular neuron in the vestibular nucleus ($\dot{H}'$) is:

$$\frac{\dot{H}'}{\dot{H}} = \frac{\dot{H}'}{\dot{H}_c} * \frac{\dot{H}_c}{\dot{H}} = \frac{1}{1 - \frac{k}{s\,T_c + 1}} * \frac{s\,T_c}{s\,T_c + 1} = \frac{s\left[\frac{T_c}{1-k}\right]}{s\left[\frac{T_c}{1-k}\right] + 1} = \frac{s\,T_{VOR}}{s\,T_{VOR} + 1}. \quad (4)$$

Robinson suggested values of k around 0.7 (in darkness) so that with T_c=6 sec, T_{VOR}=6/0.3=20 sec, thus effectively prolonging the time constant to the values experimentally recorded.

It has been shown that the relationship between eye position E and discharge rate of motor neurons M is approximately:

$$\frac{E(s)}{M(s)} = \frac{1}{s\,T_e + 1}; \tag{5}$$

Where T_e is the time constant of the viscoelastic elements in the orbit (about 0.25 sec, first order approximation [24]). Given all these transfer functions we can easily deduce what happens between the vestibular nuclei and the motoneurons ($C(s)$, central processing).

$$\frac{\dot{E}}{\dot{H}} = \left[\frac{s\,T_c}{1 + s\,T_c}\right] * \left[\frac{T_{VOR}}{T_c} * \frac{s\,T_c + 1}{s\,T_{VOR} + 1}\right] * C(s) * \left[\frac{s}{s\,T_e + 1}\right]; \tag{6}$$

we have:

$$C(s) = \frac{M(s)}{\dot{H}'(s)} = g\left(T_e + \frac{1}{s}\right). \tag{7}$$

$C(s)$ tells us that the motor command sent to the motor neurons has a velocity component and a position component obtained integrating the velocity command through the *neural integrator* (see Chapter 1.2.1), in order to compensate the dynamics of the oculomotor plant [25]. Based on this observation, subsequent researches, were able to isolate the responses of neurons implementing the neural integrator [26]–[28].

The control systems approach helped researchers by indicating them what they should look for in the neural pathway starting from the mathematical equation [22]. However this approach has some restrictions: it describes how the system can be organized physically without give information about the goal and the logic of the computation; it doesn't take into account neural responses variability (noise is ignored) assuming that the activity of a pool of neurons can be approximated by a typical neuron [29].

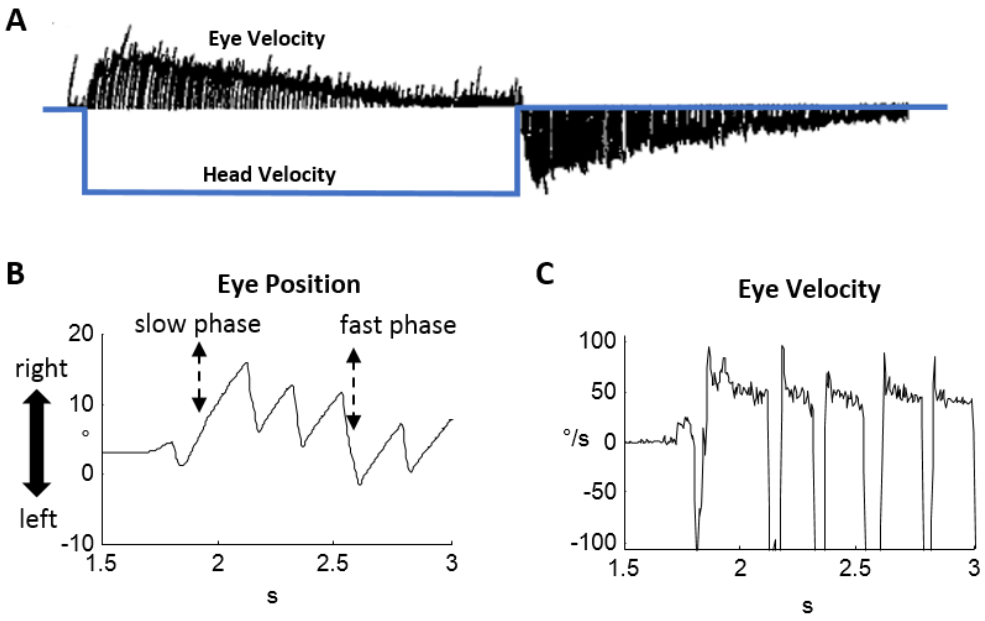

Figure 1.4 A) Eye velocity and position response to a velocity step rotation in darkness. Slow phase eye velocity exponentially decays. When the velocity step stops the eye rotate in the opposite direction and the response exponentially decays (post rotatory response) (adapted from [9]). B, C) Position and velocity trace of a typical vestibular nystagmus.

1.3. Disorders of the peripheral vestibular system

Vestibular disorders occur frequently and can affect people of all ages. The main symptoms, such as dizziness, vertigo, imbalance, are difficult to describe, and are associated to many conditions (peripheral vestibular dysfunction, central nervous system lesion, psychiatric disorders, and nonspecific dizziness).

Peripheral vestibular disorders can involve vestibular inner ear structures and vestibular nerve, altering available sensory information about head orientation and motion.

Central vestibular disorders involve the vestibular nuclear complex and the cerebellum. These pathologies affect integration and processing of sensory input. The most common include cerebellar infarct and tumors, brainstem strokes, multiple sclerosis, migraine related vestibulopathies and head trauma [30].

In this paragraph I review the pathophysiology of the more common peripheral vestibular disorders.

1.3.1. Benign Paroxysmal Positional Vertigo (BPPV)

Benign paroxysmal positional vertigo (BPPV) is the most common cause of vertigo, it occurs when crystals of calcium carbonate detach from the

otolithic membrane in the utricle and move to one of the semicircular canals.

The classic explanation suggests that the otoconial material is deposited in the cupola making it denser than the surrounding endolymph and then susceptible to gravity [31] (cupulolithiasis). A second theory, canalithiasis, suggest that the debris are free-floating in the canal and when head moves in the plane of that canal the debris fall causing endolymph movement and turbulence that stimulates the cupula [32]. BPPV is typically unilateral but in some cases bilateral.

Symptoms of BPPV, in addition to vertigo, are dizziness, imbalance and nausea and become worse changing the head position with respect to gravity. In people under 50 years of age the most common causes of BPPV are the result of forces that displace the otoconia (head injury), while in older people they are related with natural age degeneration of the otolithic membrane.

BPPV is a self-limiting disorder and usually resolves within 6-12 months; however, there are several liberatory maneuvers [33]–[35] with which most patients can be treated successfully (the period of recovery varies from immediately after the maneuver to six weeks after).

1.3.2. Vestibular Neuritis and Labyrinthitis

Vestibular neuritis is the second common cause of vertigo. A definitive cause was never proved, but etiology is compatible with a viral infection [36]: dizziness is attributed to a viral infection of the vestibular nerve (disruption of the transmission of sensory information between the ear and the brain). It is a type of unilateral vestibular dysfunction; when one of the vestibular nerves is infected, there is an imbalance between the two sides, causing vertigo. If the infection affects also the inner ear, is called Labyrinthitis, resulting in the symptoms of vestibular neuritis, with the addiction of hearing symptoms. In vestibular neuritis, the virus that causes the infection is thought to be a member of the herpes family; rarely it can be due to a bacterial middle ear infection.

The symptoms are the acute onset of prolonged severe rotational vertigo (enhanced by the movement of the head), spontaneous horizontal rotatory nystagmus beating toward the good ear, postural imbalance, nausea and vomiting. The onset of the symptoms is very sudden (acute phase) and severe dizziness develops quickly during daily activity. The symptoms usually decrease after 48-72 hours and gradual return to normal balance in about 6 weeks. However, rapid movement versus the affected side can cause oscillopsia of the visual scene (subjective motion illusion due to lack of gaze stabilization).

The initial treatment consists in vestibular suppressants and bed rest. After the most severe vertigo and nausea have passed, the patient may resume ambulation and administration of vestibular suppressor should be progressively reduced and stopped. After the acute phase vestibular

rehabilitation, exercise speeds up the recovery stimulating the adaptation of the central nervous system [37].

1.3.3. Ménière's Disease

Ménière's disease is a disorder of the inner ear function causing hearing damage and vestibular symptoms. It was linked to endolymphatic hydrops, i.e. an excess of fluid in the inner ear. The development of endolymphatic hydrops is generally function of malabsorption of endolymph in the endolymphatic duct and sac [38]. Ménière's disease evolves over a course of many years; when drainage is blocked, pressure increases causing damages and fractures in the temporal bone. Symptoms are caused both by direct compression of sensory structures (cochlea and vestibular labyrinth).

Ménière's starts with one symptom and gradually progress. Classic Ménière's symptoms are: attack of rotational vertigo (nausea, vomiting, disequilibrium, and nystagmus, generally lasting no longer than 24 hours) combines with transient hearing loss; progressive (unilateral or bilateral) hearing loss; tinnitus and sensation of pressure in one or both ears. As the disease progresses, hearing fails to return after the attack, and after many years, vertigo symptoms gradually diminish [39]. Moreover, the incidence of migraine is probably increased in patients with Ménière's syndrome [40].

Treatment aims to reduce frequency of attacks and preserve hearing. First of all a dietetic program, including restriction of salt, water, nicotine, caffeine and alcohol and avoidance of exposure to low temperatures is prescribed. Intra-tympanic infusions with ototoxic antibiotics (gentamicin sulfate) selectively damage the secretory epithelium (improving endolymphatic hydrops) but significantly affect vestibular and cochlear function [41]. A successful treatment is vestibular nerve section. Ablative surgical procedures are also possible, but may cause long lasting postural imbalance in elderly patients. Vestibular exercises are not appropriate unless patients have permanent loss of vestibular function.

1.3.4. Perilymphatic Fistula and Vestibular Paroxysmia

Perilymphatic Fistula is an abnormal opening in the bony capsule of the inner ear causing a loss of perilymph from semicircular canals into the middle ear [42]. Head or ear trauma is the most common cause of fistulas, but they can develop after a rapid increase and pulsation of intracranial pressure against the bone of the scull.

Perilymphatic Fistula causes dizziness, episodic vertigo, motion imbalance and hearing loss.

After the sudden onset of hearing loss or dizziness, treatment consists of absolute bedrest for 5-10 days, mild sedation with tranquillizer. If

symptoms persist, if Perilymphatic Fistula is diagnosed, a surgical intervention may be considered.

Vestibular Paroxysmia is a neurovascular cross-compression of the root entry zone of the vestibular nerve eliciting disabling positional vertigo [43]. Medical treatment consists in antiepileptic drugs and surgical neurovascular decompression.

Chapter 2

Sensory-motor organization of the VOR: neural computation and adaptation

The physical properties of the human motor system (large number of degrees of freedom and actuators) make it redundant, because there is often an infinite number of ways to execute a task. Despite this multitude of solutions, humans and other animals make highly stereotyped movements. There is a regularity in how we move our eyes (speed and duration of saccades), or how we move our arms during reaching or our legs while walking. There is then a regularity in how our brain perceives the external word, reacts to sensory stimuli and controls the movements. Regularity in nature lead to the formulation of theories expressed formulaically, i.e. using mathematics [44][45]. In the last twenty years, a large number of theoretical and experimental work has been directed to understand the computational basis of motor control particularly for voluntary visually guided reaching movements [46]–[49]. These computational theories describe brain function at the behavioral level because at present little is known about the neural implementation of these mechanisms. On the other hand, the vestibular system represents a good model system to study the neural processing of the computational mechanisms of sensory-motor control [29], [50] because of the well-known neural circuitry (see Chapter 1.2.1) and a solid computational framework based on control system theory (see Chapter 1.2.4).

Computational principles in sensory-motor control concern also motor learning [51], [52]. During life, indeed, both development and aging (long timescales) and fatigue and daily interaction with the environment (short timescales), change the properties of the muscular and nervous system. Our CNS learns and adapts our control strategies to overcome these changes and make skilled and correct movements. The cerebellum is an

evolutionarily conserved structure that is critical for motor learning (in addition to its direct role in motor control) in vertebrates. Several theoretical models have been developed to explain sensorimotor calibration in terms of synaptic plasticity within the cerebellum emerging from studies of the VOR [19], [53], [54].

Indeed, studies of the vestibular system provided neurophysiological evidence for general concepts of sensory-motor organization (e.g. neural implementation of forward and inverse models, concept of reafference, sensory integration, motor learning) that are common to all sensory-motor system [50], [55]. This chapter, focusing on the neural implementation in the VOR, is a review of some computational mechanisms that the brain may use in motor control: the concept of internal models, state estimation, Bayesian theory and Kalman filtering [29], [44]. Afterwards, motor memory and computational models of plasticity [44] are discussed.

2.1. Internal models

Internal models are an important theoretical concept in motor control, supported by behavioral and neurophysiological data. Internal models are neural mechanisms that mimic the input/output characteristic (or the inverse) of a motor system. Inverse internal models calculate the feed-forward motor commands for a desired trajectory; forward internal models predict sensory consequences of a motor command from an efference copy of the command [46]. The theories of motor control and learning in the limb control system suggest that these processes involve neural populations that implement inverse and forward models of the motor effector and the external world [48], [56]. Here, I will focus on the implementation of these principles in the vestibular system, which provides important evidences of neural processing and computation in the brain.

2.1.1. Inverse models: compute motor commands

Inverse motor models map the desired movement into the appropriate motor command allowing to control motor movement and achieve the desired motor output (Figure 2.1 A). Clearly, such mapping depends on the dynamics of the motor plant being considered.

The first evidence of an inverse dynamic model was pioneered by Robinson and colleagues for the rVOR [25]. Afferents from the semicircular canals encode head velocity over a wide frequency range (>0.03 Hz), while the relationship between eye position and motor neurons' firing rate can be approximated with a first order low pass filter (bandwidth 0.5-0.6 Hz). If the semicircular canals' signals were simply projected in a feed forward fashion directly to extra-ocular motor neurons, eye velocity would be proportional to head velocity only for frequency above 0.5 Hz (Figure 2.1C blue curve). It has instead been shown that the rVOR response

has a bandwidth extending to very low frequencies (Figure 2.1 C red curve). This implies and additional processing stage that compensates the dynamics of the eyeball by filtering the canal afferent signal with an inverse dynamic model of the eye plant (Figure 2.1 A).

Robinson and colleagues hypothesized that the velocity signal was conveyed to motor neurons both directly and indirectly via a *neural integrator* (Figure 2.1 B). The *parallel pathway* model compensates the viscoelastic forces of the eyeball and can be thought of as an inverse model of a simplified (first order) eye plant (see Chapter 1.3).

The neural implementation of the model [50], [57] was later supported by the discovery of *burst tonic* and *tonic* neurons in the prepositus hypoglossi (PH) and adjacent medial vestibular nuclei (VN) (collectively called PH-BT). PH-BT neurons have firing rates that correlate with eye position during static fixation and low frequency slow eye movements and do not respond to head movements during rVOR suppression (fixation of a target that moves with the head); therefore PH-BT neurons were thought to encode the position component of the inverse model (E* in Figure 2.1 C). Other populations within the VN (position-vestibular-pause PVP and eye-head EH neurons; PVP/EH) carry different combinations of head velocity and eye velocity signals and appear to directly project to motor neurons.

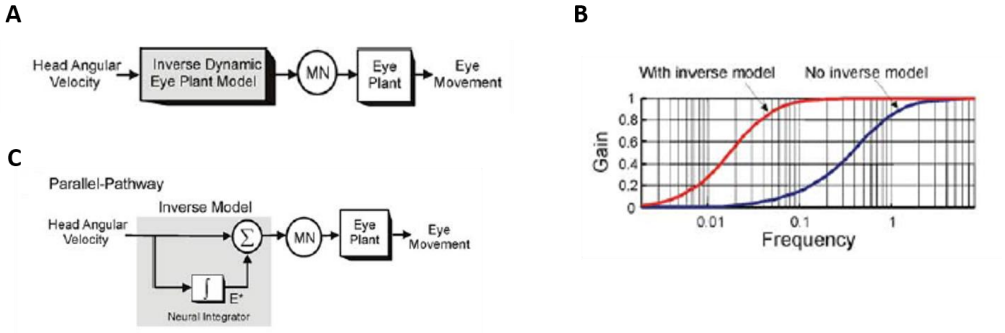

Figure 2.1: A) An inverse model transforms desired action in the appropriate motor command. In the rVOR response, angular velocity signals from semicircular canals (desired eye velocity) are processed by an inverse dynamic model and conveyed to MN. B) Frequency response of the rVOR with (red line) or without (blue line) the processing of the inverse model. C) Parallel pathway implementation of the inverse model. The inverse model (gray shaded box) is a weighted sum of angular velocity and integrated angular velocity (E* estimate of desired eye position). (Taken from [50])

2.1.2. Forward models: predict sensory consequences

Forward motor models, instead, are a neural implementation of the physics of the motor plant and convert an efference copy of the motor command into an internal estimate of the executed movement (Figures 2.2), most likely in terms of its sensory consequences.

Why should the brain predict the sensory consequences of motor commands? The first reason is the delay of sensory feedback. Delay in sensory measurements can cause instability during the execution of movements. Relying on prediction of the executed movement helps to overcome this delay. The second important principle is that our perception (i.e. the ability to estimate the state of our body and the external world) is a combination of how the brain predicts what we should sense and how the sensory system reports what was sensed (Figure 2.2). The result is that our perception will be better than if we had to rely on sensory measurement alone. Therefore, predicting the sensory consequence of the motor command helps to overcome the sensory delay and to sense the world better than using the sensory feedback alone.

Comparing prediction of the executed movement with sensed movement, also helps verifying if the plant is working properly, and maintaining calibration and robust motor control even when the dynamics of the plant change (e.g. development, injury, aging, fatigue).

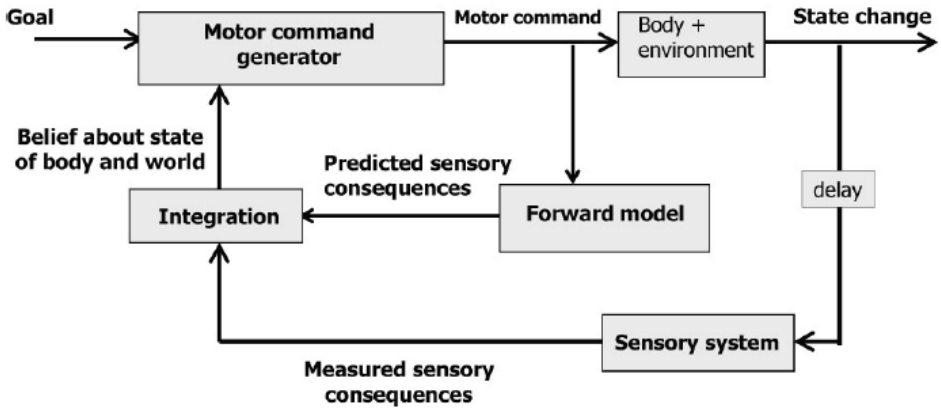

Figure 2.2: Schematic implementation of the control of voluntary movements. Motor command changes the state of the body and the external world. The sensory system measures the sensory consequences of the movement. The brain predicts the sensory consequences of the movement through a forward model, using an efference copy of the motor command. The integration of predicted and measured sensory consequences forms our belief about the state of our body and of the world. (Taken from [44]).

A forward model in the cerebellum?

Studies on limb control [46], [58] and eye movements [55], [59], [60] suggested that the cerebellum might be the site of the implementation of the forward model. The main neural circuit of the VOR in brainstem and cerebellum works as follow (Figure 2.3 A):

- VN in the brainstem receive signals related to head movement from the vestibular nerve and project to motor neurons (MN);
- as discussed before, PH-BT cells in PH and VN code the output of the inverse dynamic model and transmit to the *cerebellar*

floccular complex (FC) the efference copy of the eye movement command sent to MN;

- *mossy fibers* (MF) provide vestibular input to the cerebellum;
- a feedback of the presumed forward model in FC could be used to update the brainstem motor command via the Purkinje cells (PC) projections onto the *floccular target neurons* (FTN) in VN (PC inhibit VOR interneurons in VN).

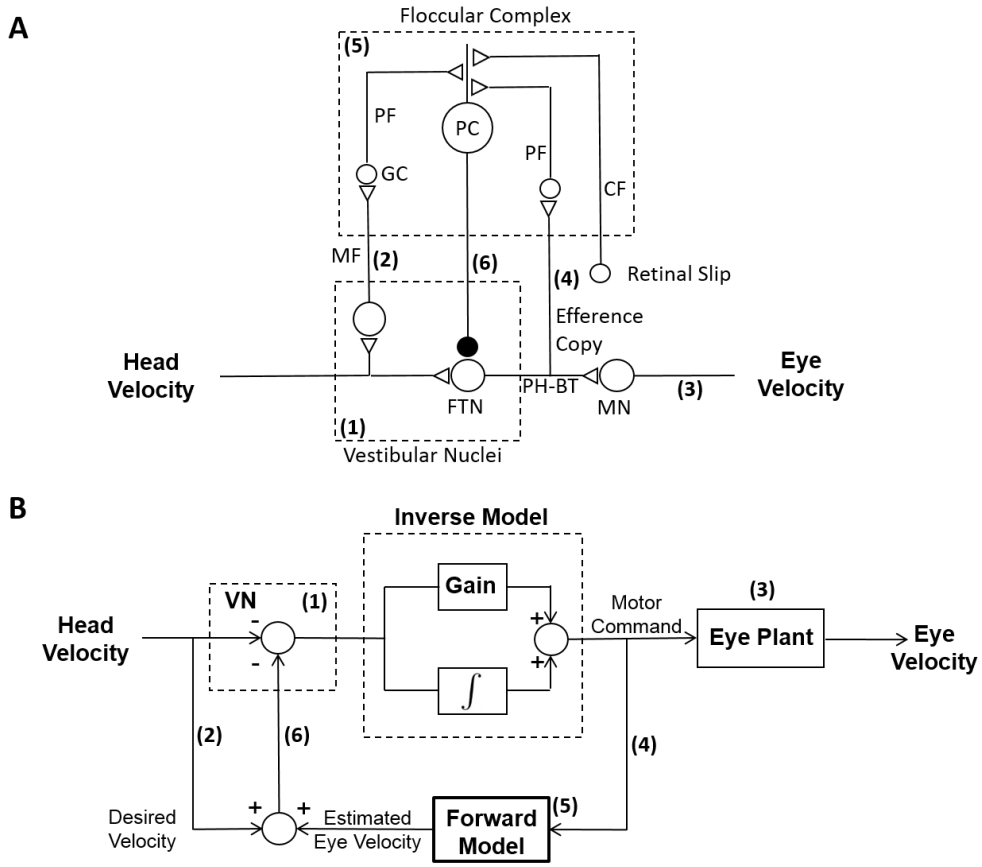

Figure 2.3: A) Brainstem/cerebellar neural circuitry responsible of the plasticity of VOR (adapted from [55]). B) Schematic of the implementation of the motor control structures (adapted from [59]). Numbers indicate: (1) vestibular nuclei; (2) vestibular input to the cerebellum; (3) plant; (4) efference copy of the motor command; (5) floccular complex in the cerebellum; (6) Purkinje cells projections on VN. Climbing fibers CF carry to the cerebellum the retinal slip signal (error in the function of the VOR), which is the instructing signal guiding plasticity.

The hypothesis of the implementation of a forward model in the cerebellar flocculus was supported by the finding of the encoding of 3D ocular kinematics during smooth pursuit eye movement [60]. Visually guided 3D eye movements are subject to Listing's law (see Chapter 1.2.3). When eye movements are made from eccentric positions, the angular velocity axis of the eye does not remain confined to Listing's plane but deviates in the same direction as gaze by approximately half as

much (half-angle rule [61]). Extra-ocular motor neurons do not encode the half-angle rule that appear to be generated by the mechanical properties of the eyeball [62], thus there is a difference between the motor command and the actual executed eye movement. Indeed, PH-BT cells, like motor neurons, showed little adherence to the half-angle rule [60] (PH-BT represent the output of the inverse model i.e. the motor command). EH neurons (in VN), instead, showed a dependency with eye position consistent with the half-angle rule, closely related to the actual executed eye velocity [60] (EH cells receive projections from the cerebellar flocculus that might implement the forward model). Moreover, Purkinje cells in the cerebellar flocculus receive also head velocity signals and combine eye and head velocity to compute an estimation of gaze velocity [55] (Figure 2.3 B). Anyway, at present there is no firm evidence of a neural implementation of that forward model.

Figure 2.3 B shows a possible implementation of inverse and forward model in feedback loop for the VOR [59]: the inverse model implements the direct and indirect integrator pathways, simplifying the dynamics of the motor plant (first order approximation); the forward model predicts eye velocity, thus the difference between predicted and desired eye velocity is used in the feedback loop to update motor command. This implementation resembles to the current models of cerebellar function considered for the adaptation of the VOR [19] (Figure 2.1 A, Figure 2.7; see Chapter 2.3.2).

2.1.3. Internal models of the physical laws

In addition to the models of sensory and motor dynamics, the brain also implements internal models of physical laws. An example is the resolution of tilt/translation ambiguity [63], [64] essential in body orientation sensing.

Body orientation is estimated by sensing gravitational force; however it is indistinguishable from inertial linear acceleration (Einstein's equivalent principle [65]). The otolith organs in the inner ear transduce linear acceleration (see Chapter 1.1.4), responding identically to translational and gravitational acceleration; therefore only their sum can be sensed:

$$a = t - g; \tag{1}$$

where a is the linear acceleration sensed by the otolith sensors, t and g are translational and gravitational acceleration. In normal conditions, however, we sense both the orientation of the head relative to the vertical even with the eyes closed, and significant accelerations.

First the brain filters the otolith signals, so that low-frequency signals are interpreted as tilt angle change relative to gravity, and high frequency signals are interpreted as related to linear acceleration [66].

In addition, the brain combines and integrates otolith and semicircular canal signals [64]: to estimate translation t, the otolith sensed acceleration a is combined with an internal estimate of head tilt computed from angular

velocity signal ω (head velocity is used to keep track of change in orientation of the gravity vector relative to the head Eq. 2).

$$\dot{g} = g \times \omega; \tag{2}$$

$$t = a - \int \omega \times g \, dt. \tag{3}$$

The otolith-canal integration necessary to implement Eq. 3 takes place in the *vestibular-only* (VO) cells within brainstem-cerebellar circuits involving VN, *rostral fastigial nuclei* (rFN) and *nodulus* and *ventral uvula* regions of the *caudal cerebellar vermis* (NU). To investigate how neurons combine canal and otolith signals Angelaki and Green [67] measured neuronal activity (otolith afferent Figure 2.4.B and VN neuron Figure 2.4 C) during four stimuli: translation, tilt and two combinations in which translational and gravitational accelerations are summed or cancelled (tilt + translation, tilt – translation; Figure 2.4 A). The VN neuron responds during tilt-translation motion (Figure 2.4 C), when the resultant acceleration is zero (lack of modulation of otolith afferent; Figure 2.4 B).

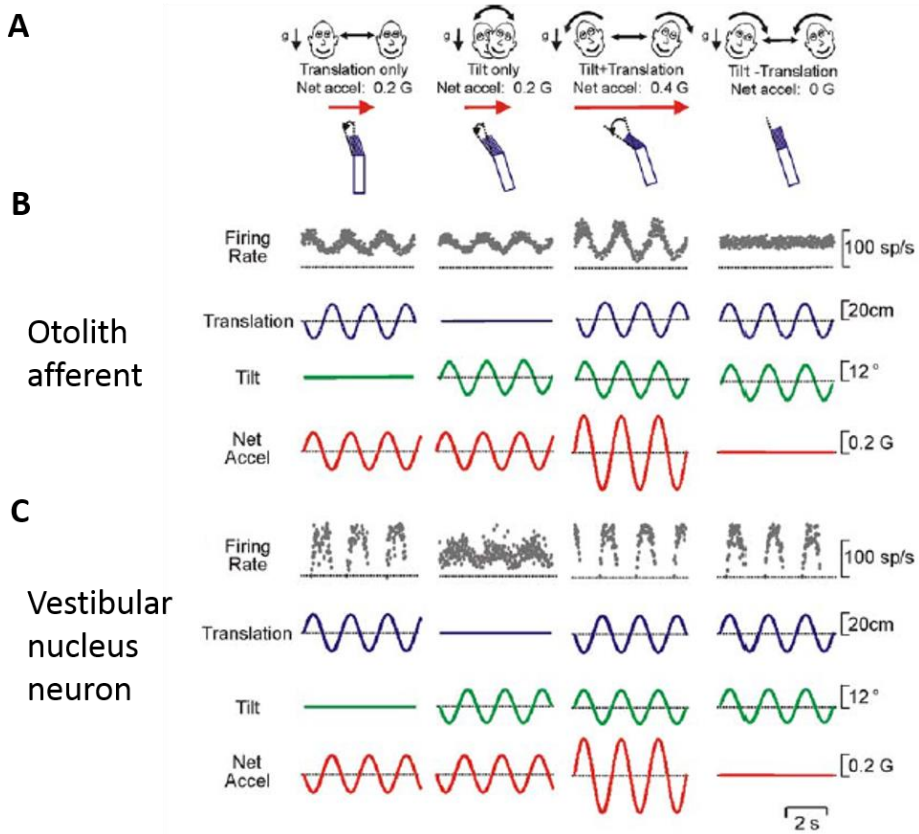

Figure 2.4: Representation of the four tilt translational stimuli, blue and green lines represent single components and red line their sum. B) Firing rate of an otolith afferent. C) Firing rate of a central VN neuron. In tilt-translation stimulus despite the resulting acceleration is zero and then the absence otolith response, VN neuron has a robust response. (Taken from [50])

The response of central neurons indicates the contribution of semicircular canals to estimate translation. Resolution of the tilt/translation ambiguity requires the nonlinear integration of linear acceleration and angular velocity as predicted by the laws of motion. The firing rates of brainstem and cerebellar neurons encode a combination of signals from the canals and the otoliths, processed to construct an internal model representation of the computation required for inertial motion detection.

2.2. State Estimation

Due to presence of noise, our sensors provide imperfect information in perceiving the world. Another fundamental problem that the brain must face is the delay. Sensory feedback information is delayed because of receptor dynamics and of conduction nerves' time. These delays are approximately 100 ms (we actually live in the past). For slow movements delays make control difficult (information can be out of date), and in the extreme case of saccades the movement duration is shorter than the sensory delay so that feedback cannot be used during the movement. Not only noise and delay cause uncertainty but there are many other sources: for example, it can be originated from the limitations in receptor density, or from the representation of an analog world in the digital neural code, or even the projection of a three-dimensional world on the two-dimensional retina.

For these reasons, our estimation of the state of the world comes from two sources of information: what we predicted and what we observed. We combine these two sources of information applying a weighed sum: the higher is the reliability of the information the more the weight that the brain assigns to it increases. Combining information of different modalities can improve the estimate. Thus, the state of the world is not only based on our sensory observation but is based also on an integration of sensory measurements with our predictions. This process is mathematically described by estimation theory [68].

2.2.1. Bayesian theory

The estimation of the state of our body (or state of external world) has two sources of information. The first is a prediction of what sensory measurements of the state should be (*prior* estimate of the state). The second is a combination of the measured quantity with the predicted one to form a *posterior* estimate of the state. The first problem is one of model building (build a forward model that predicts sensory consequences); the second problem is one of integration (form an estimate of the state based on the two sources of information). Bayes' rule describes how these sources of information are integrated:

$$p(x|y) = \frac{p(y|x) * p(x)}{p(y)}. \quad (4)$$

The term *p(x|y)* is the posterior probability e.g. the probability of the hidden state *x* given the observation *y*. The term *p(x)* is the prior probability distribution, which expresses the probability of the state, even in absence of any information. The term *p(y|x)* is called *likelihood* and expresses the probability of an observation given the value of what we want to estimate (the hidden state *x*). The term *p(y)* is the probability of information, it simply serves to scale the probability distribution of the numerator. For some hidden states *x* and observation *y* we formulate a generative model that describes *p(y|x)* and we find and estimate $\hat{x}$ that maximizes the probability of our observations (maximum likelihood estimation):

$$\hat{x} = arg\max_{x}\big(p(y|x)\big). \quad (5)$$

The variable $\hat{x}$ is also a random variable with its expected value and its variance. If we have two independent (uncorrelated) sources of information (S_1, S_2) corrupted by noise (normally Gaussian distributed with zero mean and variance σ_1, σ_2), the optimal estimate of *x* and its variance are expressed as follows:

$$[\hat{x}] = \frac{\sigma_2^2}{\sigma_1^2 + \sigma_2^2} S_1 + \frac{\sigma_1^2}{\sigma_1^2 + \sigma_2^2} S_2; \;\; \sigma = \frac{\sigma_1^2 * \sigma_2^2}{\sigma_1^2 + \sigma_2^2}. \quad (6)$$

Thus, the optimal estimate is a weighted average of the sensory input with a single parameter based on their relative reliabilities (the source with less uncertainty has more weight). The variance is less than the variance of each source in isolation; therefore, combining two sources of information decreases the uncertainty. To estimate the properties of objects our brain combines varying sources of information in a way that is consistent with maximum likelihood estimation [69]. This approach has been successfully applied also to spatial orientation: visual cues are used to interpret ambiguous vestibular cues, the weight given to these cues was less when the cues were less reliable, consistent with the prediction of the Bayesian model [70].

The Bayes' rule combines prior and likelihood to obtain the probability distribution of the hidden state *x* given the data (posterior). The peak of the posterior is the most probable state given sensory and prior information (maximum a posteriori estimator). As the uncertainty of the sensory feedback increases, the system increases the belief in prior knowledge [71].

Bayesian models describe well perception mechanisms but have several limitations. They operate only at behavioral level (they do not consider the conversion of the sensory stimulus in neural representation and how and where the neural representation is integrated). In addition such models are

limited to discrete or static situations, while real world stimuli are dynamic and continuous. We need to estimate parameters that evolve over time, because the configuration of the body during movements changes continuously. Using the information of the motor command the CNS can estimate the state of the body continuously using internal forward (predictive) model. The combination of sensory feedback and forward model to estimate the current state is known as an *observer*. Observer theory and Bayesian framework are combined in the form of the Kalman filter [72].

2.2.2. Kalman filtering

The Kalman filter [73] is a recursive filter that estimates the current state and updates it using sensory feedback and motor commands. The Kalman filter is a Bayesian estimator for time-varying systems.

The general problem is to try to estimate the state x of a process governed by the linear stochastic difference equation:

$$x_{k+1} = A_k x_k + B_k u_k + w_k; \tag{6}$$

with a measurement y:

$$y_k = C_k x_K + v_k. \tag{7}$$

The random variables w_k and v_k are the process and the measurement noise, respectively; they are assumed to be independent, zero–mean Gaussian with variances Q and R respectively.

If we define $\hat{\underline{x}}_k$ the prior estimate of the state (and $\underline{P}_k = var[\hat{\underline{x}}_k]$) on trial k given the past *k-1* trials, and $\underline{x}_k$ the posterior estimate at step k after we make an observation y_k (and $P_k = var[\underline{x}_k]$), we can write the posterior as a combination of the prior and a weighed difference between the measurement and the prediction:

$$\underline{x}_k = \hat{\underline{x}}_k + K\left(y_k - C\hat{\underline{x}}_k\right). \tag{8}$$

The term K is the sensitivity to prediction error and reflects the uncertainty about our estimation. The difference $\left(y_k - C\hat{\underline{x}}_k\right)$ is called innovation (or residual) and reflects the discrepancy between the prediction and the measurement. K is called Kalman gain and the problem is to set it in such a way that posterior estimation is as certain as possible (minimum variance). One form of K that minimizes P_k is:

$$K_k = \underline{P}_k C_k^T (C\underline{P}_k C_k^T + R_k)^{-1}. \tag{9}$$

The Kalman gain is a ratio between our prior uncertainty $\underline{P}_k$ and our measurement uncertainty R: if we are uncertain about our prediction

(numerator > denominator, in Eq. 9), we learn a lot from prediction error; if we are uncertain about measurement (denominator > numerator, in Eq. 9), we ignore prediction error.

The posterior uncertainty is computed as follow:

$$P_k = (I - K_k C)\underline{P}_k. \tag{10}$$

Eq. 8-9-10 allow to update the estimate after making an observation. The posterior estimation is used to compute the prior estimation (and its variance) for the next trial:

$$\underline{\hat{x}}_{k+1} = A\,\underline{x}_k + Bu_k; \tag{11}$$

$$\underline{P}_{k+1} = AP_kA^T + Q. \tag{12}$$

The Kalman filter estimates the process using a form of feedback control: the filter estimates the process and receives a feedback from noisy measurement. The equations fall into two groups: the *time update* equations (Eq. 11-12) project forward in time the current state and the error covariance estimates to obtain a prior estimate of the next step, and the *measurement update* equations (Eq. 8-9-10) integrate the new measurement and the prior estimate to obtain a (minimum variance) posterior estimate. The Kalman filter is the optimal estimator when the dynamics and the sensory measurements are linear and the noise is Gaussian, and is a good approximation in other cases. This framework has been proposed in several studies examining the estimation of hand position [74], posture [75] and head velocity [76][77].

Figure 2.5 A shows the application of the observer theory to the sensory estimation during voluntary movements planning. The architecture is composed by two paths: the first causes body motion via muscles activation and is corrupted by unplanned motion, sensory noise and noisy neural computation; the second (the observer) is completely neural and consists in internal models of body and sensory system. In the observer model the filter gain K is selected by the designer: if K is small the estimate is less noisy, but decays more quickly, if K is large the estimate is closer to the actual state but noise is greater.

Figure 2.5 B shows the *velocity storage* (see Chapters 1.2.2-1.2.4) observer model [78] (simple yaw rotation; the state to estimate is the angular velocity). In contrast with the observer model which is deterministic, the Kalman filter model incorporates knowledge about noise; thus the gain is an optimal tradeoff between reducing noise in the estimate and how quickly the estimate responds [77].

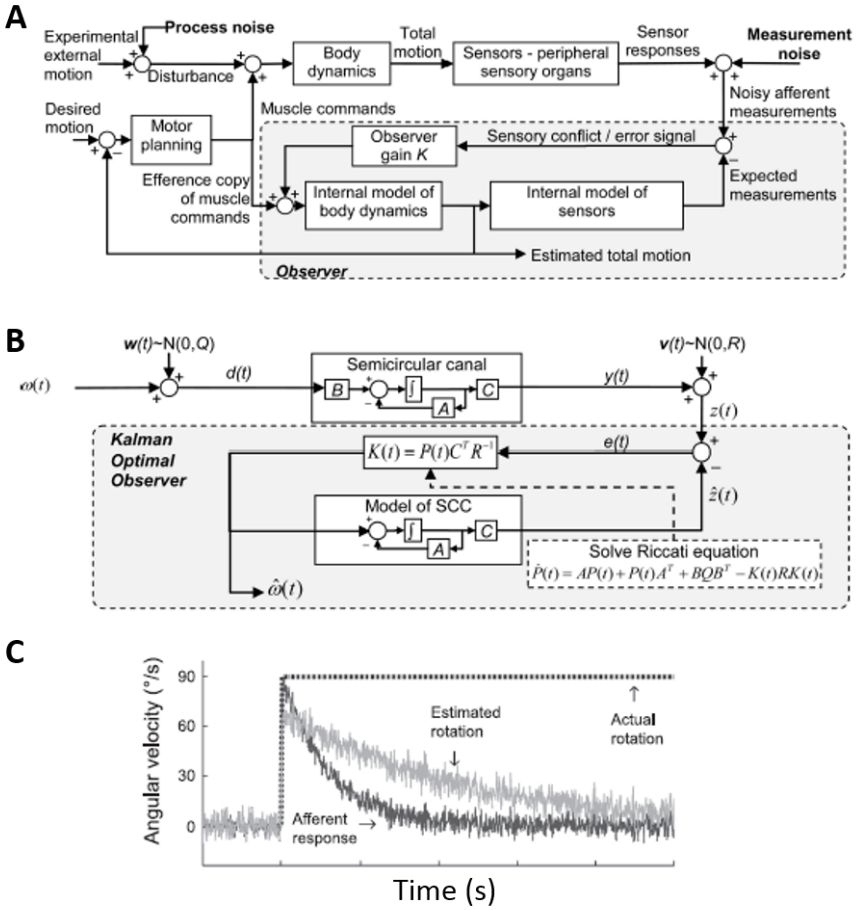

Figure 2.5 A) Observer theory model applied to the brain's control of body movement. Desired movement is subtracted from current motion to plan muscle activation for required motion. Deterministic motion is perturbed by random disturbances and the resulting motion is sensed by peripheral sensory organs. Sensory afferent information is also corrupted by noise. The observer estimates total motion using the efference copy of the motor command and internal models of body dynamics. The internal model of the sensor calculates the sensory consequences; the difference between expected and actual measurements steers the estimated state of the system. B) The general model in A is simplified for sensory estimation of passive motion: the input of the observer is set to zero (no voluntary movements), and motor dynamics set to unity (head velocity is stimulus velocity). C) Velocity storage modeling: the actual angular velocity (dashed black line) is a velocity step of 90 °/s. The afferent SCCs response (dark gray line) decays with a time constant of 5.7 s, while the Kalman filter estimate shows a longer time constant (23 s). Taken from [77].

The model (for passive yaw rotations) has some simplifications with respect to the model in Figure 2.5 A: there is no active control (motor planning) of the body but only passive perturbations; only SCCs are stimulated by motion; body dynamics are equal to the passive rotation (experimental head restraint). Measurement noise *v(t)* represents sensor inaccuracy. Disturbances represent external perturbations: the sum between experimental angular velocity and process noise *w(t)*. As in the observer model the velocity storage time constant is K+1 times the SCC time constant [78], [79], thus there is an explicit link between the velocity storage time constant and the noise characteristic (if the noise increases the time constant decreases).

Figure 2.5 C shows how the Kalman filter reproduces velocity storage in response to a step velocity stimulus. The SCCs afferent response decays with a time constant of 5.7 seconds, while the Kalman filter's estimated angular velocity shows the prolonged time constant of velocity storage (23 seconds).

The structure of Kalman filter has rigid restrictions: linear system, Gaussian noise, and explicit assumption about which signals are compared and how the feedback comes back to the system. Particle filtering is a relative new technique that introduces parallel computation of a distributed set of particles [80]. Together the particles form and propagate a probability distribution, in contrast with the Kalman filter which propagates only a signal with its estimated variance. Particle filter is a simulation technique in which these probability distributions are sampled at each time step. The samples are run through the system dynamics, subject to stochastic noise and used to create the probability distribution for the next step. This framework can be thought of as a recursive version of Bayesian inference described in Chapter 2.2.1. The particle filter doesn't need linear dynamics of the system and Gaussian noise, moreover it implements a distributed parallel computation resembling the parallel nature of neural processing. The filter has been recently applied to processing of vestibular dynamics [29], [77], [81]. On the other hand, the major disadvantage of the particle filter is that it is computationally heavy.

2.3. Learning and motor memory

Motor learning is the process responsible for improving the accuracy of our movements. It is necessary for complicated movements, but it is also important for calibrating simple movements, like reflexes, to compensate body (fatigue, injuries, and development) and environment changes over time.

As previously explained the brain combines observations with its predictions of sensory consequences to estimate the state of the body and the environment. For this reason, predictions must be unbiased estimates of

the observations. One of the fundamental problems of learning is to form accurate predictions and of keeping its representations accurate (internal models). Thus, the brain tries to predict what it observes; to make accurate predictions it builds internal models of the process that generates the data that it is observing. The problem of learning can be viewed as the problem of estimating these internal models, using the difference between predicted and sensory measures (sensory prediction error) to drive their adaptation [52]. The VOR latency (7-12 ms) is brief compared to that of visual information (100ms) so that in the initial and most important part of the response it operates in open loop Thus, the brain uses internal mechanisms such as internal feedback prediction and recalibration to optimize performance [82].

Actually, in sensorimotor control, three main classes of learning have been proposed, distinguished by the type of information that the motor system uses as a learning signal [47], [51], [83]. When a movement is made, the sensory-motor system senses the outcome and compares it to the predicted outcome: the *error-based learning* operates in order to reduce the average error to zero, thus keeping behaviors well calibrated and correcting for systematic biases. Once the error is nulled on average, error-based learning cannot improve the solution further (e.g. reduce the variability of the error). The signal that drives such learning (*reinforcement learning*) is the information about the success or the failure of the movement, thus a scalar, unsigned reward signal due to the activity of the dopamine neurons. The reward provides less information than prediction error, thus reinforcement learning tends to be slow. The third type of learning, *unsupervised use-dependent learning*, regards the state change of the motor system through the pure repetition of the movement, even if no outcome information is available. Theoretical models of learning in different parts of the brain indicate the cerebellum to be responsible for supervised learning based on the error signal encoded by the climbing fibers (Figure 2.7 A); the basal ganglia specialized for reinforcement learning based on the reward signal encoded in the dopaminergic fibers (from substantia nigra); the cerebral cortex specialized for unsupervised learning based on Hebbian plasticity and reciprocal connection within and between cortical areas [83] (Figure 2.6).

Error-based learning has been well studied with many adaptation paradigms in varying sensory-motor systems (reaching and saccadic movements, VOR; for reviews see [19], [84], [85]). Such trial-by-trial error-based learning is cerebellar based; indeed patients with cerebellar damage show impairment of adaptation.

For voluntary movements, spatial and temporal evolution of error-based adaptation has been studied extensively using linear state-space models [86]. Moreover, in the temporal domain, recent works have shown the existence of two learning processes that contribute to adaptation at different timescales: a fast one that learns and forgets quickly and a slow process that learns slowly but forgets slowly [87]. The success of these models

comes from the view of how the brain solves the control problem: in the presence of a perturbation, it adapts an appropriate internal model, which is used to drive the movement (model-based learning). Reinforcement and use-dependent learning don't need a model of the perturbation and thus can be described as model-free learning [88]. Model-free learning are thus characterized by nonlinear processes.

In this paragraph, I will talk about VOR adaptation as a model of cerebellum dependent learning. Starting with a description of the experimental procedures to induce VOR adaptation we will introduce the theories about the neural implementation of cerebellar plasticity and the evidence of the existence of different mechanisms.

Afterward I will concentrate on new theories about multiple timescales of adaptation of motor learning at behavioral level reviewing the results on saccade and reaching movements; the description of this process in VOR adaptation is object of the Chapter 3.

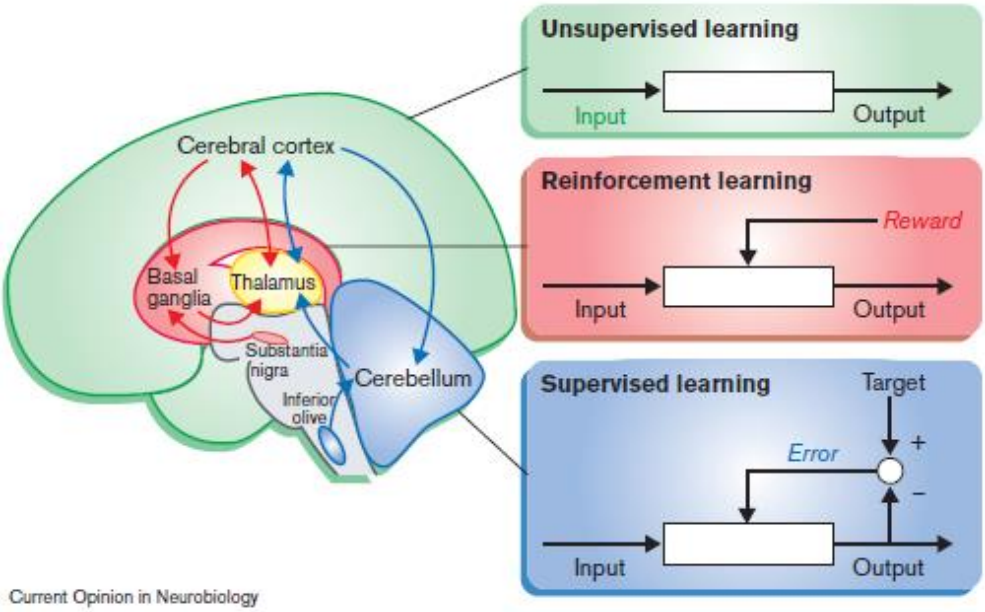

Figure 2.6: The cerebellum is specialized in supervised learning guided by the motor error carried by climbing fibers. The basal ganglia are specialized in reinforcement learning guided by the dopaminergic reward signal. The cerebral cortex is specialized for unsupervised learning guided by the statistical properties of the input signal itself. (Taken from [83])

2.3.1. Experimental rVOR adaptation

The performance of the VOR is characterized by its gain (the ratio between eye velocity and head velocity). In normal subjects, this ratio is almost one. If the VOR is uncalibrated the head movement causes image motion on the retina, resulting in blurred vision. Under such conditions, motor learning adjusts VOR gain to produce more accurate head compensation movement. Such adjustments are needed during life as

neurons and muscles develop or weaken, or for example, when a new pair of eyeglasses changes the magnification of the visual field.

Adaptive control of the VOR can be investigated in the laboratory in normal subjects and in animals by inducing artificial motion of images on the retina during head rotations. In humans, a number of rVOR adaptation studies [89] have shown the ability to recalibrate the reflex using vision, i.e. by coupling head motion with image motion to generate a velocity error signal (*retinal slip*). Image motion on the retina is a robust adaptive stimulus and depending on the direction of target motion relative to head motion, the gain of the VOR can be induced to increase or decrease. Image motion in the same direction of head rotation generates a decrease in VOR gain (gain-down stimulus), while image motion in the opposite direction of head rotation produces an increase in VOR gain (gain-up stimulus).

In pioneering studies magnifying lenses [90] and inverting prisms [91] have been used to elicit long-term adaptation. These experiments investigated plastic changes in the VOR consequent to optical reversal of vision during free head movements (horizontal reversal of VOR was produced by head-mounted dove prisms).

However, VOR adaptation can be elicited in the laboratory using artificially induced retinal slip (using a pattern target motion) during rotation of the head, from minutes to hours [92]. Traditionally, rVOR gain adaptation studies have been performed during passive, low-frequency, sinusoidal head rotations. On the other hand, recent human studies have explored gain adaptation of the rVOR during both self-generated and manually delivered passive, head-only impulsive rotations (e.g. high velocity yaw head rotations), which represent a more ecological stimulus than single frequency sinusoids [93].

Retinal slip is the most effective means to stimulate VOR adaptation, however, other error signals can also contribute: position error signals [94] (without retinal image motion), imagined motion of the target in darkness [95], strobe-light [96].

2.3.2. The role of the cerebellum in motor learning

Motor learning is mediated by plasticity mechanisms in the cerebellum. Starting from the description of cerebellar electrophysiology, the "cerebellar algorithm" was presented in the form of a microcircuit model by Marr [97] and Albus [98]. *Mossy fibers* provide sensory and motor input to the cerebellum, while *Purkinje* cells provide the sole output of cerebellar cortex. The mossy fibers inputs are connected to Purkinje cell output through *Granule* cells, as well as by inhibitory interneurons. Over a hundred thousand granule cell axons (*Parallel fibers*) project onto one single Purkinje cell (Figure 2.7 A). The Marr-Albus model proposes that changes in the strengths of Parallel fibers/ Purkinje cells connections store stimulus-response associations by linking inputs with appropriate motor outputs [19], [99].

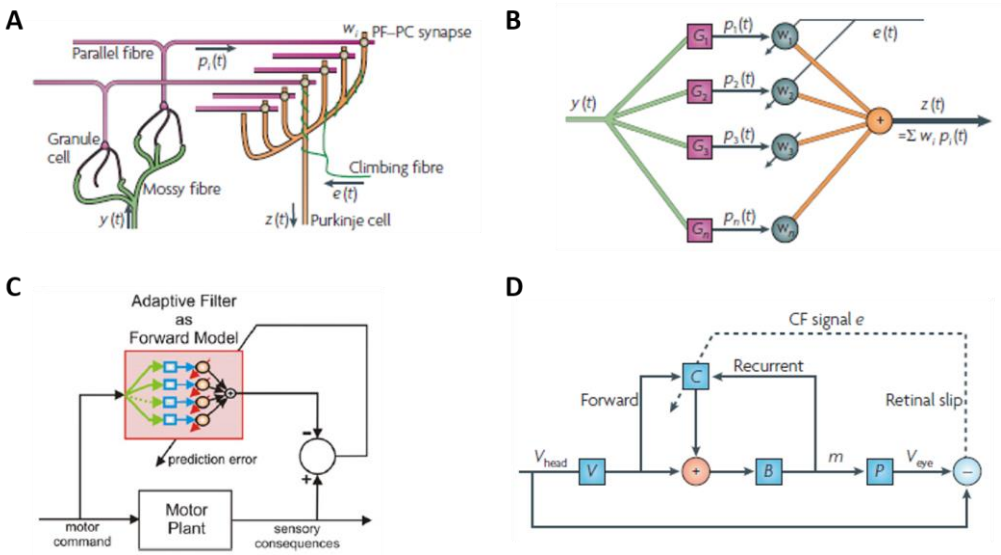

Figure 2.7 A) Simplified cerebellar microcircuit (Marr-Albus-Ito): A mossy fiber input signal is distributed over many granule cells and sent to Purkinje cells (PC) via parallel fibers (PF). Climbing fibers alter the strength of PF-PC synapses. B) The structure of the microcircuit implemented with the adaptive filter. D) Forward model architecture for the VOR adaptation (C=cerebellum, B= brainstem, P=motor plant, V=vestibular input from SCCs). (A, B, D taken from [99]; C taken from [100]).

Ito [101], [102] proposed an implementation of the Marr-Albus model in which the learned changes in the VOR are stored in the cerebellum. More precisely, Ito proposed that the *Climbing fibers* carry the error signal (retinal slip) as instructive signal that alters the weight between Parallel/Purkinje cells connections, encoding the motor memory for the adapted VOR. In 1982, Fujita [103] modeled this framework using the algorithm of the adaptive filter (Figure 2.7 B). A number of inputs ($u_{1\ldots N}$) are passed through a fixed filter G_i to produce the signals p_i which are combined with weights w_i to produce the output:

$$p_i = G[u_1 \ldots\ldots u_N]; \tag{13}$$

$$z(t) = \sum w_i\, p_i(t). \tag{14}$$

The weights w are not pre-calculated but change to improve the filter performance using the learning rule:

$$\delta w_i = -\beta\langle e(t) p_i(t)\rangle; \tag{15}$$

were β is a positive learning rate parameter and $e(t)$ is the teaching signal.

The adaptive filter can implement general concepts expressed before (internal models, Smith predictor, Kalman filter for state estimation and the

feedback-error-learning scheme for adaptive control [100]). Figure 2.7 B-C shows the implementation of the forward model that learns a model of the plant using an efference copy of the command and the difference between predicted and actual movement as teaching error signal. This architecture can implement horizontal VOR adaptation [104] (Figure 2.7 D): the direct pathway through the brainstem (B) is supplemented by the forward model in the floccular region in the cerebellum (C) that carries vestibular information (from V) and a motor efference copy (sent to the plant P). The retinal slip is the teaching error of the adaptive filter.

An alternative to Ito's hypothesis was proposed by Miles & Lisbeger [105]. They proposed that the role of the cerebellum is not to store motor memory but to compute instructive signals guiding plasticity: adaptation is implemented via Purkinje cells synapses onto floccular target neurons in the vestibular nuclei. Thus, altered Purkinje cells responses after adaptation are considered as being produced by the altered efference copy of the eye movement command carried by the mossy fibers.

These two hypotheses propose different sites of plasticity, different instructive signals and different explanations for the altered activity of Purkinje cells during adaptation. Experimental tests provide support for or against each theory [19].

2.3.3. Multiple plasticity mechanism in VOR motor learning

Neither the Marr-Albus-Ito model nor Miles-Lisberger model can account for all the experimental studies in literature. One possibility is that both mechanisms contribute to VOR adaptation. Multiple plasticity mechanisms can mediate consolidation of memory maintaining motor memories over different timescales. Thus, the role of the cerebellum may change with time and the consolidation of memory may redistribute the information to other brain areas. The storage of motor memory may initially depend on the cerebellum while long-term memory may be stored to other brain areas [19].

In addition to the temporal consolidation of motor memory also the direction of the adaptation (increase vs. decrease) suggests the existence of multiple plasticity mechanisms. The Marr-Albus-Ito model considers adaptation in both directions to occur through the same plasticity mechanism. In contrast, studies on directionality of adaptation showed different behaviors for gain increase and decrease in both the VOR [106] and the saccadic system [85], suggesting the existence of different plasticity mechanisms. Increases in VOR gain passively decay more rapidly than decreases. An increase in VOR gain can be actively reversed more rapidly than decrease [106]. Increases in VOR gain generalize less than decreases when tested in a different context (velocity or frequency) than that used for training. However, lesions of the cerebellum have similar effects on both gain-up and gain-down adaptation, going against the

hypothesis that memories for increase and decrease are stored in different areas of the brain.

Another possible solution is that gain increase and decrease could be mediated by different synaptic changes that asymmetrically cancel each other [106]: a model with complementary plasticity mechanisms (long term potentiation/depression, LTP/LTD) operating at each synapse. In terms of Boolean logic, LTD is introduced when parallel AND climbing fibers occur simultaneously, while LTP is introduced when parallel AND NOT climbing fibers activity occurs [19]. Moreover, in vitro, parallel fibers express two forms of LTP (both in absence of climbing fiber activity), one expressed presynaptically and one postsynaptically. Boyden & Raymond [106] hypothesized that postsynaptic LTD contributes to gain increase and could be fully reversed by postsynaptic LTP induced by gain decrease; on the other hand presynaptic LTP contributing to gain decrease can't be reversed by postsynaptic LTD induced by gain increase. As a result, gain increase is fully reversed by gain decrease, while gain decrease is harder to reverse by gain up training.

Thus, for a simple cerebellum-dependent motor task (VOR learning) has been shown that behavioral change are implemented at neuronal level by different plasticity mechanisms, moreover other brain areas may contribute as well [19].

2.3.4. Multiple timescales of memory

Behavioral studies on short term motor learning in higher-level movements (saccadic and reaching) suggested that motor adaptation depends on at least two distinct neural systems that have different sensitivity to error and retain information at different timescales [87]. These processes have been modeled with LTI (linear time invariant) state space models with multiple timescales.

2.3.4.1. Storage of learning memory

Different processes act in short-term motor learning, within timescales of minutes; the existence of these processes characterizes two fundamental properties of motor memory that allow the storage of learning history: *savings* and *spontaneous recovery*.

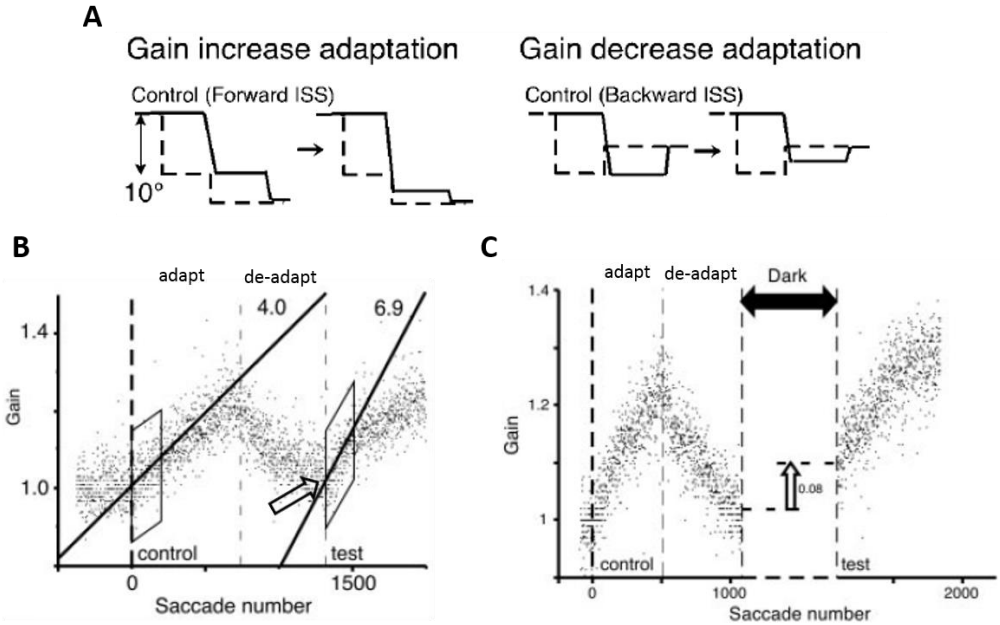

Figure 2.8 A) Double step paradigm for saccade gain adaptation: the target (dotted line) jumps in eccentric position, as the eye (black solid line) moves the target shifts backward or forward, causing a corrective saccade after the primary movement. After the repetition of the paradigm, the primary saccades increase or decrease to compensate the jump. B) Gain change profile in gain increase adaptation. The linear regression fits the first 150 trials. The slope of test adaptation is higher indicating a faster relearning. C) After a re-adaptation period, the monkey is left in darkness for thirty minutes. Test adaptation starts with a gain that is higher than the gain at recovery end; arrow indicates the entity of the jump. Taken from [107].

In 2004 Kojima and colleagues [107] inspected these processes on saccadic adaptation. During saccades visual feedback is not available, thus the gain (saccade amplitude divided by target eccentricity) is recalibrated by learning mechanisms. In laboratory saccadic adaptation can be artificially induced using the double-step paradigm [108]: the target is shown in eccentric position and as soon as the eyes start moving it jumps forward or backward (Figure 2.8 A) without the subject or animal being aware of the jump. At the end of the movement, the position error elicits a corrective saccade. With the repetition of the paradigm, the brain learns to make adapted saccades going directly on the shifted target.

Kojima and colleagues initially trained the monkeys on the gain-up task; they then followed this training with a gain-down task. This is called *extinction* because the goal is to bring back the initial adaptation to the baseline. They observed that after the extinction period the gain of the monkey comes back to baseline (i.e. gain of one; arrow in Figure 2.8 B). The question posed by the authors was if the reverse adaptation cancelled motor memory acquired in the first training. To answer this question, they exposed again (after extinction period) the monkeys to gain up training observing that the animals relearned faster (Figure 2.8 B). This faster

relearning is evidence of *savings* i.e. the fact that despite return of the behavior to the baseline, some components of the memory remember the earlier gain-up training, producing faster relearning.

Moreover, in another set of experiments the authors after the extinction period left the monkeys in a dark room for thirty minutes (the animal makes saccades but has no visual feedback information). When they retested the animals with the gain-up paradigm, they observed a sudden increase of the gain (arrow in Figure 2.8 C). This is an example of *spontaneous recovery*, which suggests that errors that reverse the direction of learning produce a new memory that competes with the original adaptation memory. With the passage of time after extinction, the memory expressed during the initial training spontaneously recovers if no feedback error drives adaptation (e.g. monkeys left in a dark room).

2.3.4.2. Two States Model of learning

In 2006 Smith and colleagues [87] proposed a simple mathematical model to account for spontaneous recovery and savings in the context of saccade gain adaptation. The idea is to represent learning as a problem of state estimation in which there are two hidden states, one that is highly sensitive to error but has poor retention and another that is poorly responsive to error but has strong retention [44].

For each trial of adaptation *n* the motor output (i.e. the learner behavior) *y* is the sum of two hidden states (x_f, x_s). Each state is affected by the error at the end of the movement *e* (the difference between perturbation *f* and motor output *y*) and the passage of time between trials:

$$y(n) = x_f(n) + x_s(n); \tag{16}$$

$$e(n) = f(n) - y(n); \tag{17}$$

$$x_f(n+1) = a_f * x_f(n) + b_f * e_m(n); \tag{18}$$

$$x_s(n+1) = a_s * x_s(n) + b_s * e_m(n). \tag{19}$$

Both the states learn from the error, but from one trial to the next partially forget what they have learned. The retention at each trial is tuned by the parameter *a*, while sensitivity to error, or learning rate, by the parameter *b*. The fast state learning rate is larger than slow state one; the fast system retention rate is smaller than the slow system one:

$$0 < a_f < a_s < 1;\ \ 0 < b_s < b_f < 1. \tag{20}$$

Figure 2.9 (A-E) shows the model simulations for the experiment of savings and Figure 2.9 (F-H) shows those for spontaneous recovery, both for a single state model and the two-state model. At the onset of adaptation

the errors are large causing rapid changes in the fast state x_f. As the training continues, errors decrease, thus in the fast state the forgetting term becomes relatively more important. As a result at the end of adaptation most of the motor adaptation is due to the slow state x_s. When the perturbation is reversed, errors are once again very large, causing a rapid change in the fast state, but not in the slow one. At the end of the de-adaptation, the motor output y is at baseline because fast and slow states are in competition, effectively cancelling each other. In the experiment of relearning the system relearns faster (showing savings) because the slow state retains the memory of the first adaptation. In the spontaneous recovery experiment, when the monkeys are in darkness (Figure 2.8 C), they have no sensory feedback thus the evolution of the hidden states is only due to forgetting terms (which is equivalent to setting the error to zero in Eq. 18-19). During this period, the fast state decays quickly, while this process is slower for the slow state. The increased gain at the beginning of relearning is thus due to spontaneous forgetting of the fast state. Simulations in Figure 2.9 show that only multi rate models can account for these memory processes.

During the darkness period, however, it is not possible to measure motor output and thus to test the prediction of the model (Figure 2.8 C). These predictions can be tested using the *error-clamp* (or *catch-trial* paradigm). In the saccadic context, an error clamp trial starts with a visual feedback, and as soon as the saccade begins, the target is turned off. After completion of the saccade the target reappears at the current location of fixation, cancelling any endpoint error [109] (in the catch paradigm the target remains turned off). An error clamp paradigm has also been proposed in the context of reaching and pointing. We will introduce our version of paradigm for VOR adaptation in Chapter 3. Thus, the error-clamp and catch trials allow measuring the evolution of motor output in the absence of feedback error. Figure 2.9 I-M shows the model prediction of the evolution of motor memory in the absence of feedback error in saccadic adaptation. At the end of nine blocks of gain down adaptation trials the motor output is mainly due to the slow state. In the block of reversal adaptation the fast state reacts and the gain returns near the baseline (the two states cancel each other). In the final set of error-clamp trials, as shown by experimental results, the model correctly predicts that the gain spontaneously recovers toward the previously adapted low gain, retained by the slow state.

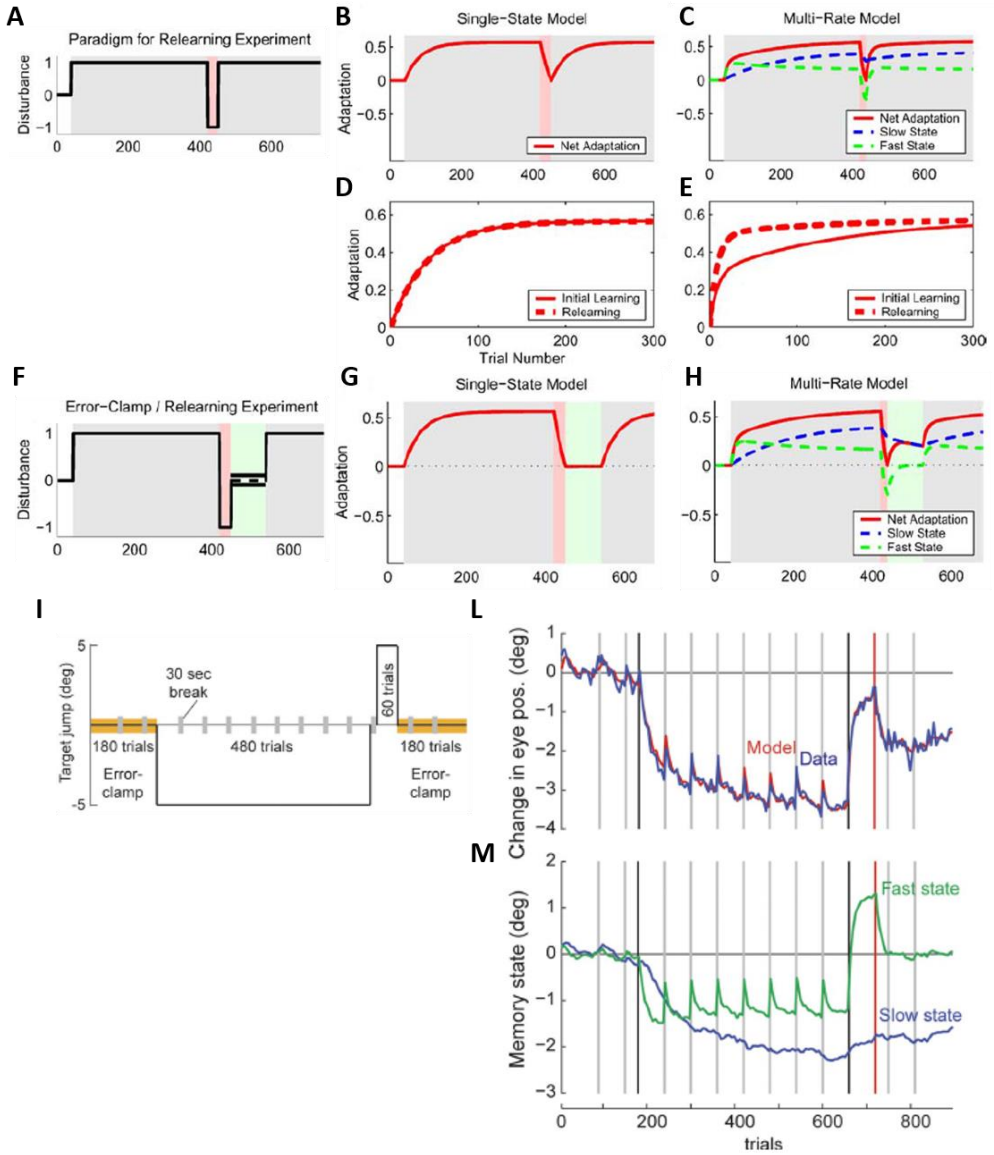

Figure 2.9: A-E) Savings experiments simulations: the perturbation is shown in A; there are an initial gain-up adaptation, a short period of reversal adaptation, and a relearning block. At the end of reversal adaptation the motor response (red line) comes back to baseline. The relearning is faster in E because the slow state (blue line) retains memory of initial adaptation. The single state model can't predict savings B,D. Taken from [87]. F-H) Spontaneous recovery simulations (perturbation in F): at the end of reversal adaptation the motor response (red line) comes back to baseline. After the period of error-clamp trials (no feedback error), the gain suddenly increases starting from the slow state level. The single state model can't predict spontaneous recovery in F. Taken from [87]. I-M) Model predictions on real saccadic adaptation data (perturbation in I): in the reversal adaptation block the gain comes back to baseline because the two states cancel each other. In the error-clamp trials the gain spontaneously recovers toward the slow state level. Taken from [109].

2.3.4.3. Nonlinear interactions and protection of motor memory

The linear two states model described above predicts complete unlearning if the de-adaptation period is as long as the adaptation period. Recent works nonetheless showed that savings can occur also after complete washout [110]–[112]. Moreover, adaptation is more rapid and complete when subjects are re-exposed to the same perturbation after an interval of hours or days [113] (thus the processes in Eq. 18-19 are back to baseline). This suggests that adaptation involves other phenomena.

A typical experiment for investigating these issues consists in exposing the subject to a perturbation A and then to a perturbation B (over an equal number of trials): the question is whether the learning in B destroys the motor memory of A. The paradigm task ABA (re-exposition to A after B) has been extensively studied to understand motor consolidation and interference of motor memory. Interference is *retrograde* when task B interferes whit the previous learning of task A. Interference is *anterograde* when performance in B (preceded by A) is worse than naive. Krakauer and colleagues [111] showed that in the ABA task the relearning of A is faster only under some conditions, such as the amount of time between initial adaptation and de-adaptation. The authors concluded that the inexpression of savings is not due to the destruction of the earlier memory but an inability to express that memory. Thus, memory acquired during adaptation may be protected during de-adaptation and re-expressed. Zarahn and colleagues [110] showed that savings can occur after complete washout, modeling this effect with a nonlinear state-space model in which the parameters a and b in Eq. 18-19 change across the phases of the adaptation experiments. Such change of the model parameters during learning corresponds to *metalearning*.

Another characteristic of adaptation is context specificity. VOR adaptation, for example, depends on the tilt angle respect to the gravity or on the frequency of the head movement [19]; saccadic adaptation depends on saccade direction, amplitude and initial eye position [85]. Moreover, in different contextual cues two opposite perturbations [114] can be learned simultaneously .

Lee and Schweighofer [115] proposed a model of adaptation composed by a single fast adaptive state and multiple slow adaptive states selected based on the context. This model predicts protection of memory of the slow state by contextual cues, while the fast state is completely erasable explaining anterograde interference (task B is worse than naïve because the fast state is adapted in opposite direction by the previous task A).

On the other hand, the recall of motor memory may be due to model-free learning process (reinforcement) regardless the updating of an internal model [88]. Thus, an error based LTI state space model may capture short-term cerebellar adaptation in which an internal model is incrementally updated to reflect the new dynamics (i.e. update the parameters of a forward model), while the deviation from LTI models (i.e. protection and

consolidation of memory) represent an additional learning process (not necessary error based) [88], [116].

2.3.4.4. Credit assignment

Many studies showed several differences in the adaptation process depending on whether the perturbation is introduced suddenly or gradually. During reaching in a force field a gradual error condition produces an update of the representation of the arm dynamics, thus adaptation of the right arm does not generalize to the left arm (subjects update the internal model of the right arm) [117]. An abrupt error condition produces an update of the representation of the dynamics of the tool (i.e. the robot), thus adaptation transfers from left to right arm (subjects learn an internal model of the tool) [118]. Moreover, gradual perturbation reduces the decay rate of the acquired memory (i.e. stronger retention) [119], [120].

These results are related to how the CNS assigns the origin of the causes of errors: a change in the dynamics of the body or a change in the context. A possible explanation is that the brain may assign larger errors to an internal model of the context [121], [122]. These results have been formalized in a Bayesian model in which the allocation of the credit to internal or external causes depends on both prior experience and on the source that is most consistent with the perturbation [123].

Thus, the brain estimates the relevance of the error in assessing its motor performance and adapts strongly only to errors due to motor causes, thus the adaptation is a nonlinear function of error size [124].

Chapter 3

Multiple timescales in the adaptation of the rotational VOR

Goal directed movements such as pointing and saccades have been shown to share similar neural architectures in spite of the different neuromuscular systems producing them. As explained in Chapter 2.1 such structure involves an inverse model of the actuator being controlled, which produces the commands innervating the muscles, and a forward model of the actuator, which predicts the sensory consequences of such commands and allows online corrections of ongoing movements. Recent studies have shown that goal directed movements also share similar motor learning and motor memory mechanisms, which are based on multiple timescales (see Chapter 2.3.4). The hypothesis that also a reflex movement such as the rotational vestibulo-ocular reflex (rVOR) may be based on a similar architecture exploiting internal models has recently been presented. Investigating the mechanism governing motor learning in rVOR adaptation could provide further evidence for such hypothesis. We hypothesize that multiple timescales are the brain's solution to the plasticity-stability dilemma, allowing it to adapt to temporary and sudden changes, while keeping stable motor control abilities. If that was the case, then we would expect also the adaptation of reflex movements to follow the same principles. We thus studied rVOR gain adaptation in eight healthy human subjects using a custom paradigm aimed at investigating the existence of a spontaneous recovery phenomenon, which we considered as the hallmark of multiple timescales in motor learning. We thus developed a mathematical model of rVOR adaptation based on two hidden state processes, which adapts the cerebellar forward model of the ocular motor plant and show that it accurately simulates our experimental data on rVOR gain adaptation, while a single timescale learning process fails to do so.

This chapter reports the study under second review submitted to Journal of Neurophysiology.

3.1. Overview

Research on how the brain produces precise and rapid goal directed movements in spite of the variability of both internal and external factors has made great progress over the past 20 years. How do we learn to control reaching movements e.g. while turning or under the water? How does the brain cope with muscle fatigue and ageing? The neural mechanisms producing movements are constantly monitored in terms of their performance; motor learning is the process that tunes their synaptic weights to keep actions quick and accurate (see Chapter 2.3). A key concept in the current understanding of motor control principles is that of an internal model, i.e. a neural mechanism that can mimic the input-output characteristics of an actuator, or its inverse [125]. Indeed, several studies have shown that goal directed movements, such as pointing and reaching movements or saccades, share a similar control structure based on the involvement of at least two internal models: an inverse internal model of the actuator being controlled [126], [127], which produces the appropriate commands once the motor plan has been chosen, and a forward internal model predicting the sensory consequences of such commands prior to the availability of sensory feedback and providing the basis for state estimation [128], [129]. Such forward models were hypothesized to lie in the cerebellar cortex [130] and to be fed by an efference copy of the motor command, i.e. the output of the inverse model, to predict the sensory consequences of a movement before sensory feedback is available and thus allow its online correction in case of a discrepancy with the desired movement (see Chapter 2.1). These theories, although mainly developed in studies of upper limb movements in time-varying force fields, found neurophysiological grounds only when considered in the domain of eye movements [50], [55].

Indeed, although the term internal model had not yet been introduced, studies on the VOR frequency response led David A. Robinson and colleagues to the hypothesis that the sum of weighted direct and integrator pathways acts as an inverse model of the eye plant dynamics and is used to transform the desired action into the corresponding motor command [25], [131]. Recent neurophysiological studies have shown that burst-tonic/tonic neurons in the nucleus prepositus hypoglossi (commonly referred to as PH-BT cells) encode and relay an efference copy of the motor command, i.e. the output of the inverse model [57], thus confirming the early hypotheses (see Chapter 2.1.1). Also the existence of a forward model in a cerebellar feedback loop was suggested by Robinson and colleagues in the context of the saccadic mechanism: the ability, found in two patients with spinocerebellar degeneration showing slow saccades, to reverse these saccades in midflight led to hypothesizing the existence of a local feedback loop in the cerebellum [132], later perfected by Jürgens and colleagues with the concept of a resettable integrator [133]. This integrator is fed with an efference copy of the command to the ocular motor plant and produces

an internal estimate of eye displacement allowing saccades to precisely stop on target despite that they are usually over by the time visual feedback is available (see [134] for a review). Several recent studies have explicitly hypothesized the existence of a forward model of the ocular motor plant in the cerebellar flocculus [50], [55], [57], [59] emphasizing that the organization of the vestibulo-ocular system may be similar to that proposed for the control of goal directed movements.

More recently, several studies on motor adaptation in response to external perturbations such as force fields affecting arm movements or target shifts in the context of saccadic eye movements, have shown that motor memory of goal directed movements evolves through at least two processes with different time scales, establishing a continuum between short-term, i.e. in the order of hours or less [87], [107], and long-term, i.e. in the order of days, adaptation [123], [135]. The model proposed by Smith et colleagues [87] is based on two hidden states, a fast one that learns quickly from motor error but has poor retention and a slow one that learns slowly but has stronger retention (see Chapter 2.3.4.2). Such approach can account for different adaptation phenomena, such as saving, i.e. a faster re-learning of the same task after the first adaptation, and spontaneous recovery, i.e. the re-emergence of a previously learned adapted state after its extinction [136]. Motor learning probably includes several timescales with time constants ranging from minutes to days and longer [137], which explains the way the brain learns new behaviors and calibrates reflexive movements. Multiple timescales thus appear to be a constant characteristic of adaptive processes involving voluntary movements. Our study thus aimed at investigating whether the VOR shares such learning principles with goal directed movements, in order to understand whether the hypothesis that the rVOR shares the organization of volitional movements [50] also extends to sharing similar adaptation processes.

Despite several studies that account for adaptation in saccadic and in reaching movements with multiple time scales of memory, little is known about these processes in the adaptation of reflex movements in humans, such as the rVOR. Moreover the existence of multiple plasticity mechanisms in the adaptation of the horizontal rVOR was shown in mice by testing the interaction [138] and the generalization [138] (in mice and in monkey) of both gain increase and gain decrease adaptation.

The vestibulo-ocular reflex (VOR) is a phylogenetically old reflex that uses head velocity information transduced by the semicircular canals to drive the movement of the eyes in order to maintain a stable gaze, and hence clear vision, during head movements (see Chapter 1). Its neural circuitry comprises a classic three-neuron arc with vestibular afferents projecting to the vestibular nuclei, which in turn project to the abducens nuclei innervating the lateral recti, and a side circuit involving the cerebellum receiving input from mossy fibers and exerting an inhibitory action on floccular target neurons (FTN) in the vestibular nuclei, which in turn project to ocular motor neurons [139] through Purkinje cells. The VOR is a very short latency (7-10ms) reflex, a characteristic that makes it the

best tool available to the brain to respond to head movement perturbations. Such timing, nonetheless, is too brief to use visual feedback to correct for errors in performance at least during the first 100 ms after the beginning of the head movement [140]–[142]. Thus, the VOR operates as an open loop control system at least during such initial part of the response, so that adaptive process are required to consistently keep the VOR calibrated.

In humans, a number of rVOR adaptation studies (see Chapter 2.3.1) have shown the ability to recalibrate the reflex using vision, i.e. by coupling head motion with target motion to generate a velocity error signal (retinal slip). Retinal slip is a strong adaptive stimulus, demonstrated for instance by the pioneering studies on long-term adaptation by Gauthier and Robinson [90] who used magnifying lenses and those by Gonshor and Melvill Jones [91] who used inverting prisms. However, other error signals, such as position errors [94], can also be used to induce adaptation of the rVOR.

Traditionally, rVOR gain adaptation studies have been performed during passive, low-frequency, sinusoidal head rotations, as in most studies carried out in the 1970s and 1980s. On the other hand recent human studies have explored gain adaptation of the rVOR during both self-generated and manually delivered passive head-only impulsive rotations (high velocity yaw head rotations), which represent a more physiological stimulus than single frequency sinusoids. These studies have shown that the rVOR can be efficiently adapted using a retinal velocity error (retinal slip) signal with a gradually increasing adaptive demand [93], [143]. Similarly, Zhou and colleagues showed the efficacy of brief passive head translations toward the adaptation of translational VOR in monkeys [144].

Being easily adaptable the VOR has been long considered as a model system for motor adaptation and the first hypotheses on the involvement of cerebellar control in the long-term adaptation of the rVOR date back to the early 1970s [145]. The cerebellar flocculus is necessary for learning in gain adaptation of the rVOR [146], [147] and recent evidence in cats and monkeys has shown that early (short-term) and late (long-term) motor memories are stored at different loci: the floccular complex and the brainstem nuclei, respectively [148], [149] (see Chapter 2.3.2).

The main purpose of this study was to understand whether multiple timescales exist also in human rVOR adaptation and thereby provide further evidence to support the hypothesis that reflex movements are not only controlled by the brain using the same approach as with goal directed movements, but also their learning mechanism is similar. We therefore chose to study whether short-term gain-down rVOR adaptation followed by a shorter gain-up de-adaptation would give rise to spontaneous recovery when movements are performed without visual feedback. We thus used catch-trials in which the visual stimulus is turned off as soon as the movement starts to observe whether rVOR gain reverted to a previously learned low-gain state. We then modeled motor memory in the VOR as a two hidden states model learning the parameters of the cerebellar forward

model of the ocular motor plant and studied whether it could explain our experimental data, also in comparison to a single hidden state model.

3.2. Materials and Methods

3.2.1. Subjects and experimental paradigm

Subjects: We recorded 8 healthy human subjects (7 males, 1 female: mean age=37 SD=9.8) at the Department of Neurology, University Hospital Zurich, Switzerland. Participation in this study was voluntary and all subjects signed a written consent form prior to taking part in the study; the experimental protocol was approved by the local ethics committee.

Vestibular stimulation: rotational stimuli were delivered in complete darkness by a three-axis rotational stimulator driven by three servo-controlled motorized axes (Acutronic, Switzerland), controlled with Acutrol software and hardware, and interfaced with LabVIEW software. Subjects were comfortably seated in a chair so that the center of the head was positioned at the center of rotations, in order to obtain purely rotational stimuli. Individually adjusted masks, made of a thermoplastic material, were molded to the contour of the head after warming, with openings in the mask made for the eyes, video-oculography system and mouth. The mask was attached to the back of the chair, and restricted head movements very effectively without causing discomfort. Rotational stimuli consisted of 120 ms of constant acceleration at 460 deg/s^2 immediately followed by a symmetric deceleration interval, resulting in a peak head velocity of about 100 deg/s and an overall rotation of about 20 deg (Figure 3.1 D). Subjects were instructed to hold their gaze on a projected laser dot or, during catch trials, on the location they remembered the laser dot at. Each stimulus lasted 5.42 seconds: 3 seconds of rest (composed by 1 second in darkness, a 1.5 seconds flash of a lateral white LED lamp aimed at the eyes of the subject to limit dark adaptation and 0.5 seconds with the laser on); 0.42 seconds of chair rotation; 2 seconds to reposition the chair and bring it back to the start position.

Laser projection: We used a red laser and real-time 2D mirror deflection system for displaying a 2 cm diameter visual target on a curved isovergence projection screen at 140 cm in front of the subject. Laser position was controlled using on-line horizontal position of the chair.

We considered three types of trials: 1) Space Fixed trials aimed at assessing rVOR in normal visuo-vestibular interaction conditions, 2) Catch trials for assessing rVOR gain in the absence of visual feedback and 3) Adaptation Stimulus trials for inducing gain adaptation. During these different types of trials, the visual stimulus behaved as follows.

Space fixed (SF): the laser dot turned on 0.5 s before the beginning of chair rotation in the straight ahead position and remained fixed in space for the entire rotation duration, asking for a ideal rVOR gain of ~1 (Figure 3.1 A).

Catch Trial (CH): the laser dot turned on 0.5 s before chair rotation in straight ahead position, turned off when the chair started rotating, and stayed off until the following trial. Thus, this condition provided no error feedback, with the following visual target being displayed only after chair repositioning (Figure 3.1 A).

Adaptation stimulus (AS): the laser dot turned on 0.5 s before chair rotation in the straight-ahead position and moved during the rotation with a percentage of the chair velocity, depending on the planned adaptation requirement (Figure 3.1 D). If the target moved in the direction of head rotation, its fixation requires rVOR gain reduction, while a movement in the opposite direction asks for rVOR gain enhancement (Figure 3.1 A). In this study we induced short-term adaptation of the rVOR using a gradually increasing target movement and hence rVOR gain adaptation request [93]. Such approach was chosen both to avoid subjects' awareness of the target movement manipulation and to adopt a paradigm that would more likely induce adaptation of the reflex, based on literature results. Thus, during such adaptation trials the visual stimulus behavior, i.e. the coefficient determining the laser movement as a fraction of the head movement, was gradually and progressively changed to induce an increasing retinal slip either for gain reduction or for gain increase.

Experimental paradigm: The overall experimental paradigm (shown in Figure 3.1 B) was then organized as follows: rVOR gain was first assessed with a block of 20 SF trials (i.e. rVOR gain request of 1) followed by a block of 20 CH trials. These were followed by one block of 150 AS trials asking for a decrease in rVOR gain from 1.0 to 0.6, i.e. the target movement was a fraction of the chair movement that increased by about 0.0027 (0.27%) on each trial, and a last block of 50 trials constantly asking for a gain of 0.6 (40% reduction, see dashed line in Figure 3.2 A). Subjects then underwent a block of 70 AS trials of reversed, i.e. gain-up, incremental adaptation asking for an increase in rVOR from 1.0 to 1.2, i.e. the target moved opposite the chair increasing its velocity by about 0.0028 (0.28%) of chair velocity at each trial. A final block of 80 CH trials was then supplied to evaluate whether spontaneous recovery of motor memory occurred.

Control paradigm (CHcontrol): after at least one month, six of the original eight subjects were recorded again in a protocol consisting in 20 SF trials and 80 CH trials, without previous adaptation stimuli. Such paradigm was aimed at verifying whether the block of catch trials per se induced any rVOR gain reduction.

3.2.2. Data acquisition and analysis

Data Acquisition: horizontal and vertical right eye position was measured using the EyeSeeCam infrared video system (sampling rate 220 Hz). Head angular velocity was measured using the EyeSeeCam three-axis IMU sensor. Target position and chair position signals were recorded at 220 Hz with 16 bits resolution through a NI USB-6211 DAQ system. All data were acquired and synchronized by the EyeSeeCam System software and saved in Matlab format for offline analysis. A fifteen-point grid (from -20° to +20° with a 10° step on the horizontal axis, from -10° to +10° with a 10° step on the vertical axis) shown on the isovergence projection screen was used to calibrate eye position. To limit dark adaptation and avoid the risk of loosing the tracking of the eye due to excessive pupil dilation, the recorded eye was briefly (1.5 s) illuminated using a white light from a battery of LEDs, lying outside the subject's field of view, at the beginning of each trial. Such technique was efficient in limiting the size of the pupil during the head movement and in allowing its proper tracking.

Data Analysis: data were analyzed off-line using Matlab (Mathworks Inc., Natick, MA) custom developed software [150]. Raw eye position was calibrated using a second order polynomial fit and filtered using a second order Butterworth low-pass filter (30 Hz cutoff frequency). Eye velocity data were calculated using the Savitzky-Golay four point derivative filter (Ramat et al., 1999). Onset of each head movement was found using a fitting curve composed of a constant value and a quadratic function, and all trials were aligned based on such instant in time [151].

We have chosen to analyze the gain of rVOR responses around 100 ms from head onset, thus measuring the open loop response of the rVOR, before the availability of visual feedback. Any trials in which the subject broke fixation or made a saccade within the first 120 ms from the onset of the head movement were manually rejected.

The effect of motor learning was evaluated by computing the adjustment of eye velocity in terms of adaptive change (Adaptation Ratio, AR) with respect to the basal SF trials. AR of the nth trial was thus computed as follows:

$$AR(n) = \frac{VM(n) - VM_p}{VM_p} \quad (1)$$

where VM is the mean eye velocity computed between 80 and 120 ms from head movement onset and VMp is the mean VM assessed in the initial 20 SF trials.

Statistical Analysis: Student's t-test was used to assess the difference between the initial 10 *SF* ((1) in Figure 3.2 A) and the last 10 movements of *AS* ((2) in Figure 3.2 A) to test adaptation; the difference between the initial 10 *SF* ((1) in Figure 3.2 A) and the first 10 movements of reversal

AS ((2) in Figure 3.2 A) to test retention, and the difference between the first 10 reversal *AS* ((3) in Figure 3.2 A) and the last 10 movements of reversal *AS* ((4) in Figure 3.2 A) to test de-adaptation.

To assess *spontaneous recovery* we analyzed the trend of *AR* data relative to the initial 20 *SF* and the final set of 80 *CH* trials of the main and the control experiments (Figure 3.2 C,D). Data were normalized with respect to the initial 20 *SF* trials, then, for each subject, we binned consecutive movements in groups of 10, thus obtaining 10 average values (first two for SF trials, last eight for *CH* trials, Figure 3.2 D). The bins were then compared with a repeated measure ANOVA followed by a multiple comparison correction using Tukey's least significant difference procedure. In analyzing the main experiment data we therefore obtained eight mean values for each bin, corresponding to the eight participants. The comparison of the main and control experiments considered six values for each bin, corresponding to the six subjects who performed both experiments.

A further analysis assessed the gain trend within the first 40 *CH* performed at the end of adaptation and in the control experiment, by testing the correlation of *AR* against the trial number (Figure 3.2 C). The significance of such correlation is reported as an indicator of its reliability. We chose 40 trials because the model predicts a decay of the fast state in 30-35 trials ($5*\tau_f$, see Results section).

Moreover for individual comparisons (Student's t-test) adaptation level was assessed between trials 41-50 ((5) in Figure 3.2 A) and compared with the last 10 movements of reversal *AS* ((4) in Figure 3.2 A).

3.2.3. Mathematical Modeling

Semicircular canals afferents encode head velocity signals representing the vestibular contribution to the desired compensatory eye movement response to head rotation; velocity signals produced by the vestibular nuclei responsible for multisensory integration (see [152] for a review) and velocity storage [20], [23] are conveyed to motoneurons both directly and indirectly via a neural integrator. The parallel pathway model [25], [131] represents an implementation of an inverse dynamic model of the eye plant dynamics. A forward model of the same motor dynamics, possibly lying in the cerebellar flocculus, could be used to compute the predicted sensory consequences of the motor command. The estimated eye velocity may be used to compute the error between predicted and desired action, and such error exploited in a feedback loop to refine the motor command [50], [57], [59], [60] (see Chapter 2.1.2).

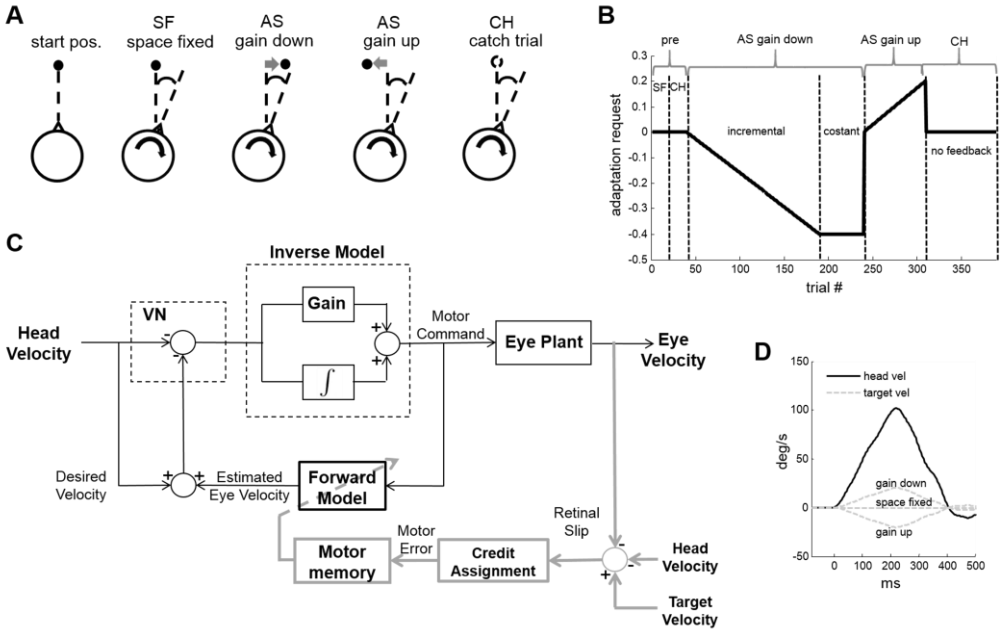

Figure 3.1 A: schematic representation of the visual stimulus during head rotation. In the *SF* stimulus the dot remains fixed in space for the entire rotation duration, in the *CH* stimulus the target turns off when the chair starts rotating and in the *AS* the dot moves during the rotation with a percentage of the chair velocity, depending on the planned adaptation requirement. B) Experimental paradigm: 20 SF and 20 CH stimuli to assess basal condition; 150 AS trials of gradual gain down adaptation; 50 AS trials of constant gain down adaptation; 70 AS trials of gradual gain up adaptation; 80 CH trials. C: block diagram of the rVOR model and its motor learning mechanism (gray lines). Head velocity estimated by the vestibular nuclei is conveyed to motor neurons both directly and indirectly via a neural integrator, forming an inverse model of the ocular motor plant; an efference copy of the innervation sent to the ocular motor nuclei is conveyed from the output of the inverse model to the forward model in the floccular feedback loop to estimate the resulting eye velocity. The latter is then compared to the desired eye velocity to compute the error and refine the motor command. The movement of the target causes retinal slip, and such error is assigned in part to an inaccurate eye movement (a motor error) and in part to world disturbances (an externally caused error) by the Credit Assignment block. Only the part credited to a motor error leads to the recalibration of the forward model of the eye plant. D: head velocity (black solid line), and target velocity (gray dotted line) during chair rotation.

The schematic in Figure 3.1 C shows the proposed rVOR model, based on that proposed by Glasauer [59] and combining it with the proposed motor learning mechanism to the lower right. We modeled the oculomotor plant (the relationship between eye velocity $\dot{E}$ and motoneurons rate M) with a second order linear system with time constants of 224 and 13 ms [153]:

$$\frac{\dot{\mathrm{E}}(\mathrm{s})}{\mathrm{M}(\mathrm{s})} = \frac{\mathrm{s}}{(1 + 0.224\mathrm{s})(1 + 0.013\ \mathrm{s})}. \qquad (2)$$

We converted the transfer function to its state-space form:

$$\dot{x}(t) = Ax(t) + Bu(t); \tag{3}$$

$$y = Cx(t); \tag{4}$$

$$A = \begin{bmatrix} -81.72 & -344.82 \\ 1 & 0 \end{bmatrix}; B = \begin{bmatrix} 1 \\ 0 \end{bmatrix}; C = [344.82 \quad 0]; D = 0. \tag{5}$$

The plant is thus a second order system, so that matrices *A*, *B* and *C* are 2x2, 2x1 and 1x2, respectively (Eq. 5).

To obtain an inverse model of the simplified first order eye plant, which produces the motor command *u(t)*, the gain of the parallel pathway was set to 0.224 s, equal to the dominant eye plant time constant and thus effectively cancelling its pole in the overall transfer function of the final ocular motor pathway [25].

The cerebellar forward model reproduces the dynamics of the ocular motor plant and thus predicts the state of the eye, i.e. its velocity, based on the previous state and the efference copy of the motor command *u(t)*:

$$\hat{x}(t+1) = \hat{A}\hat{x}(t) + \hat{B}u(t); \tag{6}$$

$$\hat{y}(t) = \hat{C}\hat{x}(t). \tag{7}$$

$\hat{A}$, $\hat{B}$ and $\hat{C}$ are estimates of matrices *A*, *B* and *C* in Eq. 3-4. The cerebellar estimate of eye velocity is compared with the desired eye velocity carried by the mossy fibers to estimate an error in the ongoing movement, which is used in a feedback loop to correct the motor command.

We then transformed the model transfer functions (forward and inverse model and plant; in Figure 3.1 C) to discrete time using a time step of 4.5 ms, corresponding to the sampling time of the data acquired through the EyeSeeCam system.

Sensory feedback is computed at the retina in the form of retinal slip (err): the velocity with which the image of the visual target moves on the retina, quickly deteriorating vision, i.e. *err= Tv-Hv-Ev+b*, where *Hv*, *Ev* and *Tv* are the mean over the interval between 80 and 120 ms from chair movement onset of head velocity, eye velocity and target velocity, respectively, and *b* represents a bias, that is the portion of head velocity, measured over the same interval, that is not compensated by the VOR during the initial SF trials [154]. Retinal slip is a strong adaptive stimulus, which induces the brain to modify its motor response to cancel it, and has been frequently used for inducing rVOR adaptation [90], [91]. Recent studies suggest that, depending on the size of the error information, the nervous system assigns the potential cause of an observed error in part to a motor error, i.e. an inaccurate eye movement, and in part to external disturbances, i.e. some change occurred in the external world (see Chapter 2.3.4.4). This process tends to assign small errors as mainly due to internal

causes, i.e. motor error, and, as the size of the error increases, an increasing portion of it is assigned to external causes. Thus, the brain estimates the relevance of the error in its motor performance and adapts strongly only to errors due to motor causes (e_m) [121], [122], [124]. We modeled this *credit assignment* (Figure 3.1 C) problem with a normalized probability of relevance varying with the size of error: the value is 1, i.e. the error is assigned entirely to motor causes, for 0 deg/s of retinal slip disturbance and it decreases with increasing error size. Given a sensory error err the estimate of the corresponding motor error was thus given by:

$$e_m(n) = e^{\frac{-err(n)^2}{2\sigma^2}}; \quad (8)$$

where σ is a parameter to be estimated based on experimental data. When a motor error occurs the brain estimates that the forward model is not accurately reproducing the dynamics of the eye plant. Therefore, during adaptation the motor learning process responds to motor error by updating the estimate $\hat{B}$ modulating the effect of the efference copy of the motor command *u(t)* in the forward model, following the rule $\hat{B}(n+1) = \hat{B}(n) + \delta(n+1)$, where δ is the learning parameter computed by motor learning. The latter was modeled as a two hidden states linear system [87] with one state representing a fast process that adapts quickly but has poor retention and one representing a slow process that learns slowly but has better retention (see Chapter 2.3.4.2). Each state was modeled with a linear differential equation with a learning term and a forgetting term. The update equations were therefore the following:

$$\delta(n) = \delta_f(n) + \delta_s(n); \quad (9)$$

$$\delta_f(n+1) = a_f * \delta_f(n) + b_f * e_m(n); \quad (10)$$

$$\delta_s(n+1) = a_s * \delta_s(n) + b_s * e_m(n). \quad (11)$$

The learning rates for the fast and slow states (δ_f and δ_s, respectively) are $1>b_f>b_s>0$ and their forgetting rates are $1>a_s>a_f>0$.

We then used the model to study the predicted changes in eye velocity caused by the adaptation of the forward model parameters, following an approach similar to that used in the context of saccadic adaptation [109], [122]. We considered that at the beginning of the experiments the system is well calibrated and $\hat{A} = A$, $\hat{B} = B$ and $\hat{C} = C$, i.e. the forward model is a perfect replica of the plant. The learning and forgetting parameters a_s, a_f, b_s, b_f as well as the σ parameter which determines the coefficient of the credit assignment problem were then estimated by minimizing the root mean square error between experimental and simulated *VM* data using a nonlinear least-squares solver (Matlab, Mathworks Inc. Natick, MA).

The goodness of fit of the model simulations was evaluated using the r^2 coefficient of determination. Based on the r^2 statistics we compared these

results with those obtained by following the same fitting procedures and credit assignment function, yet using a single hidden state model for determining the update of $\hat{B}$ in the cerebellar forward model of the plant. In order to assess whether the expected increase in goodness-of-fit related to the use of more model parameters reflected overfitting or a more appropriate model for explaining the data, we compared the two models using the Bayesian Information Criterion (BIC) statistics [155] which, considering that our models were fitted using least squares, can be computed as [156]:

$$\mathrm{BIC} = \mathrm{n} \cdot \ln\left(\widehat{\sigma_e^2}\right) + \mathrm{k} \cdot \ln(\mathrm{n})\,; \tag{12}$$

where n is the number of data points (350 in our case), k is the number of parameters in the model, i.e. 3 for the single hidden state model (a and b in the state space equation and σ in the credit assignment function) and 5 for the two hidden states model (a_s, a_f, b_s, b_f and σ), and $\left(\widehat{\sigma_e^2}\right)$ is the estimate of the variance of the error, computed as the sum of squared errors (residuals) normalized by the number of samples. Using such criterion, which penalizes the increase in the number of variables more than the Akaike criterion does, models with lower BIC are preferable for explaining the observed data.

3.3. Results

3.3.1. Time course of adaptation

We induced rVOR adaptation during passive impulsive whole-body rotations (at constant acceleration) in 8 healthy human subjects, using an incremental velocity error stimulus. As described, we used five sets of stimuli in our experiment: *SF* trials assessing the baseline rVOR gain in natural conditions followed by *CH* to assess gain in the absence of visual feedback. A set of four blocks of *AS* trials inducing gain down rVOR adaptation followed by a set of reversal *AS* trials aimed at rVOR gain up adaptation. In the fifth set of trials we assessed the state of the rVOR gain without introducing visual endpoint error feedback, using *CH* trials. The effect and the course of motor learning was evaluated by computing the change in mean of eye velocity (*VM*) between 80 ms and 120 ms from head movement onset, with respect to the baseline response assessed in the *SF* trials (see Methods).

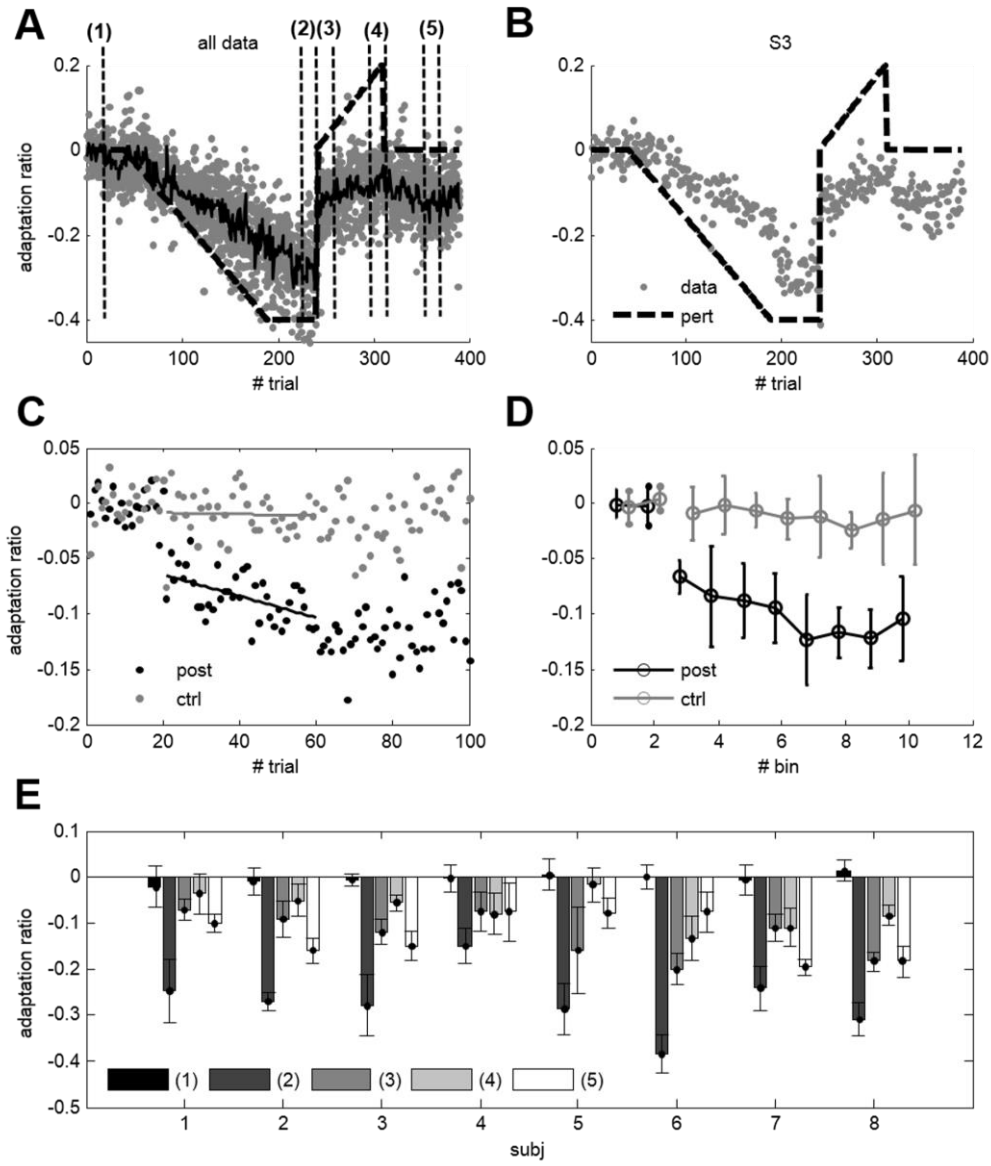

Figure 3.2 A: *adaptation ratio* for all subjects (gray points); black solid line represents the mean *AR* averaged over all subjects at each trial. The labels indicate the group of movement used in statistical analysis and in E: (1) first 10 SF; (2) last 10 AS gain down; (3) first 10 AS gain up; (4) last 10 AS gain up; (5) from 41 to 50 CH. B: *adaptation ratio* for one representative subject (S3). C, D: Comparison of catch trials recorded during the main experiment and in the control experiment. C: Mean data over all subjects in the main and the control experiments, and linear regression of the first 60 *CH*. D: Each data point represents the mean together with the standard deviation of the six values obtained by averaging 10 consecutive movements for each subject. The first 2 values are referred to *SF* trials, the last 8 to *CH* trials. One way ANOVA does not reveal any significant difference for CHcontrol (gray line). *CH* after adaptation (black line) are significantly lower than *SF*, and post hoc analysis reveals a statistically significant difference between the first bin of *CH* (group 3) and the last four bins ($p<0.001$ for bins7, 8, 9 and $p<0.05$ for 10). E: *adaptation ratio* for the movements labeled in A. Bar plots represent the mean and standard deviation of *AR* for each subject in each condition.

Figure 3.2 A shows the evolution during the entire experiment of the mean *adaptation ratio* (*AR*, Eqation 1) computed over all subjects on a trial-by-trial basis, while Figure 3.2 B shows the *AR* evolution for a representative subject (S3). Figure 3.2 E shows, for each tested subject, the mean and standard deviation of *AR* as assessed during the various phases of the experiment, shown in Figure 3.2 A. Statistical analysis on adaptation data was thus performed on each subject based on the Wilcoxon rank sum test, comparing experiment phases using the same data shown in Figure 3.2 E.

Statistical analysis provided the following results:

- All subjects had a consistent *AR* reduction (mean -28.1%, SD(1%), for a final request of -40%) at the end of the gain-down adaptation ($p<0.001$) *AS* trials (difference between (1) and (2) in Figure 3.2 A,E), showing the efficacy of the designed gain down adaptation paradigm.
- To test adaptation retention we assessed the level of adaptation at the beginning (first 10 trials) of the reversal gain-up adaptation block, during which the target movement went from 0 to 2.7% of chair movement, and was thus almost fixed in space. *AR* resulted significantly smaller compared to initial *SF* trials (mean -11%, SD (2%), $p<0.001$) in all subjects (difference between (1) and (3) in Figure 3.2 A, E).
- Reversed, gain up adaptation, was successful in inducing an increase of rVOR gain as six subjects showed a significant increase in *AR* in the last 10 trials of reversal adaptation with respect to the beginning 10 trials (mean +7%, SD 3%, $p<0.05$), while S4 and S7 showed no statistically significant *AR* changes (difference between (3) and (4) in Figure 3.2 A, E).

3.3.2. Spontaneous Recovery

The final set of 80 *CH* trials was then analyzed to investigate the evolution of eye velocity in the absence of visual feedback, and assess whether spontaneous recovery toward the previously learned low-gain state occurred in our subjects.

We performed an analysis on single subjects that underwent the main experiment (8 subjects) comparing AR between phases (4) and (5) in Figure 3.2 A, E: six subjects showed a significant AR reduction ($p<0.05$), consistent with the occurrence of spontaneous recovery, while S4 and S6 showed no statistically significant changes.

We then compared the trend of AR in the main and the control experiments (of the six subjects that performed the control experiment) using repeated-measures ANOVA (over each of the 10 bins in Figure 3.2 D):

- In the main experiment (Figure 3.2 D, black line) the test rejected the null hypothesis that all bins were equal ($p<0.001$, both considering the eight subjects that performed the main experiment and limiting the subjects to the six who performed the control); multiple comparison post hoc test showed that *AR* values in the first bin of *CH* (bin 3 in Figure 3.2D) were significantly lower than those during *SF* ($p<0.001$). Furthermore, *AR* values in the first bin of *CH* (bin #3) were significantly higher than during the last four bins (bin #7, 8, 9, 10 in Figure 3.2 D, $p<0.05$).
- In the control experiment (Figure 3.2 D, gray line) the test did not reject the null hypothesis that all bins were equal ($p=0.9$).

A further test showed that the correlation of *AR* with trial number in the first 40 *CH* (averaged over all subjects) was not statistically significant for the control experiment ($p=0.11$), while an highly significant negative correlation was found for the *CH* recorded after adaptation ($p<<0.001$) (Figure 3.2 C).

Both tests prove that, in the main experiment, CH trials showed a decreasing trend toward the low gain state acquired during the first gain down adaptation (i.e. arguing for spontaneous recovery), while in control experiment CH did not show any trend.

3.3.3. Multiple states of motor memory and forward model adaptation

We tried to explain the changes in eye velocity during rVOR adaptation in terms of recalibration of the cerebellar forward model of the eye plant that, by predicting the sensory consequences of the movement along the floccular feedback loop (Figure 3.1 C), allows online movement correction. The motor memory process controlling the adaptation of the estimated eye plant dynamics in the forward model was modeled as a linear state-space model (Eq. 9-10-11) supported by two hidden states [87], [109], [122]. The states adapt as a function of their value in the previous trial (coefficient a_s, a_f) and of the motor error observed on each trial (coefficient b_s, b_s).

Retinal slip (target velocity-head velocity) was assigned to two different sources based on its size: motor error or external causes, such as target displacement. Only the part assigned to a motor error leads to a recalibration of the rVOR gain. The credit-assignment was ruled by Gaussian functions such as that shown in Figure 3.3 G where the results of fitting Eq. 8 to the overall mean data (Eq. 8: $\sigma=6.9$) and to individual subjects are presented, respectively. In our experiment the error is induced gradually: at the start of training, when the error is relatively small, the model attributes the whole error to motor causes and, as training proceeds and the error becomes larger, the model progressively assigns part of the error to external causes, e.g. a target displacement (Figure 3.3 B).

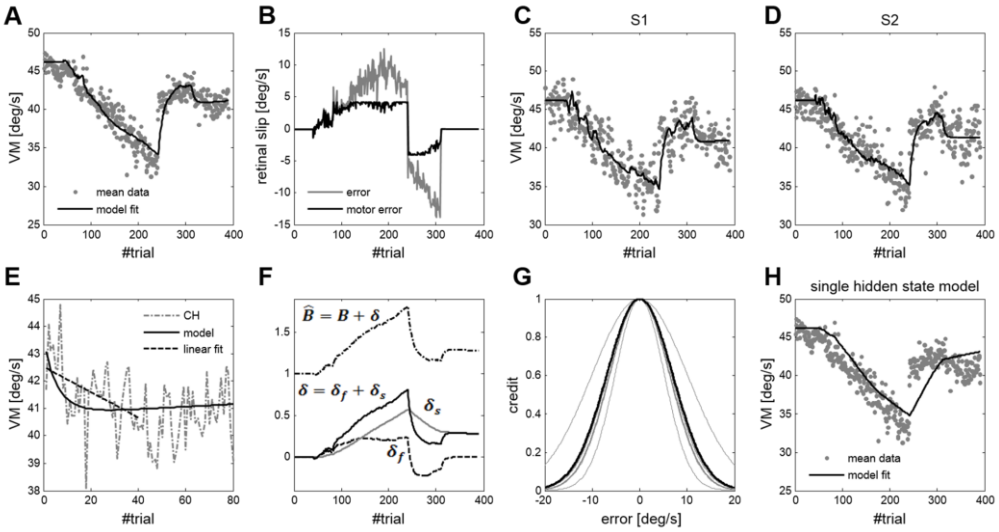

Figure 3.3: Model predictions. A: Mean velocity between 80 and 120 ms from head movement onset (*VM*) for the simulated movement (black solid line) and recorded data averaged on all subjects (grey data points). Goodness of fit: r^2=0.83. B: Error magnitude (retinal slip velocity: difference between the required and the recorded eye velocity, *err*) and motor error (black line, e_m). C,D: Model fitting on two representative subjects. E: Final CH trials (gray dotted line), prediction of the model (solid black line), and linear fit of the first 40 trials (dotted black line). F: Adaptation is the result of the recalibration of the forward model of the eye plant by changing the value of the coefficient ($\hat{B}$ black dotted line) that increases or decreases the effect of the motor command. The update of the parameter was modeled with one fast process (δ_f black dotted line) that adapts quickly but has poor retention and one slow process (δ_s gray line) that learns slowly but has better retention. G: Credit assignment function for individual subjects (gray lines), and for mean data simulations (black line). Smaller errors are more likely to be assigned to motor error, i.e. function values close to 1, due to a non-calibrated forward model of the eye plant. H: Single hidden state model fit on average data.

At the beginning of adaptation the fast state quickly responds to error (Eq. 10-11: b_f=0.0085, b_s=0.0009 b_f/b_s ~10), but at the end of the gain reduction adaptation trials most of the motor adaptation is due to the slow state (Figure 3.3 F, δ_s, dark gray dotted line). In the reverse adaptation period, the errors reverse sign and are suddenly large, so that in spite of credit assignment, the large motor error produces a rapid change in the fast state (δ_f) and a slower change in the slow state. The reverse adaptation block is followed by a set of catch-trials during which the fast state rapidly returns to zero, while the slow state declines more slowly. In this condition, the system is autonomous, i.e. it is not driven by an input *em(n)* and changes in the memory states are only due to the forgetting terms (Eq. 10-11: a_s=0.999; a_f=0.85). The different time constants governing the retention of the slow (τ_s=1000 trials, i.e. 83 min) and fast states (τ_f~7 trials, i.e. 35 s) thus result in the model prediction of spontaneous recovery of the previously learned behavior, as illustrated in Figure 3.3 A,E. The eye

velocity trajectories simulated by the model in the different stages of the experiment are also reported in Figure 3.4, in panels A-D, showing good agreement with the recorded data. Note that model simulations of both the mean data and that of individual subjects, clearly predict spontaneous recovery, correctly following the trend of the experimental data, in spite of the fact that the eye velocity predicted at the end of reversed adaptation is still lower than that at the initial, non-adapted state.

As a quantitative test for the existence of multiple timescales in rVOR adaptation we set out to verify how the alternative hypothesis of a single timescale process governing rVOR gain adaptation would explain the experimental data. The r^2 goodness-of-fit results for each subject and for the mean over all subjects are compared for the two models in Table 3.1. Values for the two hidden states model are significantly higher than those for the one state model ($p=0.01$). The single state model simulation of the mean data is presented in Figure 3.3 H, showing how the single state model fails to predict the fast increase of gain following the beginning of reversed adaptation, as well as spontaneous recovery, as the value of the single state can only continue to decrease towards the non-adapted state.

The BIC computed on the mean data simulation was 686 for the one hidden state and 125 for the two hidden states model.

Subject	R^2 two hidden states	R^2 one hidden state	BIC two HS	BIC one HS
S1	0.65	0.31	895	646
S2	0.67	0.28	849	561
S3	0.74	0.61	741	603
S4	0.39	0.34	939	923
S5	0.49	0.26	1105	971
S6	0.71	0.61	926	821
S7	0.46	0.17	910	761
S8	0.55	0.13	1024	745
Mean	0.83	0.55	686	125

Table 3.1 Comparison of r^2 statistics and BIC values between predictions of the single hidden state and the two hidden state models on individual subjects' and mean data.

3.4. Discussion

In order to deepen our understanding of the analogies between the control of goal-directed movements and the control of reflex movements such as the rVOR, we investigated the time course of short-term motor learning in the rVOR and developed a mathematical model to account for our experimental results. As an experimental proof of the existence of multiple timescales in the short-term motor learning of the rVOR we

specifically sought to investigate whether it would show the phenomenon of spontaneous recovery [107], [109], [157]. Thus, we developed a custom (Figure 3.1 A) paradigm exposing the rVOR to an initial assessment of gain, followed by an adaptive paradigm calling for gain reduction, a shorter period of reversed, gain increase adaptation, and a final set of catch trials in which the subjects had no feedback on their rVOR performance as the target disappeared at the beginning of the head movement.

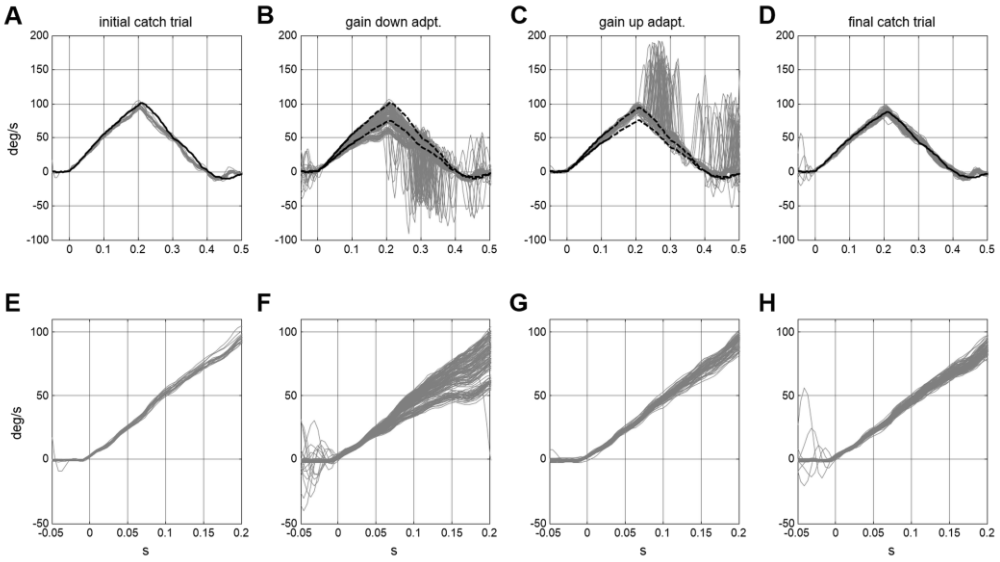

Figure 3.4: A,B,C,D) Black lines are model simulated eye velocities and gray lines recorded movements of one representative subject (S3). Dashed lines represent the rVOR outside the open loop response. A: initial catch trials and one simulation. B: recorded movements during gain-down adaptation and simulations at the beginning and at the end of adaptation. Only after at least 200 ms, at or after peak head velocity covert saccades are generated to regain fixation. C: recorded movements during gain-up adaptation and simulations at the beginning and at end of adaptation. D: final catch trials and one simulation. E, F, G, H) Detail of the data recorded during the first 200 ms corresponding to panels A, B, C, and D, respectively.

Short-term incremental rVOR adaptation using passive head (and body) impulses and spontaneous recovery.

Our experimental results show that the incremental adaptation paradigm was successful in inducing a statistically significant reduction of the gain of the rVOR in all tested subjects, obtaining a mean decrease in gain with respect to the initial baseline of 28% for a request of 40% (difference between phases 1 and 2 in Figure 3.2 A). The amount of adaptation assessed as the average over the first 10 movements at the beginning of the de-adaptation (phase 3 in Figure 2 A) trials was significantly lower than that achieved at the end of the gain down adaptation session (phase 2 in Figure 2 A). Yet, as can be appreciated both on the mean and on individual subjects data (Fig 3 A and C-D) such difference is mainly due to the rapid-de-adaptation that occurs during the 10 repetitions considered for the

assessment. The 70 repetitions of the reversal adaptation trials were also successful in significantly increasing rVOR gain in 6 out of the 8 tested subjects, with subjects S4 and S7 showing no significant change between the beginning and the end of the reversed adaptation paradigm (difference between phases 3 and 4 in Figure 2 A). The average adaptation ratio achieved at the end of reversal adaptation was still lower than the baseline by 7% (phase 4 in Figure 2 A).

AR values showed a significant reduction of gain during the final set of catch trials, arguing for the phenomenon of spontaneous recovery toward the previously learned lower gain state. Both individual subject and averaged data showed a slowly increasing, yet not statistically significant, gain in the last 20 trials of the CH paradigm (Figure 3.2 A, black line), which may reflect the autonomous behavior of the motor learning process once the fast state has returned to zero and only the slow state still shows residual adaptation. Only the first 40 trials, i.e. about 6 fast state's time constants, were then considered to assess the evolution of adaptation during catch trials and the maximum level of spontaneous recovery (data reported in Figure 3.2 E and Table 1).

Comparison of the AR behavior in such final set of catch trials with that recorded during the control experiment consisting of the same number of catch trials, yet not preceded by adaptation, showed that subjects presented no significant trend in gain during the control experiment, while a highly significant decrease in gain was shown during the main experiment.

A common architecture for motor control

Previous studies have demonstrated that the brain may deal with the tuning and continuous recalibration of the rVOR through a control circuitry that is similar to that used for goal directed movements: a forward model of the actuator in a cerebellar feedback loop is fed with an efference copy of the motor command and provides the brain with a prediction of the consequences of movements before sensory feedback is available [129]. The error being made during the online movement can then be monitored by comparing the sensory feedback signal with the prediction, and may be used for online correction. Motor commands, on the other hand, are produced by an inverse model of the same actuator, thereby cancelling its dynamics and issuing a command that will cause a movement faithfully reproducing the desired behavior [127]. Neural correlates for such a control structure were found for the control of eye movements and the control of the rVOR in particular: the existence of an inverse model was first hypothesized by Robinson [25] and then recently confirmed by Green and colleagues [57], which found that the "burst-tonic" and "tonic" cells in the praepositus hypoglossi and medial vestibular nuclei (PH-BT cells) encode the output of the inverse model, i.e. an efference copy of the motor command. The existence of a cerebellar forward model for eye movements was also hypothesized by Robinson and colleagues [132] and later by several other studies (see [50] for a review), and the finding that PH-BT neurons project to the flocculus, thereby providing the input to the forward

model, together with the similarity between the activity of eye-head (EH) neurons receiving projections from the cerebellar flocculus and eye velocity [60], provide support for such hypothesis [50].

Mathematical model of motor learning dynamics

We thus developed a mathematical model of the rVOR circuitry implementing the described control structure and including such inverse and forward models based on the model proposed by Glasauer [59]. We provided the model with a motor learning mechanism based on credit assignment [124] and a two hidden states process [87] acting on the parameters of the cerebellar forward model. The latter is the motor learning process, comprising a fast state that quickly learns from motor error but has poor retention and a slow state that learns more slowly but has greater retention. The mechanism behind adaptation of the rVOR response through adaptive changes of the cerebellar forward model is the following. During gain-down adaptation the nervous system faces a consistent retinal slip as the VOR produces eye velocities that are faster than required for target stabilization (Figure 3.4 B corrective saccades in opposite direction than rVOR). With our incremental adaptation paradigm the error is initially small and is thus entirely assigned to motor error. The brain then starts to believe that the motor command sent to the motor plant has a stronger effect on the dynamics of the eye than its forward model predicts i.e. the eyes are faster than predicted. The motor learning process Eq. 4-7 thus increases the effect of the motor command *u(t)* in Eq.3 by increasing the value of $\hat{B}$, which causes the forward model to predict a faster eye movement for a given command. A higher predicted eye velocity in turn reduces or changes sign to the feedback error, which diminishes the velocity command to the eyes. During gain up adaptation the situation is reversed and the eye movements are consistently less than compensatory (Figure 3.4 C corrective saccades in the same direction as the rVOR), thus the contribution of *u(t)* in the predicted eye velocity is decreased and the resulting command is increased.

Error signal for rVOR motor learning

One issue that is still debated with respect to motor learning in the saccadic system is that of the error signal used by the brain in the motor learning mechanism. Saccades are goal directed eye movements for which a well-defined error value may be computed for each movement performed. Based on the motor control model in Figure 3.1 C several signals may be available: a sensory error computed at the retina based on visual feedback and corresponding to the difference between real movement and intended movement, a predictive error between the desired and the predicted movement outcome and a predictive error between the predicted and the actual movement outcome, with the two latter signals being based on the output of the cerebellar forward model [158], [159] which signal is being considered, though, saccade error naturally corresponds to a scalar value for each movement performed. This is not the case with the rVOR, whose

goal is that of maintaining the image of the external world stable on the retina throughout the entire duration of the head rotation, so that a time based vector of instantaneous errors may be computed in terms of real or predicted retinal slip, i.e. a velocity based error signal, for each trial. We thus hypothesized that the brain might use a scalar error value computed for each trial based on an average performance over time, i.e. we computed the error in a single trial as the average of the corresponding time based signal over the same 80 – 120 ms interval from head movement onset that we considered for the analysis of experimental data. Such choice evidently represents an assumption for which we have no direct proof, i.e. we do not know how the brain evaluates the performance of the rVOR. Nonetheless, considering a time interval within the open-loop portion of the ocular motor response may be ecological, in the sense that it would provide the brain with useful information related to the performance of the sole rVOR. This would be advantageous with respect to a measure including the performance of the visually mediated movements such as pursuit or the optokinetic reflex, since it is the performance of the rVOR, which is critical in the open loop in response to high frequency perturbations, that benefits more from a correctly calibrated pair of forward and inverse internal models.

Credit assignment

Credit assignment is a mechanism that, given the information on an error, estimates its relevance to motor adaptation by assigning it to internal or external causes based on the size of the error and considering that only the error attributed to internal causes, i.e. the motor error, should be taken into account for motor learning [122], [124]. Following the principle that when facing small errors the brain is more likely to assign them to internal causes, we fitted the variance of a zero-mean Gaussian curve to our data considering retinal slip as global error and the probability of it being of motor origin as the portion of such error attributed to motor causes, and thus driving adaptation. The standard deviation of the Gaussian distribution found for credit assignment was 7.1 deg/s when simulating the mean data; the mean value over the 8 subjects was 6.6 ± 1.4 deg/s. Further research specifically tailored to the understanding of credit assignment is needed to explore such phenomenon in detail and evaluate its potential implications, for instance with vestibular rehabilitation or training paradigms.

Motor learning in the rVOR

As a theoretical argument on the structure of the motor learning process, we compared the ability to fit the experimental data, i.e. the AR evolution curve, between a single hidden state and a two hidden states model. We thus fit each model to the experimental data and assessed the goodness of fit of each simulation using the R2 coefficient of determination statistics. All fits were improved using the two hidden states model (R2 ranging 0.32-0.68, mean 0.57) with respect to the single hidden state one (R2 ranging -0.13-0.57, mean 0.25). The BIC provided further support in favor of a two

hidden states memory process showing that the increase in goodness of fit for the second order model was indeed an indicator of a more appropriate model for the experimental data and not a consequence of overfitting.

We have thus shown that the rVOR may quickly adapt its gain in response to consistent visual errors in the form of retinal slip, and that such adaptation may in fact result from changes in the forward model of the ocular motor plant, possibly residing in the cerebellar flocculus. Here, the main adaptation paradigm consisted in 200 trials, corresponding to about 18 minutes, and the entire experiment of 390, lasting 35 minutes altogether. Such short-term adaptation may reflect, for instance, the general mechanism by which the brain maintains an appropriate reflex performance when facing muscle fatigue, or adapts to the needs for a new sensorimotor transformation such as that required by wearing glasses. On the other hand, it would seem odd that, if the need for an altered response becomes permanent, such as with ageing, the brain achieves such adaptation by maintaining a wrong forward model of the plant in its cerebellar synapses. Indeed studies on cats [148], mouse [160] and monkeys [149] have shown that motor memories for adaptation of the horizontal rVOR are stored at different sites depending on their consolidation. Motor memories acquired with short term adaptive training are immediately stored in the cerebellar flocculus so that its pharmacological inactivation disrupts the recently learned changes, while the changes learned during the previous day's training are preserved, and are therefore stored elsewhere, possibly in the brainstem [149]. These and other studies [116], [161] have shown that when a memory learning process is explained by a two-hidden states model, it is the slow state that may form a long term memory being consolidated while the fast state only reflects short-term learning. These issues go beyond the scope of our study as we have not investigated retention of the learned behaviors to longer time intervals, yet it would appear reasonable that adaptive changes deserving to be consolidated become incorporated in the brainstem inverse model of the ocular motor plant, while always leaving to the floccular forward model the task of learning the changes needed to respond to short-term adaptation requests.

In conclusion, both our experimental data and our modeling results strongly support the hypotheses that short-term adaptation of the rVOR is mediated by the adaptation of a forward model of the ocular motor plant residing in the cerebellar flocculus, and that such adaptation is controlled by a multiple hidden states process that modifies the parameters of the forward model based on motor error. For movements to be quick and accurate, the commands controlling them need to be continuously adjusted to reflect the state of our body, such as the level of fatigue, and of our interaction with the environment. The brain then faces the classical plasticity-stability dilemma, i.e. the need to find a compromise allowing sufficient plasticity to adapt to changes while being stable enough to benefit from learning and behave consistently. Our results showing that the brain faces adaptation even of a reflex movement using the same approach

used with goal directed movements lead to the hypothesis that multiple timescales in motor learning may be considered as a general principle, a general purpose solution of the central nervous system to the cited dilemma, allowing the system to quickly adapt to errors while having a relatively stable, slowly evolving reference behavior.

Chapter 4

Clinical evaluation of vestibular function: the Head Impulse Test Device (HITD)

The main symptoms of vestibular disorders (see Chapter 1.3), such as dizziness, vertigo or imbalance are difficult to describe, and are associated to several different conditions. For this reason, the exact number of affected people is hard to quantify. In order to understand the impact of vestibular disorders on the public health service I report data from reliable quantitative studies carried out in the United States. As reported in [162], dizziness is the third most common medical symptom reported in general medical clinics [163] and accounts for 3-5% of visits across care settings [164]; this translates to 10 million ambulatory visits per year related to dizziness [165], with 25% of these visits being to emergency departments [164]. Moreover, between 2001 and 2004, about 35% of adults aged 45 years and older suffered from vestibular dysfunctions [166].

Management of the dizzy patient consists in clinical history inspection, bedside examination and laboratory testing. History allows determining the onset of the problem, description of the symptoms and the impact on lifestyle. The bedside clinical examination, mostly based on the qualitative evaluation of eye movements, allows distinguishing peripheral from central vestibular problems and the extent of the loss. Laboratory tests quantify the degree of loss and the central compensation.

Despite peripheral causes (see Chapter 1.3) are more common, dangerous central causes, in particular ischemic stroke in the brainstem or cerebellum, can mimic benign vestibular causes closely [162]. Therefore accurate diagnosis of dizzy patients at an early stage is important and can avoid potentially fatal complication and improve patients' outcome [167].

Thus, vestibular tests are important both in the diagnosis and in evaluating the effects of rehabilitation. In the first section of this Chapter I

reviewed the classical laboratory tests [2], the Head Impulse Test (HIT) that is the gold standard for clinical testing, and the functional testing approaches that assess the reflex (without directly measuring eyes movements) by evaluating the ability to stabilize gaze in space allowing clear vision during head movement. Afterward, the functional test proposed by our group, the HITD [168], [169] that exploits impulsive head rotations while requiring the subject to identify optotypes briefly displayed on a screen, is presented. The percentage of correct answers at different head accelerations represents an evaluation of the efficiency of the rVOR without directly measuring eye movements. Finally, in order to validate the HITD, the vHITD tool [150] is described. This research tool allows the synchronized recording of eye and head movements, together with a feedback on visual display timing. The goal is to understand the relation between the functional (percentage of reading) and quantitative (gain) measure and thus to compare HITD outcome with traditional evaluation tests. Paragraph 4.3, presenting the HITD and paragraph 4.3 presenting the vHITD are excerpts of our papers [150], [168], respectively.

4.1. Traditional vestibular function tests

After the examination of history and the clinical examination, vestibular tests help to determine if dizziness is caused by the inner ear or by brain problems.

By measuring eye movements in response to specific sensory stimulations, it is possible to quantify vestibulo-ocular and optokinetic responses in order to characterize and quantify the loss of function.

4.1.1. Caloric Test

Caloric testing induces a nystagmus that can be measured with electro-oculography (EOG) or video-oculography (VOG). The caloric response is due to two separate effects of the stimulus: convection currents induced in the endolymph and the effect of temperature on the discharging of the vestibular nerve. During the test, the patient is supine with the head tilted up 30 degrees placing the horizontal canal in the vertical lane. After checking that the tympanic membrane is intact (otherwise air instead of water can be used as stimulus) the procedure consists of a first infusion of water at 44 ^{o}C for 40 seconds into one ear (recording the ensuing nystagmus). After 5 minutes of recovery, the same stimulus is repeated for the opposite ear. Then each ear is stimulated with water at 30 ^{o}C. With cold-water infusion, the endolymph falls within the semicircular canal, causing the movement of the cupula away from the utricle and an inhibition of the firing rate of the vestibular nerve. That causes a nystagmus with its slow phase directed toward the side of irrigation. When warm water (44°) is infused, the opposite response occurs. Absent reactive eye movements

suggest vestibular impairment of the horizontal semicircular canal of the stimulated side.

Caloric testing is the considered as the best approach to determining whether a disorder is central or peripheral and to identifying the affected side, yet it assesses only the function of the horizontal canal and cannot be used to assess bilateral vestibular loss or to determine central compensation.

4.1.2. Rotary Chair Testing

Rotary chair testing should be performed in darkness with eye movements measured using EOG, VOG or eye coils. During a sustained chair rotation, the VOR first drives the eyes away from the center position (slow phase) and then triggers a quick phase movement (produced by the saccadic mechanism) in the opposite direction (see Figure 1.4). A sustained sequence of slow and quick phases is called *nystagmus*, and in this case *vestibular nystagmus*.

The *VOR gain* (i.e., eye velocity/chair velocity) can be obtained by measuring peak slow phase eye velocity in response to step of angular velocity. During a velocity step also the *time constant of decay* of the slow phase eye movements can be measured. VOR gain and phase (offset between peak eye velocity and peak chair velocity) can also be measured in response to sinusoidal rotations. In sinusoidal rotary chair stimulations, the chair rotations are commonly performed at 0.125, 0.05, 0.2, 0.4 and 0.8 Hz. A velocity step instead consists in sudden sustained rotation at 50 or 100 deg/s.

Rotatory testing can give more accurate and reproducible results with respect to the caloric test in patients with bilateral vestibular loss. This test can be used to determine central compensation after rehabilitation.

The test can assess only the horizontal semicircular canal on a normal rotary chair; moreover, because rotation affects both sides, it is more difficult to identify unilateral loss with respect to caloric testing. The equipment is very expensive and requires frequent calibration and maintenance.

4.1.3. Vestibular Evoked Myogenic Potential

The vestibular evoked myogenic potential (VEMP) is a technique for assessing the function of the saccule and of its central projections, including the inferior vestibular nerve. The test consists in stimulating the ear with acoustic tones while recording the tone of the sternocleidomastoid with surface electromyography (EMG). The stimulus can be tones or clicks with intensity between 60 and 94 dB and frequency of 5 Hz. Usually the output of the test is the average of the responses in 128 trials. The response, in healthy subjects, is a biphasic positive negativity with amplitude

depending from the intensity of the tone and muscle contraction. Absence or delay or reduced amplitude of the response indicate damage of the saccule on that side. This test cannot be used to assess central compensation.

Recently the ocular vestibular evoked myogenic potential (oVEMP) has been introduced and validated. It refers to the myogenic potentials recorded by surface EMG on the eye muscles in response to bone conducted vibration stimulation of the head or air conducted sound [170].

4.1.4. Subjective Visual Vertical Test

The subjective visual vertical test (SVV) assesses utricle function and its central connection, including the superior vestibular nerve. It is a subjective measure of ocular torsion due to damage to the utricle. The patient, sitting in a dark room, has to align a projected tilted line with his perceived vertical. The mean and the standard deviation, from true vertical, of ten readjustments is then computed. Usually, up to 2 degrees of tilt is considered as normal. If the utricle of one side or the vestibular nerve is damaged, the perception of the earth vertical reflects the asymmetry in utricular input.

The SVV response can be used to assess central compensation (looking at changes in the same individual). It will not detect bilateral utricular injury.

4.1.5. Head Impulse Test

The head impulse (or head trust) test, introduced by Halmagyi and Curthoys [171], provides important results in the examination of vestibular hypo-function. Head impulses are brief, rapid and unpredictable rotations of the head on the trunk (Figure 4.1). The rotations are of low amplitude (10^o-20^o) and high acceleration (up to 6000 ^{o}/s). If the VOR is healthy, the compensatory vestibular eye rotation has exactly the same velocity as the head impulse but in the opposite direction (Figures 4.1 A, 4.3 A, C). In case of vestibular loss, the patient's gaze will be dragged in the direction of the head impulse and the patient must make corrective saccades to bring back the eyes on the target (Figures 4.1 B, 4.3 B, D).

The semicircular canals (SCC), are organized in push-pull arrangement (see Chapter 1.1.3), thus, for example, during a rotation in the horizontal canal's plane, an ampullofugal (inhibitory) flow within a canal will be accompanied by an ampullopetal (excitatory) in the contralateral one. Anyway, each SCC transduces angular acceleration in a non-linear manner, but the normal VOR is linear because each SCC is paired with its co-planar partner. In each SCC, for Ewald's second law [172], the excitatory response is greater than the inhibitory response, which has lower sensitivity and which can be saturated [173], [174]. Therefore, a high acceleration

rotation drives in inhibitory cut-off the inhibited semicircular canal (i.e. the afferents from that canal stop firing) and in the case of unilateral vestibular hypo-function, this results in an asymmetric gain of the VOR [175].

To carry out the test the physician, sitting in front of the patient, instructs him/her to maintain the gaze on the examiner's nose while rapidly turning the head to about 20°. If the eyes stay locked on the examiner nose, the VOR is intact (Figure 4.1 A). If the VOR is impaired, the eyes move with the head, and then come back with a corrective saccade to the experimenter's nose (Figure 4.1 B). In unilateral vestibular loss, the response is defective when the head is rotated toward the side of the lesion.

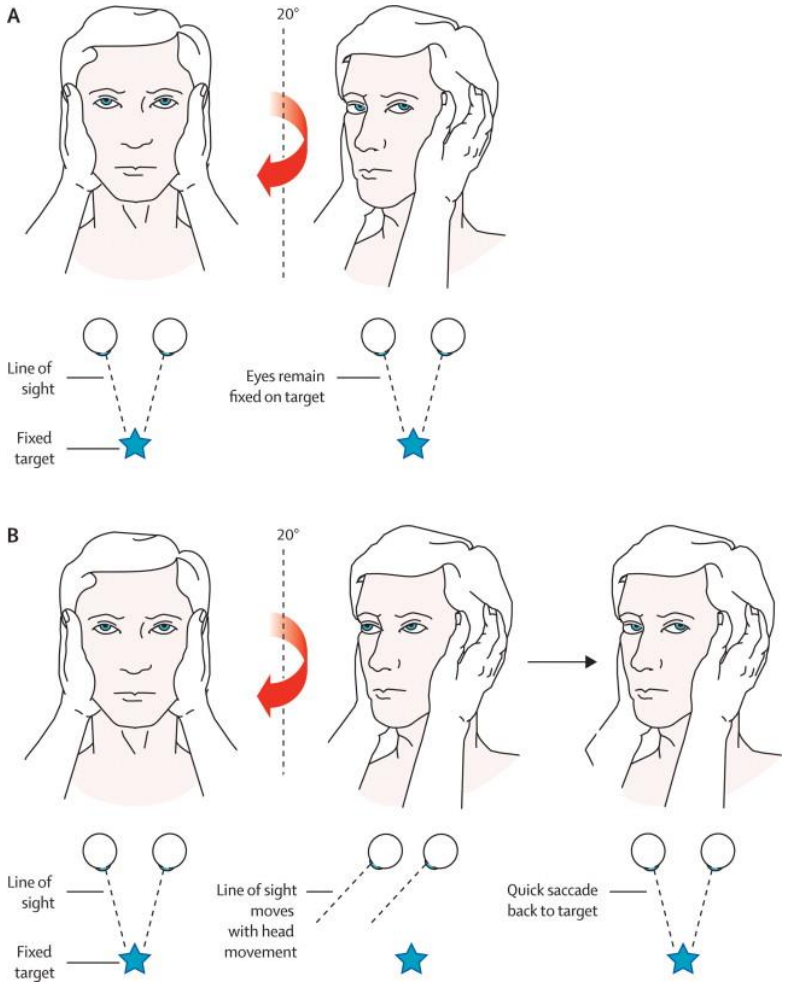

Figure 4.1: A) Normal head impulse test to the right. Initial starting position is with the patient's gaze on the experimenter's nose. Upon stopping the head thrust, the eyes are still on target and no corrective saccade is observed. B) Abnormal head impulse test to the right. Initial starting position with the patient's gaze focused on the experimenter's nose. As the head is rapidly turned to the left, the eyes move with the eye and lose the target. The subject must make a corrective saccade to bring back the eyes on the target. (Taken from [167]).

The head impulse test is useful to distinguish acute peripheral vestibulopathy from cerebellar stroke [167] because the primary VOR pathway bypasses the cerebellum. In acute vestibular syndrome patients, a negative head impulse test (normal VOR) is a strong predictor of a cerebellar stroke diagnosis, while an abnormal test requires additional clinical features (direction fixed nystagmus, absent skew deviation) before a central lesion can be excluded [176]..

The head impulse test, in addition, tests the VOR with natural high-acceleration head rotations while the caloric test provides unnatural stimulation equivalent to a very low frequency head rotation [177] (this is also true for the stimulus frequencies that can be tested by rotatory chair). Moreover, after the acute phase, when vestibular diagnosis becomes more difficult due to the central nervous system compensation, testing the VOR with high frequency stimuli, can still reveal the deficit.

Usually the head impulse test is a bedside test, but it can be also assessed quantitatively by simultaneously recording eye and head movements (Figures 4.3, 4.5-7). The quantitative measure shows the pattern of slow phases and saccades and allows computing the VOR *gain* (actually the ratio of output/input velocities to the VOR system, computed as eye velocity/head velocity). The gold standard for the head impulse test measure is the *search coil* technique [154], [178],. However, this technique is not practical for acute patients because it requires the subject to wear an uncomfortable contact lens, technical knowledge and it's quite expensive. However, lightweight, high speed VOG systems were recently developed which allow performing the head impulse test [179], [180].

4.2. The Head Impulse Test Device (HITD)

Peripheral vestibular function may be tested quantitatively, by measuring the gain of the rotational vestibulo-ocular reflex (rVOR), or functionally, by assessing how well the rVOR performs with respect to its goal of stabilizing gaze in space and thus allow to acquire visual information during the head movement (e.g. an optotype briefly showed during head movement). If the rVOR works properly, the gaze remains fixed in space and the subject can read the optotype (Figure 4.3 A, C); otherwise, the eyes move with the head, the image slips on the retina and the subject cannot read (Figure 4.3 B, D).

We developed the head impulse testing device (HITD) based on an inertial sensing system with the goal of proposing a tool allowing to investigate the functional performance of the rotational vestibulo-ocular reflex (VOR). We aimed at testing its gaze stabilization ability (in terms of percentage of reading) independently from the subject's visual acuity and in response to head impulses at different head angular accelerations ranging from 2000 to 7000 deg/s^2. This paragraph summarizes the work published in [168].

4.2.1. The functional assessment of the VOR

Even a few degrees/second of image slippage on the retina seriously deteriorate vision, so that during a head rotation that unveils a vestibular deficit, vision is impaired. This observation provides the grounds for protocols aiming at the evaluation of vestibular function, i.e., evaluating the VOR in terms of its efficacy toward the stabilization of the visual scene during head rotations.

One early example is the dynamic visual acuity test (DVAT), which measures visual acuity during active, sinusoidal, head rotations [181], [182]. The subject must recognize the orientation of the letter "E" appearing on the screen when head velocity falls between 120 and 180 deg/s. The size of the shown letter is progressively decreased until that corresponding to normal visual acuity is reached. The test has proven clinically reliable [181], [183] in detecting vestibular dysfunction. Nonetheless, its effectiveness with compensated patients is limited, since voluntary head movements imply that the CNS may use the available information, e.g., the efference copy of the commands to neck muscles, to activate predictive mechanisms that do not rely on peripheral function [184], [185]. A new version of the DVAT using passive, impulsive head rotations has recently been suggested [186], [187]. In the Schubert study, when head velocity is within the 120–180 deg/s range for at least 40 ms a letter "E" optotype appears on the computer monitor and the subject must recognize its orientation. During the test the size of the letter is varied based on the rate of correct answers and the outcome is a measure of visual acuity, i.e., the minimum angle between the features of the shown character, as seen from the patient, needed for correctly discerning it (in logMAR, minimum angle of resolution). The diagnosis of a vestibular deficit is based on the comparison of the static visual acuity measure with that of the dynamic one. A patient is considered pathological when the latter is at least 0.3 logMAR smaller than the former [188]. Further research has recently been devoted to improving the DVAT by designing a new version of the test using Landolt rings in eight orientations, thereby reducing the probability of obtaining a correct answer by chance, and exploiting an adaptive algorithm for changing the size of the presented letters allowing to speed-up the execution of the test [189].

The gaze stabilization test (GST) [190]–[192] evaluates the contribution of the VOR to gaze stabilization by measuring the peak head velocity that allows discerning the orientation of a randomly presented, fixed-size optotype (the letter "E") during active head shaking (sinusoidal head movements at relatively high frequency, about 2 Hz). The size of the optotype is fixed at 0.3 logMAR above each subject's static visual acuity level and the visual stimulus is shown for at most 75 ms when head velocity exceeds a predefined threshold for at least 40 ms. The threshold is increased or decreased adaptively depending on the patient's performance. The GST allows discerning vestibular patients. Yet, the use of active head

movements exposes this technique to the same limitations described above for the sinusoidal and the active DVAT. Surprisingly, no normative data exists on both DVAT and GST.

The above-mentioned quantitative testing techniques indicate the presence, or absence, of a deficit, yet their measurements are not directly correlated with the patient's percept of his own disability. In fact, during DVA testing, vision plays a fundamental role in determining the output of the technique and, although the diagnosis is based on a comparison with the static visual acuity level, the relationship of the absolute DVA value to the patient's percept of his abilities cannot provide a direct measure of vestibular functionality.

HITD assesses the function of the VOR without directly measuring the movement of the eyes. The suggested approach differs from that of DVA assessment as it focuses on the characteristics of the head movement, and not those of the visual stimulus, in affecting the subject's ability to stabilize gaze in space. Thus, the goal of the HITD is that of assessing vestibular function to different head angular accelerations, while facing equally challenging visual stimuli, in order to provide indications that may be closely correlated to each patient's daily activities.

We tested the HITD in a group of normal subjects, and we suggest a method for the definition of normal limits for the evaluation of a single patient. This method was tested on a group of patients with various stabilized vestibular disorders, and the results were compared with those obtained by clinical HIT.

4.2.2. Methods

The Test

The rationale of the proposed testing approach is as follows: a patient wearing a head mounted sensor sits in front of a computer monitor with the experimenter manually imposing head impulses standing behind his/her back (Figure 4.3 F). Static visual acuity is first assessed using an eye chart displayed on the monitor with letter sizes scaled based on the subject's viewing distance. The size of the visual stimuli used during the test is then determined based on the assessed visual acuity by increasing that of the smallest seen line by 0.8 logMAR. Such stimulus size, which is eight lines bigger than the best static visual acuity, will then remain constant during the test.

When the imposed head angular acceleration exceeds a user-defined threshold, a character drawn from the Sloan letter set is briefly displayed on the screen for a user adjustable number of video frames and with a user adjustable time lag.

In our experiments the duration of the letter display was set to two frames (about 33 ms with a regular 60 Hz refresh rate) with no delay. This setting resulted in the visual stimulus being displayed around the time of

maximum head acceleration, as we verified by recording the output of a photo diode applied to the screen.

Hardware implementation of the protocol is exposed in Appendix A.

Subjects and patients

We have recorded the responses of 39 patients (age range 35–80) with different vestibular disorders and those of 22 age-matched controls (age range 22–68). In patients, the HITD evaluation and the HITD vs HIT comparison were not performed during the acute phase of their disorders.

The experimental protocol was approved by the local ethics committee, and all individuals were investigated on a voluntary basis and gave written informed consent to participate in it.

All patients underwent a careful collection of their clinical history and a full clinical vestibular examination. Moreover, some patients, those who were referred to an ENT department in Siena, underwent caloric and mastoid vibration testing, whereas some other patients, who were referred to a neurological department in Pavia, underwent to rotatory testing, subjective visual vertical evaluation and vestibular evoked potentials recording.

On these bases the patients were divided in five diagnostic groups: vestibular neuritis (VN, seven patients, age range 35–66), Ménière's disease (MD, five, age range 40–65), UVD (14, age range 42–66), bilateral vestibular deficit (BVD, seven, age range 45–80), central vestibular deficit (CVD, six, age range 50–71).

Vestibular neuritis was diagnosed on the basis of the clinical history (sudden onset of rotatory vertigo, quite severe in the first days, and then followed by a spontaneous and progressive improvement without recurrence) and of clinical and instrumental signs detectable in the acute phase of the disease. Instrumental signs included caloric canal paresis [193], VOR gain significant asymmetry at rotatory test, abnormally tilted subjective visual vertical, asymmetrical vestibular evoked potentials. MD was diagnosed on the basis of the AAON-HHS criteria [194]. In order to be included in the UVD group, patients had to show a clinical or instrumental vestibular deficit (asymmetry), but without any further features to be included in another diagnostic group (in particular the VN or the MD groups).

The BVD included subjects who complained of oscillopsia during head motion (for instance when walking) and who showed no response to caloric and/or to rotatory stimulation bilaterally; in all subjects BVD was idiopathic.

The CVD group included four patients with vestibular migraine and two subjects with idiopathic down beat nystagmus.

Data analysis

Data was divided in 1000 deg/s^2 wide bins based on peak head angular acceleration reached during each head impulse that triggered the display of

the letter. Only patients that were tested for at least eight head impulses in each direction were considered for the specific bin and direction. Thresholds ranged 2000–7000 deg/s^2 and the data was therefore organized in six bins for each subject.

Statistical analysis was performed by comparing the rate of correct answers in each patient against the population of controls considering two independent samples. We considered separately clockwise (CW) and counterclockwise (CCW) head impulses and performed the comparisons both considering individual acceleration bins and pooling bins together.

For each comparison we considered r1 correct answers over n1 total trials for controls and r2 correct answers over n2 trials for each patient, and the corresponding rates p1 = r1/n1 and p2 = r2/n2.

Thus, we tested the null hypothesis that p1 = p2 by considering the expected rate of correct answers in the population (2) and computing the standardized normal deviate:

$$[E_{correct}] = \frac{r1 + r2}{n1 + n2}; \tag{1}$$

$$z = \frac{p1 - p2}{E_{correct} \times (1 - E_{correct}) \times ({}^{1}/_{n1} + {}^{1}/_{n2})}. \tag{2}$$

The patient was considered as being not normal if z fell outside the 99% of the two tailed z distribution.

Such approach was applied twice for each patient: once by considering each acceleration bin individually (individual bin approach) and once by pooling all the acceleration bins together (pooled bin approach). The individual bin approach labeled as abnormal the subjects who showed a rate of correct answers lower than expected in at least one acceleration bin.

The percentage of patients showing an abnormal HIT and/or HITD test for each diagnostic group and for each direction (healthy and affected side) were compared by Fisher's exact test.

4.2.3. Results

In controls, the percentage of correct answers ranged from 98 to 100, both for CW and CCW impulses independently from the acceleration bin they belonged to. When all acceleration bins were pooled together, the percentage of correct answers was 99 for CW and 98 for CCW impulses.

The distribution of the performance of control subjects in response to the six levels of head angular acceleration is shown in Figure 4.2 A, together with the number of subjects considered for each bin. For all bins except the highest CCW acceleration, the median of the sample of control subjects was one.

The same graphical representation is shown for patients in Figure 4.2 B, where the median of correct response ratios is shown to be lower than in controls (Figure 4.2 B), especially for higher acceleration bins.

In 30 of the 39 patients HITD proved to be abnormal in at least one direction, and only in five patients the abnormality was detectable for acceleration thresholds less than 4000 deg/s^2, i.e., for 2000 and/or for 3000 deg/s^2 bins. On the other hand, only two patients proved to be abnormal only for the 7000 deg/s^2 bin.

The abnormalities detectable by the HITD and the HIT were comparable both from the affected or the healthy sides in the VN, UVD, MD, and BVD groups. The two tests proved the CVD group to be significantly different, with a higher number of abnormalities detected by the HITD than by the HIT both for the individual (Fisher's exact test, $p = 0.007$) and for the pooled (Fisher's exact test, $p = 0.04$) approach.

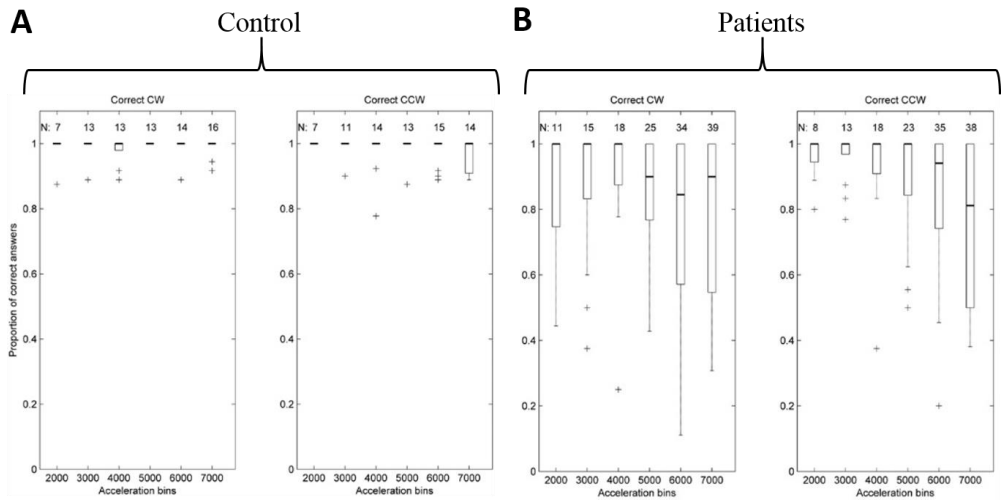

Figure 4.2: box plot representation of the distribution of correct answers ratios per acceleration bin, in control subject A and in patients B. Each acceleration bin is labeled using the lower acceleration threshold. In each box plot, the thick horizontal line indicates the median of the sample, and the thin line at the lower and upper extremity of the box is the 25 and 75 percentile. Whiskers extend to the extreme data points considered in the distribution, while crosses indicate individual outlier data points.

4.3. The video Head Impulse Test Device (vHITD)

Several relevant parameters of the functional testing approach, such as the best timing of the visual display, of its duration on screen or its temporal relationship to the head movement, significantly differ both among the different described techniques (i.e. DVAT, GST and HITD) and within the DVAT approach itself when carried out by the different cited groups or studies. Certainly, a true understanding of these parameters and their optimization for diagnostic purposes would be important for establishing a reliable and easy to use diagnostic approach.

On the other hand, recent work by Weber and colleagues [179], [195] investigating the video head impulse test aimed at measuring non-invasively the gain of the VOR during HIT, found that vestibular patients could produce compensatory saccades during the head movement, which they called *"covert"* saccades (Figure 4.3 B), that would likely be missed by the clinician during clinical HIT. Although such compensatory *"covert"* saccades have been described in the literature [196]–[198], their functional consequences, i.e. whether they are effective at improving gaze stabilization during the head movement, and thus the ability to correctly identify the stimuli in functional testing paradigms, or whether their function is that of bringing the eyes back on the fixation point sooner than with the delayed *"overt"* saccade (Figure 4.3 B) yet without improving vision while in motion, has never been investigated so far.

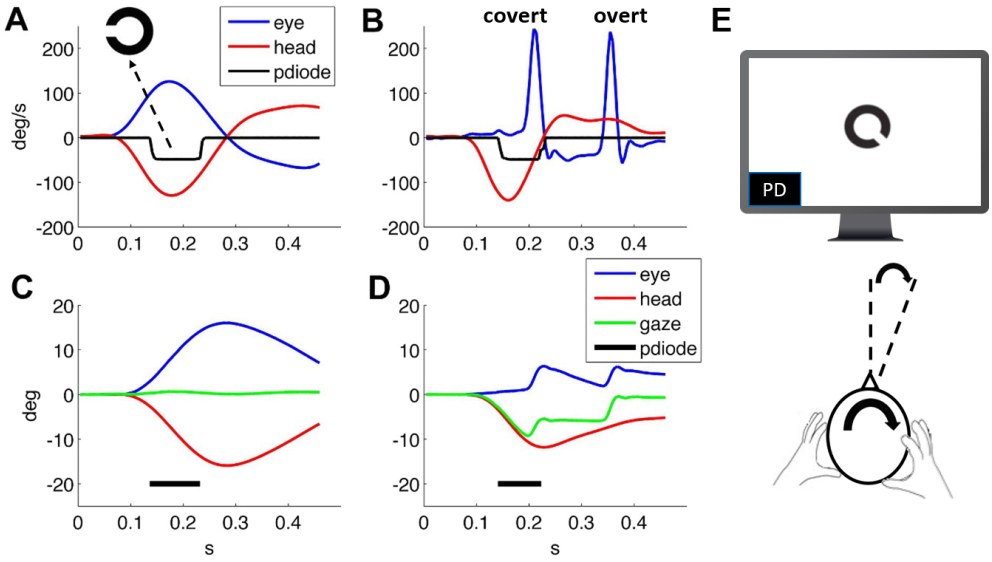

Figure 4.3: A, B) Head and eye velocity response, and optotype (Landolt C) presentation from a normal subject and a patient, respectively, with (left) unilateral vestibular neuritis. In B are labeled Covert saccade made during the head movement and delayed overt saccade when the head is stopped. C, D) Head, eye and gaze position, together with optotype timing for the responses in A, B, respectively. Compared with the healthy subject, the gaze of the patient is not stable during the optotype presentation, and his answer was indeed not correct. The derivative of the gaze is the *retinal slip*. F) Experimental setup: the sits in front of a monitor with the experimenter manually imposing head impulses standing behind his/her back. A photodiode (PD) attached to the test screen detects a square that pops up together with the letter.

Furthermore, when working with commercial operating systems (OS) the timing variability related to the screen refreshing rate, the acquisition and processing software performance, CPU load and the known other factors related to a non-real-time OS, introduce uncertainty about the adherence of the testing procedure to the intended protocol. Since an

impulsive head movement lasts 150-200 ms considering all these issue may help to improve functional testing.

This paragraph reports the study published in [150]: the goal was that of developing a new research tool allowing the synchronized recording of eye and head movements, together with a feedback on visual display timing (Figure 4.3), which we believe are crucial information to truly understand functional rVOR testing, that is:

- define which experimental parameters are critical for optimizing the diagnostic power of functional rVOR testing;
- study the effectiveness of covert saccades towards image stabilization;
- understand the relation between the functional (percentage of reading) and quantitative (gain) measure.

4.3.1. Methods

The test

The project aimed at integrating our head impulse testing device, HITD [168], [169] (Chapter 4.2, Appendix A) with the EyeSeeCam video-oculography system [180] available in our lab. The choice of such eye movement recording tool was driven by the need for a lightweight device, thereby limiting the consequences of inertial forces, while avoiding the scleral search coil for the inevitable disruption of visual clarity it implies. The experimental paradigms were then developed as Matlab (MATLAB R2009b, The MathWorks, Inc.) scripts handling both the stimulation and data acquisition through data structures made available on-line by the EyeSeeCam software package in the Matlab workspace. Hardware implementation is discussed in Appendix B.

The test works as the traditional HITD, with the difference that the subject wears the EyeSeeCam system. In respect to the HITD test, the optotype size is increased by 0.6 logMAR and we chose the Landolt C optotype instead of Sloan letters (explanations are exposed in Appendix B). Moreover, the static visual acuity is tested requiring the patient to identify the orientation of a sequence of Landolt C rings of size calculated with an adaptive algorithm searching the visual acuity threshold.

Subject and patients

We investigated 29 subjects suffering from vestibular neuritis (VN, see Chapter 1.3.2), 12 right and 16 left, aged between 24 and 81 years (mean: 54.6 years). We compared them with a group of 13 normal subjects (aged between 23 and 54 years; mean age 36.5 years). VN was defined as acute onset non-positional rotatory vertigo, presenting with unidirectional horizontal-torsional spontaneous nystagmus, positive clinical HIT, absent or reduced caloric response, normal neurological examination. The patients were examined the first time after 3 to 10 days from symptom onset, and

re-tested after about 3 months. Patients underwent vHITD, rotatory chair test (RT), vestibular evoked myogenic potential evoked by air conducted auditory stimuli (VEMP and oVEMP) and subjective visual vertical (SVV). At second examination, the patients self-feeling about their balance was assessed by 3 questionnaires: Dizziness Handicap Inventory [199], Situational Vertigo Questionnaire [200], Activities-Specific Balance Confidence [201].

4.3.2. Functional and quantitative assessment of the VOR

Figure 4.3 shows the detail of two representative responses to head impulses triggering the optotype presentation: one from a healthy subject and one from a patient recorded 3 days after the onset of a right vestibular neuritis. When at rotatory testing she showed an ipsilesional gain of 0.07 and a contralesional gain of 0.16; the subjective visual vertical was 7.8 deg. The gains measured over all impulses delivered during HITD testing were 0.14±0.07 ipsilesionally and 0.74±0.04 contralesionally. In the normal subject (Panel A) the eyes rotate in the opposite direction of the head (with the same velocity), gaze (Panel C) remains basically stable and the subject is indeed able to correctly recognize the optotype.

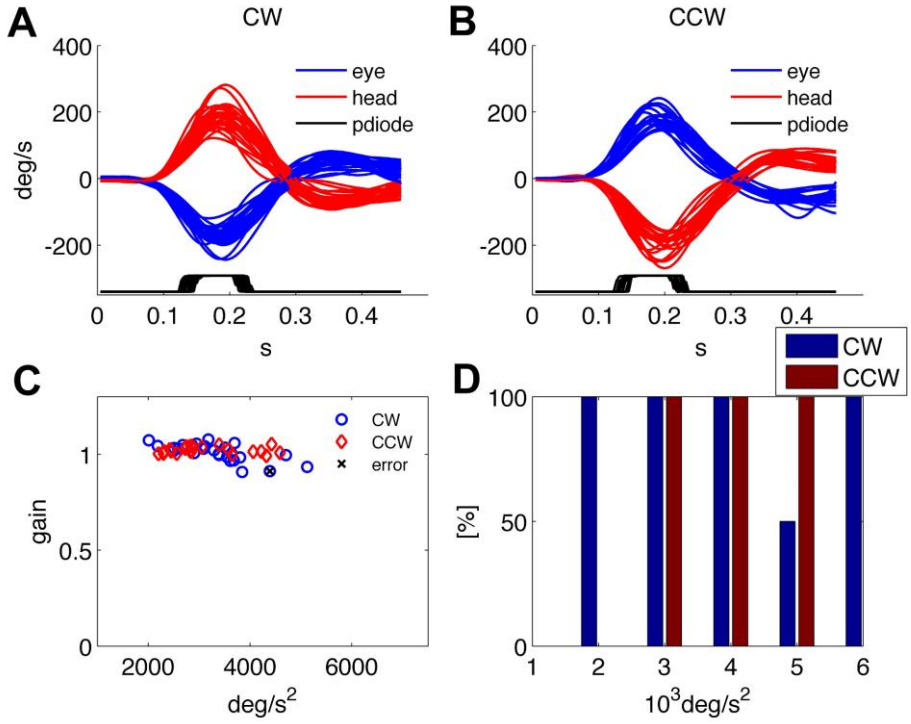

Figure 4.4: results of the vHITD test on a healthy subject. A, B) Head and eye movements for CW and CCW rotations, respectively. C) Plot of VOR gain values computed for each movement. D) Percentage of correct answers for each acceleration bin (97% CW; 100% CCW).

In the patient response (Panel B), the eyes move together with the head and saccades are triggered to regain fixation. The first is a covert saccade occurring during the presentation of the optotype with a latency of about 100 ms from the onset of the head movement, while the second is an overt saccade allowing the patient to regain fixation. Compared with the healthy subject, the gaze of the patient (Panel D) is not stable during the optotype presentation, and his answer was indeed not correct. Gaze returns to the target, at 0 deg, only after the end of head rotation.

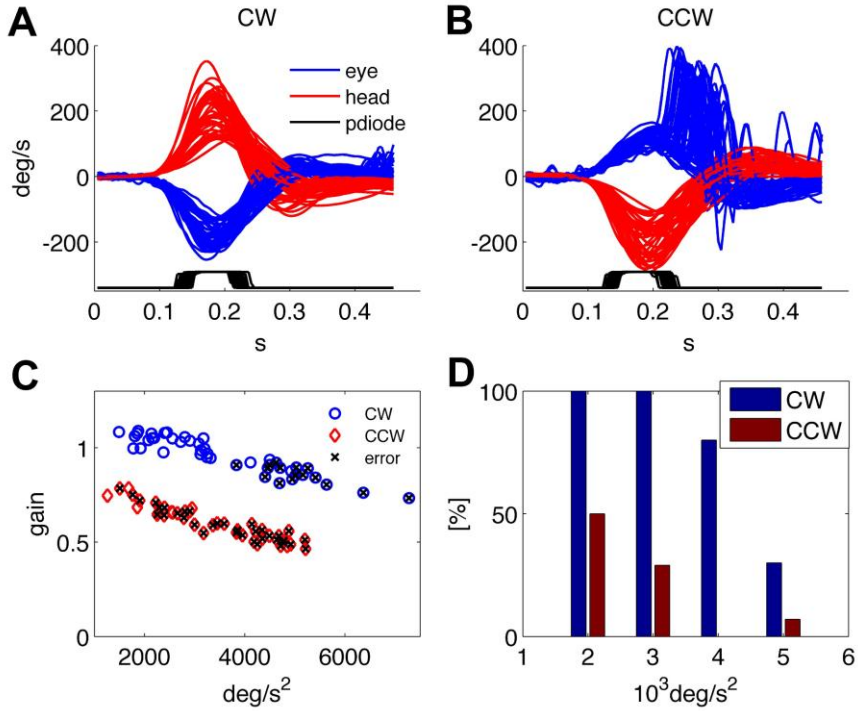

Figure 4.5: results of the vHITD test on a patient with vestibular neuritis. A, B) Head and eye movements for CW and CCW rotations, respectively. C) Plot of VOR gain values computed for each movement. D) Percentage of correct answers for each acceleration bin. Overall percentage of correct answers: 18% toward the affected side, 62% toward the contralateral.

The vHITD system proved to be a useful tool to evaluate and follow up patients. It is well tolerated and lasts about 20 minutes if the entire range of accelerations is explored. The analysis of the data takes about 5 additional minutes and provides two parameters, the gain and the percentage of correct answers, which evaluate the VOR performance both from a neurophysiological and from a functional point of view.

Besides providing all the collected data to the examiner in order to allow further analysis and the investigation of specific aspects through customized programs, a predefined set of results is presented by the system at the end of each examination. An example of such standard results panel is shown in Figure 4.4 for a representative healthy subject, and in Figure 4.5 for a patient affected by a left side vestibular deficit. The results report

the traces of all recorded head and eye movements for each direction of head rotation (clockwise, CW, and counterclockwise, CCW) together with the trace showing the timing of the optotype presentation (recorded from the photodiode); the gain of the VOR in response to each head impulse is plotted against its peak head acceleration; the percentage of correct answers in every direction for each acceleration bin.

The patient in Figure 4.5 was recorded 4 days after the onset of a left vestibular neuritis. He had severe problems in identifying the optotype when the head was rotated towards the affected (left) side and a low rate of correct answers was also found during high acceleration rotations towards the contralateral side; indeed, as recently reported [179], the gain decreases with increasing accelerations in both the ipsilesional and the contralesional directions.

4.3.3. Results

The vHITD tools allowed us to understand how the performance of the optotype presentation are influenced by the experimental setup and the role of residual VOR response (i.e. the gain) and of corrective saccadic movements in riding the optotype. Moreover, in this section, the comparison of HITD outcome with traditional test parameters is discussed.

4.3.3.1. System performance

Figure 4.6 shows the timing performance of the system as tested using two different screens: one with refresh rate of 75 Hz and resolution 1280x1024 and one with refresh rate of 60 Hz and resolution 1920x1080. The thresholds were set to 10 deg/s for angular velocity and 300 deg/s^2 for angular acceleration. The delay of the optotype with threshold detection was set to zero and its on-screen duration to 80 ms or 83 ms, corresponding to 6 frames at 75 Hz and 5 frames at 60 Hz vertical refresh rates, respectively.

We then verified the performance using a 75 Hz screen and found a mean optotype delay of 25 ms (25±8 ms) due to both the system performance and the one frame uncertainty related to the asynchronous presentation command. The presentation time is of about 80 ms (80±8 ms) as planned by the experimental paradigm. With the 60Hz screen the delay was 62±20 ms and the duration on screen was 84±10 ms.

Figure 4.6 A shows that when the optotype is presented with the 60 Hz screen, it can still be displayed while the head velocity crosses 0 deg/s and changes sign, this can in theory distort the results of the test since even a few ms of stable retinal image can allow a correct optotype recognition.

Figure 4.4 (A-B) shows data relative to an acquisition with the 75Hz screen of about 60 head thrusts on a healthy subject; the variability of the

timing results from the asynchronous command and the discrete timing of the screen quantized by its frame rate.

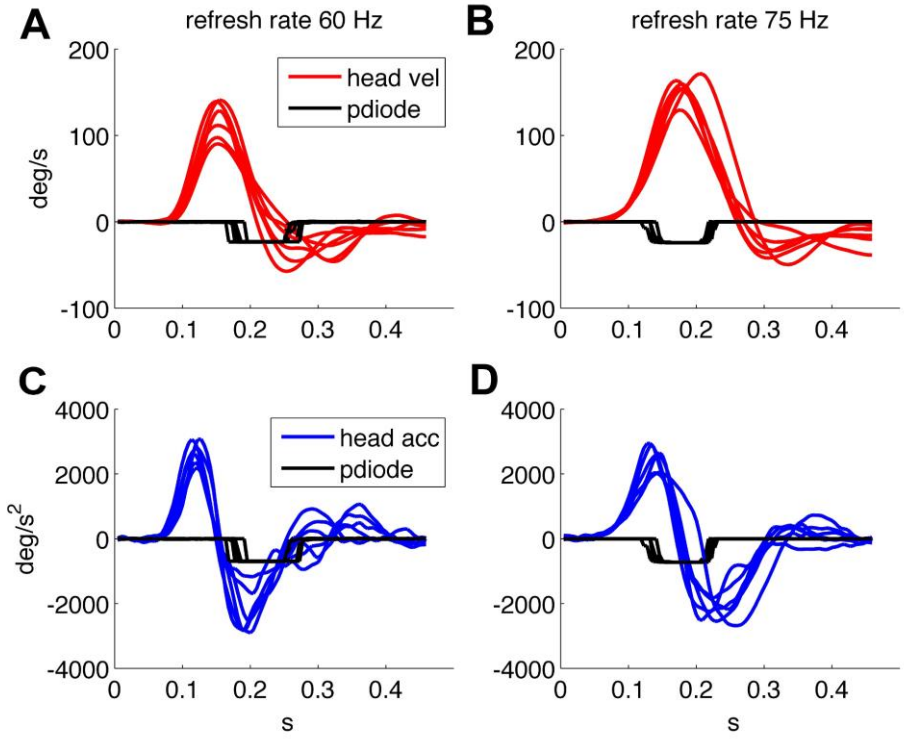

Figure 4.6: Timing performance of the system using a screen running at 60 Hz (A, C) and at 75 Hz (B, D). A, B) head velocity and sensor output. C, D) head acceleration and sensor output. When the optotype is presented with the 60 Hz screen, it can still be displayed while the head velocity crosses 0 deg/s and changes sign.

4.3.3.2. Corrective saccades, retinal slip and gaze error

Figure 4.7 A shows the frequency distribution of the first and the second corrective saccades (see Figure 4.3 B) in the acute phase, for all subjects. The first saccade has a mean latency of 136 ms, while the second saccade of 250 ms from head movement onset.

With our test setup only the 11% of corrective saccades finished while the optotype was still on the screen and only in 23% of these cases, the subject was able to read. In the second examination 12% of saccades finished while the optotype was still on the screen and in 60% of these cases, the subject read. Since the optotype disappeared before the large majority of the saccades ended, we could not establish the involvement of covert saccades in reading the optotype. On the other hand, from the effectiveness of the test point of view, this means that the percentage of reading is almost unaffected by covert saccades, especially in the acute phase. In this study the optotype was shown on screen sooner than in our recent work on opioids [202], which was carried out in a different laboratory, explaining our different findings with respect to the role of covert saccades on HITD results.

We computed the retinal slip (i.e. the velocity of gaze in space) and the gaze error (i.e. the eccentricity of gaze with respect to the optotype) while the optotype is shown on the screen (see Figure 4.3 D). The probability of reading the optotype decreases very quickly with both the increase of gaze position error and of retinal slip (Figure 4.7 C, D). In particular, if the optotype falls outside the central visual field, namely outside the fovea (~2 deg), the probability of reading is less than 0.2.

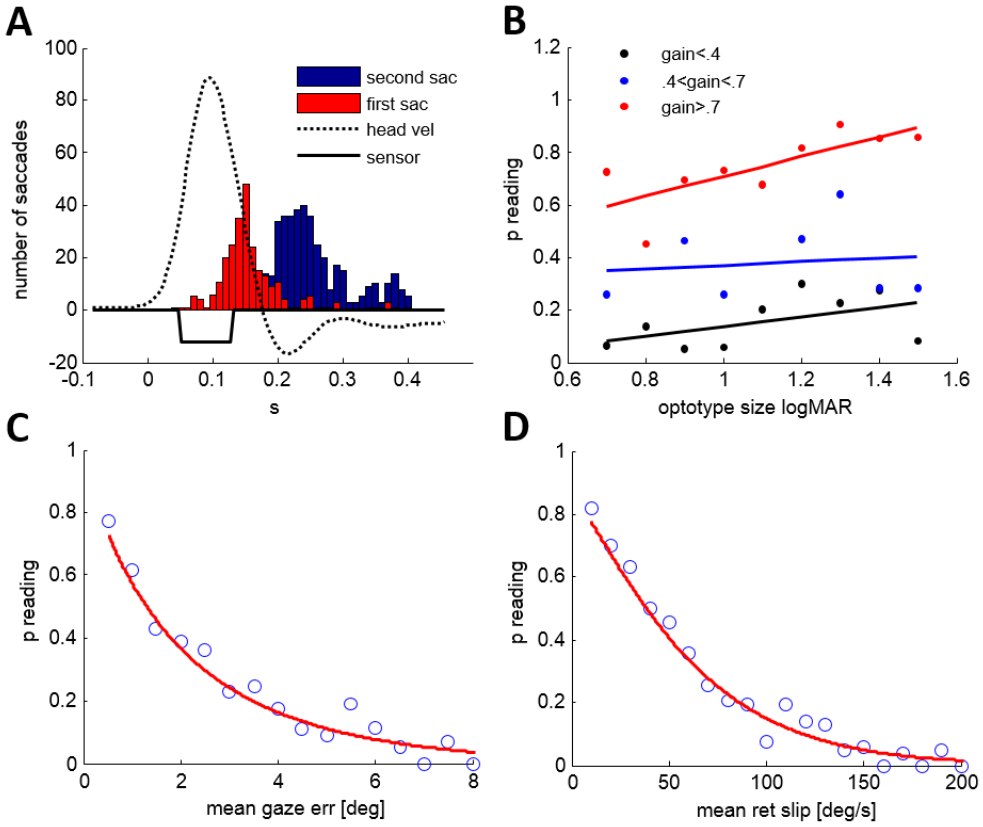

Figure 4.7: A) Frequency distribution of the latency of the first and the second corrective saccades for all subjects. An averaged head velocity profile and the optotype timing are superimposed. B) Correlation between probability of reading and optotype size at different bands of gain (less than 0.4, between 0.4 and 0.7 and greater than 0.7). Probability of reading is correlated ($r=0.75$, $p<0.05$) with the optotype size only for gains greater than 0.7. C) Probability of reading as a function of gaze error. D) Probability of reading as a function of retinal slip. Data in C, D are fitted with a reverse Weibull psychometric function (red line).

In order to understand if the size of the optotype distorts the results of the test, we computed the correlation between the probability of reading and optotype size. This relation is also influenced by the gain, because the lower is the gain, the bigger is the position error. Thus, we computed the correlation for three different gain intervals: lower than 0.4, between 0.4 and 0.7 and higher than 0.7 (Figure 4.7 B). The probability of reading was not correlated with optotype size in the first to intervals, while we found a

correlation ($r=0.75$, $p<0.05$) for gains higher than 0.7. Therefore, if the gain is higher than 0.7 and the optotype size is higher than 1.5 logMAR the percentage of correct answers may result to be higher because the gaze error is smaller than the optotype size. Taking into account this consideration, we removed two subjects from our population for which the optotype size, after normalization based on static visual acuity, resulted in 1.7 and 1.8 logMAR.

4.3.3.3. Comparison with traditional vestibular tests

Single patient evaluation

At first examination (acute phase):

- the ipsilesional gain values (Gipsi1) were abnormal in 27/27 (100%) subjects, whereas contralesional (Gcontra1) values were abnormal in 11/27 (40.7%) subjects (gain is considered abnormal if smaller than the 99% lower limit computed on normal subjects);
- the percentage of correct answers (%CAipsi1) was abnormal in 25/27 (92.5%) subjects ipsilesionally and in 18/27 (66.6%) subjects contralesionally(%CAcontra1) (statistical analysis for percentage of correct answers is reported in Paragraph 4.2.1:data analysis);
- the per-rotatory gain of the rotatory chair test (RT) was abnormal in 18/27 (66.6%) subjects ipsilesionally and in 6/27 (22.2%) contralesionally (normal value: >0.27);
- the subjective visual vertical perception (SVV) was altered in 24/27 (88.8%) subjects (normal interval: ±2.6 deg);
- VEMPs were abnormal in 5/27 (18.5%) subjects ipsilaterally and in 7/27 (25.9%) contralaterally;
- oVEMPs were abnormal in 6/27 (22.2%) subjects ipsilaterally and in 5/27 (18.5%) contralaterally.

At second examination (3 months after the first, compensated phase):

- the ipsilesional (Gipsi2) gain values were abnormal in 17/27 (62.9%) subjects, whereas contralesional (Gcontra2) values were abnormal in 7/27 (25.9%) subjects;
- the %CA was abnormal in 17/27 (62.9%) subjects ipsilesionally (%CAipsi2) and in 7/27 (25.9%) subjects contralesionally (%CAcontra2);
- the RT was abnormal in 10/27 (37%) of subjects ipsilesionally and in 3/27 (11.1%) contralesionally;
- the SVV was abnormal in 10/27 (37%) subjects;
- VEMPs were abnormal in 5/27 (18.5%) subjects ipsilaterally and in 4/27 (14.8%) contralaterally;

- oVEMPs were abnormal in 9/27 (33.3%) subjects ipsilaterally and in 1/27 (3%) contralaterally;

In the acute phase, the ipsilesional gain was abnormal in all patients whereas %CA was not in two patients; however %CA revealed more abnormalities than traditional laboratory tests (Table 4.1).

At second examination (after compensation), VOR gain resulted abnormal in 17 patient; 15 of them resulted abnormal also in %CA while only 10 and 9 in SVV and RT, respectively. Thus, despite the HITD procedure triggers also the vestibulo-collic reflex, after compensation, it still reveals more abnormalities than SVV and RT because of the higher frequency stimulation.

	Gain	**%CA**	**RT**	**SVV**	**VEMP**	**oVEMP**
Ex. 1	100/40.7	92.8/66.6	66.6/22.2	88.8	18.5/29.5	22.5/18.5
Ex. 2	62.9/25.9	62.9/25.9	37/11.1	37	18.5/14.8	33.3/3

Table 4.1: percentage (%) of abnormalities ipsilaterally/contralaterally at first (Ex. 1) and second (Ex. 2) examination revealed by each test.

Correlations

The four %CA values (ipsi1, conra1, ipsi2, contra2) correlate with each other. The %CAipsi1 and contra1 correlate with both Gipsi1 and Gipsi2, thus ipsilaterally %CA are correlated with gain both in acute ($r=0.66$ $p<0.001$) and in compensated phases ($r=0.87$ $p<0.001$), while they are not correlated contralesionally.

At second examination, both ipsilesional gain and %CA correlate ($p<0.05$) with the score of the three questionnaires describing self-perceived effects caused by vestibular disease. Therefore, both parameters describe the subjects' self-feeling about his/her balance. Traditional laboratory tests correlate poorly with the subjects' self-feeling, indeed, only RT ipsilaterally correlates just with the Dizziness Handicap Inventory test.

An interesting result is that the ipsilateral gain values in the acute phase are correlated ($p<0.05$) with the subject's self-feeling reported in the compensated phase. Therefore a low ipsilateral gain may predict the patients that will have an incomplete recovery and thus can take advantage from vestibular rehabilitation program.

Mean value comparison

The mean values (reported in Table 4.2) were compared by repeated-measure analysis of variance. We considered two two-level within subject factors and their interactions: side (ipsi- and contra-lesionally) and time (acute and compensated phases). In the analyses we included age as a covariate.

The effect of age and of its interactions with the other two main factor never proved to be significant.

	First examination		Second examination				
	Ipsi	**Contra**	**Ipsi**	**Contra**	side	time	time* side
Gain	0.4±0.22	0.94±0.11	0.67±0.32	0.97±0.11	p<.001	p<.001	p=.367
%CA	27.4±27	63.7±20	57.14±32	82.5±14	p=.031	P=.001	p=.363

Table 4.2: Mean values (± standard deviation) of gain and %CA for patient and p values of repeated-measures analysis of variance for each factor and their interaction. Normal subjects have mean gain: CW=0.89±0.1, CCW=0.95±0.1; mean %CA: CW=87.1±7, CCW=89±7.

Both in terms of %CA and of gain, the contralesional values were significantly better than the ipsilesional ones (side factor) and the values of the compensated phase were better than those in the acute phase (time factor), but that the interactions of the two factors were never significant

More interestingly, the HITD unveiled that in the acute phase the contralesional VOR is also affected, and that this abnormality was better picked up by %CA than by gain.

4.4. Discussion

In this chapter a new approach to functional testing of the rVOR has been presented, focusing on verifying the ability of the reflex to grant visual stability during head rotations when faced with a wide range of head angular accelerations, independently from the subject's visual acuity.

Such approach was implemented using the HITD, a device that needs very little equipment to be set up, is not expensive, is user friendly and is well tolerated by the patients.

In order to validate the system and analyze the relation of the functional outcome with the quantitative evaluation of the rVOR, the rationale of the test has been implemented on a lightweight video-oculography system allowing the simultaneous recording of eye movements while performing HITD.

We found that the HITD functional test detects more abnormalities than the traditional VOR testing approaches (SVV, RT, VEMP, oVEMP). Moreover, such test is well tolerated by the patients, requires low cost equipment and is potentially suitable for clinical testing. Visual acuity, reflecting on the size of the optotype used during HITD testing, does not influence reading percentages with low rVOR gains. Nonetheless, low acuity patients with gains higher than 0.7 may appear as normal, thus requiring further testing. The percentage of reading is well correlated with

rVOR gain, while the latter is more informative as all patients had abnormal gains while two patients were not detected as being pathological by the HITD. On the other hand, measurement of gain is more complex and requires relatively expensive equipment, which makes this approach less suitable for large scale clinical use.

Chapter 5

Overall conclusions and future works

Classic studies on VOR adaptation have shown that the natural gain of the VOR can be increased and decreased. In this work, we showed that the plasticity of the reflex follows the same behavior of the voluntary movements comprising processes which learn quickly and others that are more conservative and tend to protect the memory of learned behaviors. In other words, we have shown that learning in the VOR is governed by multiple processes having different timescales carrying out storage and protection of memory. This architecture could allow the integration of new information, preventing the forgetting of previous knowledge (a possible solution to the plasticity-stability dilemma [203]). This understanding could potentially be useful for developing new paradigms to improve pathological VOR gain in vestibular rehabilitation of patients [143].

Several new rehabilitation approaches are based on theories of motor learning [204], nevertheless several problems still need to be understood: the credit assignment problem, i.e. how the brain estimates the relevance of the error in order to enable faster and stronger adaptation [124]; the generalization of the learned behavior from the context of learning to general behavior [205]; the transfer of the plasticity from the cerebellum to other brain areas during consolidation [149]. These problems are connected to each other. The magnitude of errors during training affects the generalization and the efficacy of learning, indeed a gradual introduction of adaptive perturbations is more effective than an abrupt one. The size of the error, thus the credit assigned to it, can transfer the problem from the learning of a forward model (i.e. learn to predict sensory consequences), to the learning of a new inverse model (e.g. adapting the controller to reflect an altered plant) [121]. This means that plasticity moves from the cerebellum to other brain areas [206], [207], in the case of the VOR in the brainstem, increasing the degree of generalization. On the other hand, during gradual perturbations more of the adaptation is assigned to the slow state [119], which then contributes to long term retention (stored in other

brain areas) more strongly than the faster process [161]. However, we need to consider that the adaptation at the level of the inverse model may also be due to model free learning systems driven by reinforcement of successful actions (skill learning) even when there is no perturbation [208]. Thus, it is not only the size of the error that influences adaptation.

Most likely, a rehabilitation program should involve paradigms aiming at reinforcement and unsupervised learning, depending on task success and repetition, in addition to those based on inducing a performance error.

The HITD was shown to be a reliable approach to detecting rVOR impairment by testing the ability of a subject to read an optotype briefly displayed on a screen during head rotations. During such paradigm, an insufficient rVOR causes retinal slip, i.e. the slippage of the seen image on the retina, which is a strong adaptive stimulus, such as the one we used in our adaptation experiments. In fact, in a rehabilitation setting, the device could also be used to induce adaptation of the VOR: both by adapting the threshold triggering the display on screen to the abilities of the patient, i.e. similarly to an incremental error paradigm, and by providing an immediate feedback to the patients on their correctly read letters, thereby promoting reinforcement of correct responses. Such application of the device in the development of new, adaptive rehabilitation paradigms could represent a further relevant development of this work.

Appendix A

Head Impulse Test Device (HITD)

The Device

To implement the protocol we developed an inertial motion sensor based on a three axis accelerometer (model ADXL330, Analog Devices Inc., with a linear range of ± 3 g) and a single axis gyroscope (model ADXRS300, Analog Devices Inc., with a linear range of ± 300 deg/s), packed together on a custom 2 cm by 2 cm circuit board, weighing only a few grams. Such assembly was then mounted with an elastic band to the subject's head, allowing to freely and naturally move his/her head.

The analog sensor signals were then acquired and sampled using a National Instruments USB-6211, 16 bit, 256 KS/s data acquisition card.

In order to reduce the effect of sampling noise, raw data was captured at 10 KHz and then smoothed in to 100 Hz by averaging 100 samples to provide one angular velocity or linear acceleration data point. Head angular acceleration was then computed from the gyroscope angular head velocity signal as:

$$a_n = \Delta v/\Delta t = (v_n - v_{n-1})/(t_n - t_{n-1}). \quad (1)$$

The software verified both that the axis of head rotation did not change during the angular head impulse by verifying the orientation of the sensor with respect to gravity, and that there was limited spurious head translation. Trials in which the lateral head acceleration was greater than an adaptive threshold max(4,1.1*α_T/1000), where α_T is the angular acceleration threshold set for the trial, were therefore rejected.

Appendix B

Video Head Impulse Test Device (vHITD)

EyeSeeCam System

The EyeSeeCam system is a modular device allowing to measure eye and head movements thanks to one (or two) head mounted sensors, each consisting of:

- an infrared video camera with two integrated light emitting diodes (IRLEDS) with wavelengths of above 850 nm;
- a six degrees of freedom (6DOF) inertial measurement unit (IMU).

The system is provided with an acquisition software package for the measurement of eye movements by means of an automated on-line analysis of video streams. The results of these image processing steps are stored into Matlab data (.mat) files for subsequent analysis.

The EyeSeeCam system provides an interface to Matlab that enables three distinct tasks:

- present visual stimuli;
- acquire data made available in the Matlab workspace, based on a time-controlled flow;
- analyze and show recorded data.

The EyeSeeCam is delivered with a standard set of stimulation and analysis Matlab scripts that can be customized to the needs of individual laboratories. Similarly, it is possible to extend the provided set of functions with user-written scripts. The scripts presenting visual stimuli exploit the PsychToolbox-3 [209], [210], which also allows openGL commands. The online communication with the acquisition software is granted by Matlab mex files provided with the system, which allow to access the data and to control the stimuli and experimental paradigms. Up to eight additional

analog channels may be acquired and synced with the rest of the data through National Instruments USB data acquisition devices.

The .mat file saved at the end of the acquisition contains synchronized data samples relative to the head movement (provided by the IMU), eye position (video-oculography) and the analog channel representing the photodiode output, stored in a single matrix together with its relative timestamps.

The software workflow and the interaction between the scripts are managed through a graphical user interface (GUI).

The camera frame rate determines the acquisition frequency of the whole system and can be defined by the experimenter, yet it is inversely related to the spatial resolution of each acquired frame, and thus of the resulting angular eye position. For our experiments we have chosen a sampling rate of 220 Hz, which determined frames of 188x120 pixels. Our system is monocular and was set to measure movements of the left eye.

Visual Stimulus size

For the new HITD test we chose the Landolt C optotype (Figure 4.3 A, E), a ring with a gap measuring 1/5 of the diameter that can be presented in eight possible orientations at 45 deg increments, for two main reasons. First because its use grants that all visual stimuli are equally challenging while maintaining the probability of a correct answer by chance to 0.125 (it was 0.1 in the original version of the test related to the use of the Sloan letter set [168]). Then because such optotype is relatively simple to handle using openGL functions, a software development environment constraint. Furthermore, the use of such approach simplifies the recording of the patient responses, since the answers may be provided easily by coding the orientation of the ring with the keys of a numerical keyboard.

Optotypes are displayed in black over a white background on the monitor in front of the subject (here at 1 m distance) that discerns the orientation and returns the answer using a numerical keyboard modified with arrows pointing in the direction of the gap. The size of the optotype is scaled depending on the distance from the screen based on (4):

$$Size = \frac{Distance}{\frac{1}{5 * \tan(\frac{1}{60})} * VisualAcuity}. \quad (1)$$

To improve presentation timing, the Landolt ring is pre-built at the maximum size allowed by the screen size with the gap at 0° and stored. Before being presented on screen it is rotated to one of the eight possible orientations following a pseudo-random sequence and scaled with (1).

Visual acuity in static conditions is tested at the beginning of the experiment by requiring the patient to identify the orientation of a sequence of Landolt C rings. The size of the ring (and its gap) is reduced depending on the subject rate of errors using the QUEST [211] adaptive algorithm,

which is also implemented in the Psychtoolbox. The algorithm starts from a value of 1 logMAR and estimates the viewer's static visual acuity threshold in twenty trials.

Visual stimulus and timing

For the HITD test, the size of the stimulus is obtained by increasing the static visual acuity by 0.6 logMAR. Such value is lower than previously used [25] and was chosen based on the assessed reading ability of ten healthy subjects (visual acuities ranging .1 to .7 logMAR) during passive head impulses within a restricted range of accelerations (between 2000 and 4000 deg/s^2) and using optotypes with different size increments with respect to their SVA. Ten stimuli were presented for each increment, in a pseudorandom order, and we obtained a psychometric function of the percentage of correct answers as a function of the increments. The increment of 0.5 was the first one whereby the number of errors was significantly greater than zero and we therefore chose to use a 0.6 logMAR increment.

The chosen optotype size will then remain constant through the entire dynamic testing phase. The patient has then to recognize the optotype orientation flashed on screen when the experimenter-imposed head angular acceleration exceeds a selectable threshold. The delay between the overcoming of the threshold and the optotype presentation, as well as its duration on screen may be selected by the experimenter, among multiples of frame duration, computed as the inverse of the screen's vertical refresh rate.

The user-defined timing of the optotype is obviously only nominal, as it depends on the graphic performance of the computer running the experiment, on the refresh rate of the screen, on the OS scheduling of the running processes. In order to verify the timing of the system, which is a crucial performance for the accuracy of the test, we used a photodiode attached to the test screen for detecting a square that pops up together with the letter in the lower right-hand corner of the screen. The appearance of the square is not perceived by the subject as the entire area is covered by the photodiode assembly box. The output of the photodiode is also captured via the National Instruments USB device connected to EyeSeeCam. The photodiode is a generic RS-Components diode, BPW21, RS part no. 303-719. It has a typical rise-time of 1μs, which was therefore neglected in the following analyses.

The photodiode data channel, synced with head and eye movement data, thus provides the system with the feedback on the exact timing of the optotype as its output will be high for the whole permanence of the stimulus on screen: a key information for further understanding functional VOR performance in healthy subjects, in patients and during rehabilitation.

Data from the EyeSeeCam IMU sensor are thus used to measure head angular velocity ($\dot{\theta}$) about the vertical axis (see the Data Analysis section) and thus to compute head angular acceleration as expressed in Appendix A.

Then, when head angular velocity overcomes a threshold (e.g. 10 deg/s) if the acceleration overcomes another threshold (e.g. 300 deg/s^2) a thrust is recognized and the optotype is shown.

As previously described the HITD test assesses the functionality of the VOR at different head accelerations so that the imposed head thrusts are classified in acceleration bins (width of 1000 deg/ s^2 with upper bounds ranging 2000 to 7000 deg/ s^2) based on their direction, while an online feedback is provided through the GUI reporting the number of thrusts performed per bin and the corresponding percentage of reading errors, thus helping the experimenter at delivering head thrusts in the whole field of the required accelerations. We chose to impose at least five thrusts per bin and increase such number to eight if the subject performed at least one reading mistake, to improve resolution. Plots of angular velocity and eye velocity relative to the performed thrust are also presented on the feedback GUI.

Clearly, covering the full range of accelerations is a demanding task for both the subject and the experimenter, since at least 60 head impulses are necessary. Yet, although in the context of this research study we have attempted at achieving such task, our previous studies [168] suggest that the range of head accelerations relevant to clinical HITD testing may be reduced to the 3000-6000 deg/s^2 bins, which typically requires between 40 and 50 head impulses per subject.

Data analysis

During offline processing of the acquired data, eye position is computed using rotation vectors [212]. In order to better quantify the stimulus to the horizontal canals which, with proper subject positioning (30 deg. nose down), should lie in the horizontal plane, we chose to consider only the head rotation component lying in that same plane ($\dot{\theta}_z$). We thus use the linear acceleration signals from the IMU to assess the sensor's orientation with respect to gravity and then rotate the angular velocity components from the gyro to compute the angular velocity around the vertical axis. This component is compared with ω_z (horizontal eye velocity).

Velocity gain of the VOR is then calculated as the ratio of the mean eye velocity over the mean head velocity computed over the time interval between head peak acceleration and peak velocity (duration 40±8 ms). The head acceleration value associated with each impulse is computed as the slope of the line that fits five samples of head angular velocity centered at the time of peak acceleration.

References

[1] R. J. Leigh and D. S. Zee, *The neurology of eye movements*, vol. 90. Oxford University Press New York, 1999.

[2] S. J. Herdman, *Vestibular Rehabilitation*. F. A. Davis Company, 2007.

[3] E. R. Kandel Schwartz, James H., Jessell, Thomas M.,, *Principles of neural science*. New York: McGraw-Hill, Health Professions Division, 2000.

[4] K. Cullen and S. Sadeghi, "Vestibular system," *Scholarpedia*, vol. 3, no. 1, p. 3013, Jan. 2008.

[5] T. Haslwanter, "Vestibular System," *Wikibooks/Sensory Systems*, 2011. [Online]. Available: http://en.wikibooks.org/wiki/Sensory_Systems/Vestibular_System.

[6] C. C. Della Santina, V. Potyagaylo, A. A. Migliaccio, L. B. Minor, and J. P. Carey, "Orientation of human semicircular canals measured by three-dimensional multiplanar CT reconstruction.," *J. Assoc. Res. Otolaryngol.*, vol. 6, no. 3, pp. 191–206, Sep. 2005.

[7] J. M. Goldberg and C. Fernandez, "Physiology of peripheral neurons innervating semicircular canals of the squirrel monkey. I. Resting discharge and response to constant angular accelerations," *J Neurophysiol*, vol. 34, no. 4, pp. 635–660, Jul. 1971.

[8] V. J. Wilson and G. M. Jones, *Mammalian vestibular physiology*. 1979.

[9] B. Cohen, V. Henn, T. Raphan, and D. Dennett, "Velocity storage, nystagmus, and visual-vestibular interactions in humans.," *Ann. N. Y. Acad. Sci.*, vol. 374, no. 1 Vestibular an, pp. 421–433, Nov. 1981.

[10] I. S. CURTHOYS, G. A. BETTS, A. M. BURGESS, H. G. MacDOUGALL, A. D. CARTWRIGHT, and G. M. HALMAGYI, "The Planes of the Utricular and Saccular Maculae of the Guinea Pig," *Ann. N. Y. Acad. Sci.*, vol. 871, no. 1 OTOLITH FUNCT, pp. 27–34, May 1999.

[11] R. Jaeger, A. Takagi, and T. Haslwanter, "Modeling the relation between head orientations and otolith responses in humans," *Hear. Res.*, vol. 173, no. 1–2, pp. 29–42, Nov. 2002.

[12] Y. Uchino, H. Sato, and H. Suwa, "Excitatory and Inhibitory Inputs From Saccular Afferents to Single Vestibular Neurons in the Cat," *J Neurophysiol*, vol. 78, no. 4, pp. 2186–2192, Oct. 1997.

[13] R. A. Baird, G. Desmadryl, C. Fernandez, and J. M. Goldberg, "The vestibular nerve of the chinchilla. II. Relation between afferent response properties and peripheral innervation patterns in the semicircular canals," *J Neurophysiol*, vol. 60, no. 1, pp. 182–203, Jul. 1988.

[14] S. G. Sadeghi, M. J. Chacron, M. C. Taylor, and K. E. Cullen, "Neural variability, detection thresholds, and information transmission in the vestibular system.," *J. Neurosci.*, vol. 27, no. 4, pp. 771–81, Jan. 2007.

[15] S. G. Sadeghi, L. B. Minor, and K. E. Cullen, "Response of vestibular-nerve afferents to active and passive rotations under normal conditions and after unilateral labyrinthectomy.," *J. Neurophysiol.*, vol. 97, no. 2, pp. 1503–14, Feb. 2007.

[16] J. Szentagothai, "The elementary vestibulo-ocular reflex arc.," *J Neurophysiol*, vol. 13, no. 6, pp. 395–407, Nov. 1950.

[17] E. F. Maas, W. P. Huebner, S. H. Seidman, and R. J. Leigh, "Behavior of human horizontal vestibulo-ocular reflex in response to high-acceleration stimuli," *Brain Res.*, vol. 499, no. 1, pp. 153–156, Oct. 1989.

[18] R. S. Gellman, J. R. Carl, and F. A. Miles, "Short latency ocular-following responses in man," *Vis. Neurosci.*, vol. 5, no. 02, p. 107, Jun. 2009.

[19] E. S. Boyden, A. Katoh, and J. L. Raymond, "Cerebellum-dependent learning: the role of multiple plasticity mechanisms.," *Annu. Rev. Neurosci.*, vol. 27, pp. 581–609, Jan. 2004.

[20] D. A. Robinson, "Vestibular and optokinetic symbiosis: an example of explaining by modelling.," *Control Gaze by Brain Stem Neurons, Dev. Neurosci.*, vol. 1, pp. 49–58, 1977.

[21] J. Laurens and D. E. Angelaki, "The functional significance of velocity storage and its dependence on gravity.," *Exp. Brain Res.*, vol. 210, no. 3–4, pp. 407–22, May 2011.

[22] D. A. Robinson, "The systems approach to the oculomotor system," *Vision Res.*, vol. 26, no. 1, pp. 91–99, Jan. 1986.

[23] T. Raphan, V. Matsuo, and B. Cohen, "Velocity storage in the vestibulo-ocular reflex arc (VOR)," *Exp. Brain Res.*, vol. 35, no. 2, Apr. 1979.

[24] D. A. Robinson, "The mechanics of human saccadic eye movement.," *J. Physiol.*, vol. 174, pp. 245–64, Nov. 1964.

[25] A. A. Skavenski and D. A. Robinson, "Role of abducens neurons in vestibuloocular reflex," *J Neurophysiol*, vol. 36, no. 4, pp. 724–738, Jul. 1973.

[26] M. S. Goldman, C. R. S. Kaneko, G. Major, E. Aksay, D. W. Tank, and H. S. Seung, "Linear Regression of Eye Velocity on Eye Position and Head Velocity Suggests a Common Oculomotor Neural Integrator," *J Neurophysiol*, vol. 88, no. 2, pp. 659–665, Aug. 2002.

[27] J. L. McFarland and A. F. Fuchs, "Discharge patterns in nucleus prepositus hypoglossi and adjacent medial vestibular nucleus during horizontal eye movement in behaving macaques," *J Neurophysiol*, vol. 68, no. 1, pp. 319–332, Jul. 1992.

[28] C. A. Scudder and A. F. Fuchs, "Physiological and behavioral identification of vestibular nucleus neurons mediating the horizontal vestibuloocular reflex in trained rhesus monkeys," *J Neurophysiol*, vol. 68, no. 1, pp. 244–264, Jul. 1992.

[29] P. R. MacNeilage, N. Ganesan, and D. E. Angelaki, "Computational approaches to spatial orientation: from transfer functions to dynamic Bayesian inference.," *J. Neurophysiol.*, vol. 100, no. 6, pp. 2981–96, Dec. 2008.

[30] J. M. Furman and S. L. Whitney, "Central causes of dizziness.," *Phys. Ther.*, vol. 80, no. 2, pp. 179–87, Feb. 2000.

[31] H. F. Schuknecht, "Cupulolithiasis.," *Arch. Otolaryngol.*, vol. 90, no. 6, pp. 765–78, Dec. 1969.

[32] T. Brandt and S. Steddin, "Current view of the mechanism of benign paroxysmal positioning vertigo: cupulolithiasis or canalolithiasis?," *J. Vestib. Res.*, vol. 3, no. 4, pp. 373–82, Jan. 1993.

[33] A. Semont, G. Freyss, and E. Vitte, "Curing the BPPV with a liberatory maneuver.," *Adv. Otorhinolaryngol.*, vol. 42, pp. 290–3, Jan. 1988.

[34] J. M. Epley, "The Canalith Repositioning Procedure: For Treatment of Benign Paroxysmal Positional Vertigo," *Otolaryngol. -- Head Neck Surg.*, vol. 107, no. 3, pp. 399–404, Sep. 1992.

[35] S. J. Herdman, R. J. Tusa, D. S. Zee, L. R. Proctor, and D. E. Mattox, "Single Treatment Approaches to Benign Paroxysmal Positional Vertigo," *Arch. Otolaryngol. - Head Neck Surg.*, vol. 119, no. 4, pp. 450–454, Apr. 1993.

[36] R. BALOH, I. LOPEZ, A. ISHIYAMA, P. WACKYM, and V. HONRUBIA, "Vestibular neuritis: Clinical-pathologic correlation," *Otolaryngol. - Head Neck Surg.*, vol. 114, no. 4, pp. 586–592, Apr. 1996.

[37] M. Strupp, V. Arbusow, K. P. Maag, C. Gall, and T. Brandt, "Vestibular exercises improve central vestibulospinal compensation after vestibular neuritis.," *Neurology*, vol. 51, no. 3, pp. 838–44, Sep. 1998.

[38] R. S. Kimura, "Animal models of endolymphatic hydrops," *Am. J. Otolaryngol.*, vol. 3, no. 6, pp. 447–451, Nov. 1982.

[39] J. D. J. Green, D. J. Blum, and S. G. Harner, "Longitudinal Followup of Patients with Meniere's Disease," *Otolaryngol. -- Head Neck Surg.*, vol. 104, no. 6, pp. 783–788, Jun. 1991.

[40] C. H. Rassekh and L. A. Harker, "The Prevalence of Migraine in Ménière's Disease," *Laryngoscope*, vol. 102, no. 2, p. 135???138, Feb. 1992.

[41] G. Lange, "The intratympanic treatment of Menière's disease with ototoxic antibiotics.," *Laryngol. Rhinol. Otol. (Stuttg).*, vol. 56, no. 5, pp. 409–14, May 1977.

[42] D. C. Fitzgerald, "Head trauma: hearing loss and dizziness.," *J. Trauma*, vol. 40, no. 3, pp. 488–96, Mar. 1996.

[43] P. J. Jannetta, M. B. Møller, and A. R. Møller, "Disabling positional vertigo.," *N. Engl. J. Med.*, vol. 310, no. 26, pp. 1700–5, Jun. 1984.

[44] R. Shadmehr and S. Mussa-Ivaldi, *Biological Learning and Control: How the Brain Builds Representations, Predicts Events, and Makes Decisions*. MIT Press, 2012, p. 385.

[45] E. Todorov, "Stochastic optimal control and estimation methods adapted to the noise characteristics of the sensorimotor system.," *Neural Comput.*, vol. 17, no. 5, pp. 1084–108, May 2005.

[46] D. M. Wolpert and M. Kawato, "Multiple paired forward and inverse models for motor control," *Neural Networks*, vol. 11, no. 7–8, pp. 1317–1329, Oct. 1998.

[47] D. W. Franklin and D. M. Wolpert, "Computational mechanisms of sensorimotor control.," *Neuron*, vol. 72, no. 3, pp. 425–42, Nov. 2011.

[48] R. Shadmehr and J. W. Krakauer, "A computational neuroanatomy for motor control.," *Exp. brain Res.*, vol. 185, no. 3, pp. 359–81, Mar. 2008.

[49] E. Todorov, "Optimality principles in sensorimotor control.," *Nat. Neurosci.*, vol. 7, no. 9, pp. 907–15, Sep. 2004.

[50] A. M. Green and D. E. Angelaki, "Internal models and neural computation in the vestibular system.," *Exp. brain Res.*, vol. 200, no. 3–4, pp. 197–222, Jan. 2010.

[51] D. M. Wolpert, J. Diedrichsen, and J. R. Flanagan, "Principles of sensorimotor learning.," *Nat. Rev. Neurosci.*, vol. 12, no. 12, pp. 739–51, Dec. 2011.

[52] R. Shadmehr, M. a Smith, and J. W. Krakauer, "Error correction, sensory prediction, and adaptation in motor control.," *Annu. Rev. Neurosci.*, vol. 33, pp. 89–108, Jan. 2010.

[53] P. M. Blazquez, Y. Hirata, and S. M. Highstein, "The vestibulo-ocular reflex as a model system for motor learning: what is the role of the cerebellum?," *Cerebellum*, vol. 3, no. 3, pp. 188–92, Jan. 2004.

[54] J. L. Raymond, S. G. Lisberger, and M. D. Mauk, "The Cerebellum: A Neuronal Learning Machine?," *Science (80-.).*, vol. 272, no. 5265, pp. 1126–1131, May 1996.

[55] S. G. Lisberger, "Internal models of eye movement in the floccular complex of the monkey cerebellum.," *Neuroscience*, vol. 162, no. 3, pp. 763–76, Sep. 2009.

[56] R. Shadmehr, "Generalization as a behavioral window to the neural mechanisms of learning internal models.," *Hum. Mov. Sci.*, vol. 23, no. 5, pp. 543–68, Nov. 2004.

[57] A. M. Green, H. Meng, and D. E. Angelaki, "A reevaluation of the inverse dynamic model for eye movements.," *J. Neurosci.*, vol. 27, no. 6, pp. 1346–55, Feb. 2007.

[58] M. Kawato, T. Kuroda, H. Imamizu, E. Nakano, S. Miyauchi, and T. Yoshioka, "Internal forward models in the cerebellum: fMRI study on grip force and load force coupling.," *Prog. Brain Res.*, vol. 142, pp. 171–88, Jan. 2003.

[59] S. Glasauer, "Cerebellar contribution to saccades and gaze holding: a modeling approach.," *Ann. N. Y. Acad. Sci.*, vol. 1004, pp. 206–19, Oct. 2003.

[60] F. F. Ghasia, H. Meng, and D. E. Angelaki, "Neural correlates of forward and inverse models for eye movements: evidence from three-dimensional kinematics.," *J. Neurosci.*, vol. 28, no. 19, pp. 5082–7, May 2008.

[61] D. Tweed and T. Vilis, "Geometric relations of eye position and velocity vectors during saccades," *Vision Res.*, vol. 30, no. 1, pp. 111–127, Jan. 1990.

[62] F. F. Ghasia and D. E. Angelaki, "Do motoneurons encode the noncommutativity of ocular rotations?," *Neuron*, vol. 47, no. 2, pp. 281–93, Jul. 2005.

[63] D. E. Angelaki, A. G. Shaikh, A. M. Green, and J. D. Dickman, "Neurons compute internal models of the physical laws of motion.," *Nature*, vol. 430, no. 6999, pp. 560–4, Jul. 2004.

[64] D. M. Merfeld, L. Zupan, and R. J. Peterka, "Humans use internal models to estimate gravity and linear acceleration.," *Nature*, vol. 398, no. 6728, pp. 615–8, Apr. 1999.

[65] A. Einstein, "Über das Relativitätsprinzip und die aus demselben gezogenen Folgerungen," *Jahrb. der Radioakt. und Elektron.*, 1908.

[66] F. Lacquaniti, G. Bosco, S. Gravano, I. Indovina, B. La Scaleia, V. Maffei, and M. Zago, "Multisensory integration and internal models for sensing gravity effects in primates.," *Biomed Res. Int.*, vol. 2014, p. 615854, Jan. 2014.

[67] A. M. Green, A. G. Shaikh, and D. E. Angelaki, "Sensory vestibular contributions to constructing internal models of self-motion.," *J. Neural Eng.*, vol. 2, no. 3, pp. S164–79, Sep. 2005.

[68] D. M. Wolpert, "Probabilistic models in human sensorimotor control.," *Hum. Mov. Sci.*, vol. 26, no. 4, pp. 511–24, Aug. 2007.

[69] M. O. Ernst and M. S. Banks, "Humans integrate visual and haptic information in a statistically optimal fashion.," *Nature*, vol. 415, no. 6870, pp. 429–33, Jan. 2002.

[70] P. R. MacNeilage, M. S. Banks, D. R. Berger, and H. H. Bülthoff, "A Bayesian model of the disambiguation of gravitoinertial force by visual cues.," *Exp. brain Res.*, vol. 179, no. 2, pp. 263–90, May 2007.

[71] K. P. Körding and D. M. Wolpert, “Bayesian integration in sensorimotor learning.,” *Nature*, vol. 427, no. 6971, pp. 244–7, Jan. 2004.

[72] R. E. Kalman, “A New Approach to Linear Filtering and Prediction Problems,” *J. Basic Eng.*, vol. 82, no. 1, p. 35, Mar. 1960.

[73] G. Welch and G. Bishop, “An Introduction to the Kalman Filter,” Nov. 1995.

[74] D. M. Wolpert, Z. Ghahramani, and M. I. Jordan, “An internal model for sensorimotor integration.,” *Science*, vol. 269, no. 5232, pp. 1880–2, Sep. 1995.

[75] A. D. Kuo, “An optimal control model for analyzing human postural balance.,” *IEEE Trans. Biomed. Eng.*, vol. 42, no. 1, pp. 87–101, Jan. 1995.

[76] J. Borah, L. R. Young, and R. E. Curry, “Optimal estimator model for human spatial orientation.,” *Ann. N. Y. Acad. Sci.*, vol. 545, pp. 51–73, Jan. 1988.

[77] F. Karmali and D. M. Merfeld, “A distributed, dynamic, parallel computational model: the role of noise in velocity storage.,” *J. Neurophysiol.*, vol. 108, no. 2, pp. 390–405, Jul. 2012.

[78] D. M. Merfeld, L. R. Young, C. M. Oman, and M. J. Shelhamer, “A multidimensional model of the effect of gravity on the spatial orientation of the monkey.,” *J. Vestib. Res.*, vol. 3, no. 2, pp. 141–61, Jan. 1993.

[79] P. Selva and C. M. Oman, “Relationships between observer and Kalman Filter models for human dynamic spatial orientation.,” *J. Vestib. Res.*, vol. 22, no. 2, pp. 69–80, Jan. 2012.

[80] M. S. Arulampalam, S. Maskell, N. Gordon, and T. Clapp, “A tutorial on particle filters for online nonlinear/non-Gaussian Bayesian tracking,” *IEEE Trans. Signal Process.*, vol. 50, no. 2, pp. 174–188, 2002.

[81] J. Laurens and J. Droulez, “Bayesian processing of vestibular information.,” *Biol. Cybern.*, vol. 96, no. 4, pp. 389–404, Apr. 2007.

[82] M. A. Frens and O. Donchin, “Forward models and state estimation in compensatory eye movements.,” *Front. Cell. Neurosci.*, vol. 3, p. 13, Jan. 2009.

[83] K. Doya, “Complementary roles of basal ganglia and cerebellum in learning and motor control.,” *Curr. Opin. Neurobiol.*, vol. 10, no. 6, pp. 732–9, Dec. 2000.

[84] J. R. Lackner and P. DiZio, “Motor control and learning in altered dynamic environments.,” *Curr. Opin. Neurobiol.*, vol. 15, no. 6, pp. 653–9, Dec. 2005.

[85] D. Pélisson, N. Alahyane, M. Panouillères, and C. Tilikete, “Sensorimotor adaptation of saccadic eye movements.,” *Neurosci. Biobehav. Rev.*, vol. 34, no. 8, pp. 1103–20, Jul. 2010.

[86] S. Cheng and P. N. Sabes, “Modeling sensorimotor learning with linear dynamical systems.,” *Neural Comput.*, vol. 18, no. 4, pp. 760–93, Apr. 2006.

[87] M. a Smith, A. Ghazizadeh, and R. Shadmehr, “Interacting adaptive processes with different timescales underlie short-term motor learning.,” *PLoS Biol.*, vol. 4, no. 6, p. e179, Jun. 2006.

[88] V. S. Huang, A. Haith, P. Mazzoni, and J. W. Krakauer, “Rethinking motor learning and savings in adaptation paradigms: model-free memory for successful actions combines with internal models.,” *Neuron*, vol. 70, no. 4, pp. 787–801, May 2011.

[89] M. C. Schubert and D. S. Zee, “Saccade and vestibular ocular motor adaptation.,” *Restor. Neurol. Neurosci.*, vol. 28, no. 1, pp. 9–18, Jan. 2010.

[90] G. M. Gauthier and D. A. Robinson, “Adaptation of the human vestibuloocular reflex to magnifying lenses.,” *Brain Res.*, vol. 92, no. 2, pp. 331–5, Jul. 1975.

[91] A. Gonshor and G. M. Jones, “Extreme vestibulo-ocular adaptation induced by prolonged optical reversal of vision.,” *J. Physiol.*, vol. 256, no. 2, pp. 381–414, Apr. 1976.

[92] M. Shelhamer, C. Tiliket, D. Roberts, P. D. Kramer, and D. S. Zee, “Short-term vestibulo-ocular reflex adaptation in humans. II. Error signals.,” *Exp. brain Res.*, vol. 100, no. 2, pp. 328–36, Jan. 1994.

[93] M. C. Schubert, C. C. Della Santina, and M. Shelhamer, “Incremental angular vestibulo-ocular reflex adaptation to active head rotation.,” *Exp. Brain Res.*, vol. 191, no. 4, pp. 435–46, Dec. 2008.

[94] S. D. Z. Eggers, N. De Pennington, M. F. Walker, M. Shelhamer, and D. S. Zee, “Short-term adaptation of the VOR: non-retinal-slip error signals and saccade substitution.,” *Ann. N. Y. Acad. Sci.*, vol. 1004, pp. 94–110, Oct. 2003.

[95] G. Melvill Jones, A. Berthoz, and B. Segal, “Adaptive modification of the vestibulo-ocular reflex by mental effort in darkness,” *Exp. Brain Res.*, vol. 56, no. 1, Aug. 1984.

[96] G. Mandl, G. Melvill Jones, and M. Cynader, "Adaptability of the vestibulo-ocular reflex to vision reversal in strobe reared cats.," *Brain Res.*, vol. 209, no. 1, pp. 35–45, Mar. 1981.

[97] D. Marr, "A theory of cerebellar cortex," *J. Physiol.*, vol. 202, no. 2, pp. 437–470, Jun. 1969.

[98] J. S. Albus, "A theory of cerebellar function," *Math. Biosci.*, vol. 10, no. 1–2, pp. 25–61, Feb. 1971.

[99] P. Dean, J. Porrill, C.-F. Ekerot, and H. Jörntell, "The cerebellar microcircuit as an adaptive filter: experimental and computational evidence.," *Nat. Rev. Neurosci.*, vol. 11, no. 1, pp. 30–43, Jan. 2010.

[100] J. Porrill, P. Dean, and S. R. Anderson, "Adaptive filters and internal models: multilevel description of cerebellar function.," *Neural Netw.*, vol. 47, pp. 134–49, Nov. 2013.

[101] M. Ito, "Neural design of the cerebellar motor control system.," *Brain Res.*, vol. 40, no. 1, pp. 81–4, May 1972.

[102] M. Ito, "Cerebellar control of the vestibulo-ocular reflex--around the flocculus hypothesis.," *Annu. Rev. Neurosci.*, vol. 5, pp. 275–96, Jan. 1982.

[103] M. Fujita, "Adaptive filter model of the cerebellum," *Biol. Cybern.*, vol. 45, no. 3, pp. 195–206, Nov. 2013.

[104] J. Porrill and P. Dean, "Cerebellar motor learning: when is cortical plasticity not enough?," *PLoS Comput. Biol.*, vol. 3, no. 10, pp. 1935–50, Oct. 2007.

[105] F. A. Miles and S. G. Lisberger, "Plasticity in the vestibulo-ocular reflex: a new hypothesis.," *Annu. Rev. Neurosci.*, vol. 4, pp. 273–99, Jan. 1981.

[106] E. S. Boyden and J. L. Raymond, "Active reversal of motor memories reveals rules governing memory encoding.," *Neuron*, vol. 39, no. 6, pp. 1031–42, Sep. 2003.

[107] Y. Kojima, Y. Iwamoto, and K. Yoshida, "Memory of learning facilitates saccadic adaptation in the monkey.," *J. Neurosci.*, vol. 24, no. 34, pp. 7531–9, Aug. 2004.

[108] S. C. McLaughlin, "Parametric adjustment in saccadic eye movements," *Percept. Psychophys.*, vol. 2, no. 8, pp. 359–362, Aug. 1967.

[109] V. Ethier, D. S. Zee, and R. Shadmehr, "Spontaneous recovery of motor memory during saccade adaptation.," *J. Neurophysiol.*, vol. 99, no. 5, pp. 2577–83, May 2008.

[110] E. Zarahn, G. D. Weston, J. Liang, P. Mazzoni, and J. W. Krakauer, "Explaining savings for visuomotor adaptation: linear time-invariant state-space models are not sufficient.," *J. Neurophysiol.*, vol. 100, no. 5, pp. 2537–48, Nov. 2008.

[111] J. W. Krakauer, C. Ghez, and M. F. Ghilardi, "Adaptation to visuomotor transformations: consolidation, interference, and forgetting.," *J. Neurosci.*, vol. 25, no. 2, pp. 473–8, Jan. 2005.

[112] S. E. Pekny, S. E. Criscimagna-Hemminger, and R. Shadmehr, "Protection and expression of human motor memories.," *J. Neurosci.*, vol. 31, no. 39, pp. 13829–39, Sep. 2011.

[113] R. Shadmehr and T. Brashers-Krug, "Functional Stages in the Formation of Human Long-Term Motor Memory," *J. Neurosci.*, vol. 17, no. 1, pp. 409–419, Jan. 1997.

[114] A. Aboukhalil, M. Shelhamer, and R. Clendaniel, "Acquisition of context-specific adaptation is enhanced with rest intervals between changes in context state, suggesting a new form of motor consolidation.," *Neurosci. Lett.*, vol. 369, no. 2, pp. 162–7, Oct. 2004.

[115] J.-Y. Lee and N. Schweighofer, "Dual adaptation supports a parallel architecture of motor memory.," *J. Neurosci.*, vol. 29, no. 33, pp. 10396–404, Aug. 2009.

[116] H. Tanaka, J. W. Krakauer, and T. J. Sejnowski, "Generalization and Multirate Models of Motor Adaptation." MIT Press 55 Hayward Street, Cambridge, MA 02142-1315 email: journals-info@mit.edu, 05-Mar-2012.

[117] N. Malfait and D. J. Ostry, "Is interlimb transfer of force-field adaptation a cognitive response to the sudden introduction of load?," *J. Neurosci.*, vol. 24, no. 37, pp. 8084–9, Sep. 2004.

[118] S. E. Criscimagna-Hemminger, O. Donchin, M. S. Gazzaniga, and R. Shadmehr, "Learned dynamics of reaching movements generalize from dominant to nondominant arm.," *J. Neurophysiol.*, vol. 89, no. 1, pp. 168–76, Jan. 2003.

[119] V. S. Huang and R. Shadmehr, "Persistence of motor memories reflects statistics of the learning event.," *J. Neurophysiol.*, vol. 102, no. 2, pp. 931–40, Aug. 2009.

[120] A. L. Wong and M. Shelhamer, "Saccade adaptation improves in response to a gradually introduced stimulus perturbation.," *Neurosci. Lett.*, vol. 500, no. 3, pp. 207–11, Aug. 2011.

[121] J. Kluzik, J. Diedrichsen, R. Shadmehr, and A. J. Bastian, "Reach adaptation: what determines whether we learn an internal model of the tool or adapt the model of our arm?," *J. Neurophysiol.*, vol. 100, no. 3, pp. 1455–64, Sep. 2008.

[122] H. Chen-Harris, W. M. Joiner, V. Ethier, D. S. Zee, and R. Shadmehr, "Adaptive control of saccades via internal feedback.," *J. Neurosci.*, vol. 28, no. 11, pp. 2804–13, Mar. 2008.

[123] M. Berniker and K. Kording, "Estimating the sources of motor errors for adaptation and generalization.," *Nat. Neurosci.*, vol. 11, no. 12, pp. 1454–61, Dec. 2008.

[124] K. Wei and K. Körding, "Relevance of error: what drives motor adaptation?," *J. Neurophysiol.*, vol. 101, no. 2, pp. 655–64, Feb. 2009.

[125] M. Kawato, "Internal models for motor control and trajectory planning.," *Curr. Opin. Neurobiol.*, vol. 9, no. 6, pp. 718–27, Dec. 1999.

[126] M. Shidara, K. Kawano, H. Gomi, and M. Kawato, "Inverse-dynamics model eye movement control by Purkinje cells in the cerebellum.," *Nature*, vol. 365, no. 6441, pp. 50–2, Sep. 1993.

[127] R. Shadmehr and F. Mussa-Ivaldi, "Adaptive representation of dynamics during learning of a motor task," *J. Neurosci.*, vol. 14, no. 5, pp. 3208–3224, May 1994.

[128] M. I. Jordan and D. E. Rumelhart, "Forward Models: Supervised Learning with a Distal Teacher," *Cogn. Sci.*, vol. 16, no. 3, pp. 307–354, Jul. 1992.

[129] D. M. Wolpert and R. C. Miall, "Forward Models for Physiological Motor Control.," *Neural Netw.*, vol. 9, no. 8, pp. 1265–1279, Nov. 1996.

[130] R. C. Miall, D. J. Weir, D. M. Wolpert, and J. F. Stein, "Is the cerebellum a smith predictor?," *J. Mot. Behav.*, vol. 25, no. 3, pp. 203–16, Sep. 1993.

[131] D. A. Robinson, "The use of control systems analysis in the neurophysiology of eye movements.," *Annu. Rev. Neurosci.*, vol. 4, pp. 463–503, Jan. 1981.

[132] D. S. Zee, L. M. Optican, J. D. Cook, D. A. Robinson, and W. K. Engel, "Slow saccades in spinocerebellar degeneration.," *Arch. Neurol.*, vol. 33, no. 4, pp. 243–51, Apr. 1976.

[133] R. Jurgens, W. Becker, and H. H. Kornhuber, "Natural and drug-induced variations of velocity and duration of human saccadic eye movements: Evidence for a control of the neural pulse generator by local feedback," *Biol. Cybern.*, vol. 39, no. 2, pp. 87–96, Jan. 1981.

[134] S. Ramat, R. J. Leigh, D. S. Zee, and L. M. Optican, "What clinical disorders tell us about the neural control of saccadic eye movements.," *Brain*, vol. 130, no. Pt 1, pp. 10–35, Jan. 2007.

[135] F. R. Robinson, R. Soetedjo, and C. Noto, "Distinct short-term and long-term adaptation to reduce saccade size in monkey.," *J. Neurophysiol.*, vol. 96, no. 3, pp. 1030–41, Sep. 2006.

[136] S. J. Robbins, "Mechanisms underlying spontaneous recovery in autoshaping."

[137] A. L. Wong and M. Shelhamer, "Exploring the fundamental dynamics of error-based motor learning using a stationary predictive-saccade task.," *PLoS One*, vol. 6, no. 9, p. e25225, Jan. 2011.

[138] R. R. Kimpo, E. S. Boyden, A. Katoh, M. C. Ke, and J. L. Raymond, "Distinct patterns of stimulus generalization of increases and decreases in VOR gain.," *J. Neurophysiol.*, vol. 94, no. 5, pp. 3092–100, Nov. 2005.

[139] S. G. Lisberger, T. A. Pavelko, and D. M. Broussard, "Responses during eye movements of brain stem neurons that receive monosynaptic inhibition from the flocculus and ventral paraflocculus in monkeys.," *J. Neurophysiol.*, vol. 72, no. 2, pp. 909–27, Aug. 1994.

[140] J. R. Carl and R. S. Gellman, "Human smooth pursuit: stimulus-dependent responses.," *J. Neurophysiol.*, vol. 57, no. 5, pp. 1446–63, May 1987.

[141] S. G. Lisberger and L. E. Westbrook, "Properties of visual inputs that initiate horizontal smooth pursuit eye movements in monkeys.," *J. Neurosci.*, vol. 5, no. 6, pp. 1662–73, Jun. 1985.

[142] W. Waespe and V. Henn, "Gaze stabilization in the primate. The interaction of the vestibulo-ocular reflex, optokinetic nystagmus, and smooth pursuit.," *Rev. Physiol. Biochem. Pharmacol.*, vol. 106, pp. 37–125, Jan. 1987.

[143] A. a Migliaccio and M. C. Schubert, "Unilateral adaptation of the human angular vestibulo-ocular reflex.," *J. Assoc. Res. Otolaryngol.*, vol. 14, no. 1, pp. 29–36, Feb. 2013.

[144] W. Zhou, P. Weldon, B. Tang, and W. M. King, "Rapid motor learning in the translational vestibulo-ocular reflex.," *J. Neurosci.*, vol. 23, no. 10, pp. 4288–98, May 2003.

[145] M. Ito, "The molecular organization of cerebellar long-term depression.," *Nat. Rev. Neurosci.*, vol. 3, no. 11, pp. 896–902, Nov. 2002.

[146] M. Ito, T. Shiida, N. Yagi, and M. Yamamoto, "Visual influence on rabbit horizontal vestibulo-ocular reflex presumably effected via the cerebellar flocculus," *Brain Res.*, vol. 65, no. 1, pp. 170–174, Jan. 1974.

[147] D. A. Robinson, "Adaptive gain control of vestibuloocular reflex by the cerebellum.," *J. Neurophysiol.*, vol. 39, no. 5, pp. 954–69, Sep. 1976.

[148] C. D. Kassardjian, Y.-F. Tan, J.-Y. J. Chung, R. Heskin, M. J. Peterson, and D. M. Broussard, "The site of a motor memory shifts with consolidation.," *J. Neurosci.*, vol. 25, no. 35, pp. 7979–85, Aug. 2005.

[149] M. Anzai, H. Kitazawa, and S. Nagao, "Effects of reversible pharmacological shutdown of cerebellar flocculus on the memory of long-term horizontal vestibulo-ocular reflex adaptation in monkeys.," *Neurosci. Res.*, vol. 68, no. 3, pp. 191–8, Nov. 2010.

[150] P. Colagiorgio, S. Colnaghi, M. Versino, and S. Ramat, "A New Tool for Investigating the Functional Testing of the VOR.," *Front. Neurol.*, vol. 4, no. October, p. 165, Jan. 2013.

[151] S. Ramat and D. S. Zee, "Ocular motor responses to abrupt interaural head translation in normal humans.," *J. Neurophysiol.*, vol. 90, no. 2, pp. 887–902, Aug. 2003.

[152] K. E. Cullen, "The vestibular system: multimodal integration and encoding of self-motion for motor control.," *Trends Neurosci.*, vol. 35, no. 3, pp. 185–96, Mar. 2012.

[153] E. L. Keller, "Accommodative vergence in the alert monkey. Motor unit analysis," *Vision Res.*, vol. 13, no. 8, pp. 1565–1575, Aug. 1973.

[154] S. T. Aw, G. M. Halmagyi, T. Haslwanter, I. S. Curthoys, R. A. Yavor, and M. J. Todd, "Three-dimensional vector analysis of the human vestibuloocular reflex in response to high-acceleration head rotations. II. responses in subjects with unilateral vestibular loss and selective semicircular canal occlusion.," *J. Neurophysiol.*, vol. 76, no. 6, pp. 4021–30, Dec. 1996.

[155] G. Schwarz, "Estimating the Dimension of a Model," *Ann. Stat.*, vol. 6, no. 2, pp. 461–464, Mar. 1978.

[156] K. P. Burnham and D. R. Anderson, *Model Selection and Multimodel Inference: A Practical Information-Theoretic Approach*. 2010.

[157] K. M. Myers and M. Davis, "Behavioral and neural analysis of extinction.," *Neuron*, vol. 36, no. 4, pp. 567–84, Nov. 2002.

[158] A. L. Wong and M. Shelhamer, "Sensorimotor adaptation error signals are derived from realistic predictions of movement outcomes.," *J. Neurophysiol.*, vol. 105, no. 3, pp. 1130–40, Mar. 2011.

[159] A. L. Wong and M. Shelhamer, "Using prediction errors to drive saccade adaptation: the implicit double-step task.," *Exp. brain Res.*, vol. 222, no. 1–2, pp. 55–64, Oct. 2012.

[160] F. Shutoh, M. Ohki, H. Kitazawa, S. Itohara, and S. Nagao, "Memory trace of motor learning shifts transsynaptically from cerebellar cortex to nuclei for consolidation.," *Neuroscience*, vol. 139, no. 2, pp. 767–77, May 2006.

[161] W. M. Joiner and M. A. Smith, "Long-term retention explained by a model of short-term learning in the adaptive control of reaching.," *J. Neurophysiol.*, vol. 100, no. 5, pp. 2948–55, Nov. 2008.

[162] A. A. Tarnutzer, A. L. Berkowitz, K. A. Robinson, Y.-H. Hsieh, and D. E. Newman-Toker, "Does my dizzy patient have a stroke? A systematic review of bedside diagnosis in acute vestibular syndrome.," *CMAJ*, vol. 183, no. 9, pp. E571–92, Jun. 2011.

[163] K. Kroenke and A. D. Mangelsdorff, "Common symptoms in ambulatory care: incidence, evaluation, therapy, and outcome.," *Am. J. Med.*, vol. 86, no. 3, pp. 262–6, Mar. 1989.

[164] D. E. Newman-Toker, Y.-H. Hsieh, C. A. Camargo, A. J. Pelletier, G. T. Butchy, and J. A. Edlow, "Spectrum of dizziness visits to US emergency departments: cross-sectional analysis from a nationally representative sample.," *Mayo Clin. Proc.*, vol. 83, no. 7, pp. 765–75, Jul. 2008.

[165] C. Kruschinski, E. Hummers-Pradier, D. Newman-Toker, C. A. Camargo, and J. A. Edlow, "Diagnosing dizziness in the emergency and primary care settings.," *Mayo Clin. Proc.*, vol. 83, no. 11, pp. 1297–8; author reply 1298–9, Nov. 2008.

[166] Y. Agrawal, J. P. Carey, C. C. Della Santina, M. C. Schubert, and L. B. Minor, "Disorders of balance and vestibular function in US adults: data

from the National Health and Nutrition Examination Survey, 2001-2004.," *Arch. Intern. Med.*, vol. 169, no. 10, pp. 938–44, May 2009.

[167] J. A. Edlow, D. E. Newman-Toker, and S. I. Savitz, "Diagnosis and initial management of cerebellar infarction.," *Lancet. Neurol.*, vol. 7, no. 10, pp. 951–64, Oct. 2008.

[168] S. Ramat, S. Colnaghi, A. Boehler, S. Astore, P. Falco, M. Mandalà, D. Nuti, P. Colagiorgio, and M. Versino, "A Device for the Functional Evaluation of the VOR in Clinical Settings.," *Front. Neurol.*, vol. 3, p. 39, Jan. 2012.

[169] A. Bohler, M. Mandala, and S. Ramat, "A software program for the head impulse testing device (HITD).," *Conf. Proc. IEEE Eng. Med. Biol. Soc.*, vol. 2010, pp. 6615–8, Jan. 2010.

[170] I. S. Curthoys, V. Vulovic, and L. Manzari, "Ocular vestibular-evoked myogenic potential (oVEMP) to test utricular function: neural and oculomotor evidence.," *Acta Otorhinolaryngol. Ital.*, vol. 32, no. 1, pp. 41–5, Feb. 2012.

[171] G. M. Halmagyi and I. S. Curthoys, "A clinical sign of canal paresis.," *Arch. Neurol.*, vol. 45, no. 7, pp. 737–9, Jul. 1988.

[172] J. Ewald, *Physiologische Untersuchungen über das Endorgan des Nervus octavus*. Wiesbaden: Bergmann, 1892.

[173] P. D. Cremer, G. M. Halmagyi, S. T. Aw, I. S. Curthoys, L. A. McGarvie, M. J. Todd, R. A. Black, and I. P. Hannigan, "Semicircular canal plane head impulses detect absent function of individual semicircular canals.," *Brain*, vol. 121 (Pt 4, pp. 699–716, Apr. 1998.

[174] L. B. Minor, D. M. Lasker, D. D. Backous, and T. E. Hullar, "Horizontal vestibuloocular reflex evoked by high-acceleration rotations in the squirrel monkey. I. Normal responses.," *J. Neurophysiol.*, vol. 82, no. 3, pp. 1254–70, Sep. 1999.

[175] M. Jorns-Häderli, D. Straumann, and A. Palla, "Accuracy of the bedside head impulse test in detecting vestibular hypofunction.," *J. Neurol. Neurosurg. Psychiatry*, vol. 78, no. 10, pp. 1113–8, Oct. 2007.

[176] D. E. Newman-Toker, J. C. Kattah, J. E. Alvernia, and D. Z. Wang, "Normal head impulse test differentiates acute cerebellar strokes from vestibular neuritis.," *Neurology*, vol. 70, no. 24 Pt 2, pp. 2378–85, Jun. 2008.

[177] M. C. Schubert, R. J. Tusa, L. E. Grine, and S. J. Herdman, "Optimizing the sensitivity of the head thrust test for identifying

vestibular hypofunction.," *Phys. Ther.*, vol. 84, no. 2, pp. 151–8, Feb. 2004.

[178] D. A. Robinson, "A Method of Measuring Eye Movemnent Using a Scieral Search Coil in a Magnetic Field," *Ire Trans. Biomed. Electron.*, vol. 10, no. 4, pp. 137–145, 1963.

[179] K. P. Weber, S. T. Aw, M. J. Todd, L. A. McGarvie, I. S. Curthoys, and G. M. Halmagyi, "Head impulse test in unilateral vestibular loss: vestibulo-ocular reflex and catch-up saccades.," *Neurology*, vol. 70, no. 6, pp. 454–63, Feb. 2008.

[180] K. Bartl, N. Lehnen, S. Kohlbecher, and E. Schneider, "Head impulse testing using video-oculography.," *Ann. N. Y. Acad. Sci.*, vol. 1164, pp. 331–3, May 2009.

[181] S. J. Herdman, R. J. Tusa, P. Blatt, A. Suzuki, P. J. Venuto, and D. Roberts, "Computerized dynamic visual acuity test in the assessment of vestibular deficits.," *Am. J. Otol.*, vol. 19, no. 6, pp. 790–6, Nov. 1998.

[182] J. R. Tian, I. Shubayev, and J. L. Demer, "Dynamic visual acuity during yaw rotation in normal and unilaterally vestibulopathic humans.," *Ann. N. Y. Acad. Sci.*, vol. 942, pp. 501–4, Oct. 2001.

[183] M. C. Schubert, S. J. Herdman, and R. J. Tusa, "Vertical dynamic visual acuity in normal subjects and patients with vestibular hypofunction.," *Otol. Neurotol.*, vol. 23, no. 3, pp. 372–7, May 2002.

[184] S. J. Herdman, M. C. Schubert, and R. J. Tusa, "Role of central preprogramming in dynamic visual acuity with vestibular loss.," *Arch. Otolaryngol. Head. Neck Surg.*, vol. 127, no. 10, pp. 1205–10, Oct. 2001.

[185] C. C. Della Santina, P. D. Cremer, J. P. Carey, and L. B. Minor, "Comparison of head thrust test with head autorotation test reveals that the vestibulo-ocular reflex is enhanced during voluntary head movements.," *Arch. Otolaryngol. Head. Neck Surg.*, vol. 128, no. 9, pp. 1044–54, Sep. 2002.

[186] J. Tian, I. Shubayev, and J. L. Demer, "Dynamic visual acuity during passive and self-generated transient head rotation in normal and unilaterally vestibulopathic humans.," *Exp. Brain Res.*, vol. 142, no. 4, pp. 486–95, Feb. 2002.

[187] M. C. Schubert, A. A. Migliaccio, and C. C. Della Santina, "Dynamic visual acuity during passive head thrusts in canal planes.," *J. Assoc. Res. Otolaryngol.*, vol. 7, no. 4, pp. 329–38, Dec. 2006.

[188] N. S. Longridge and A. I. Mallinson, “The dynamic illegible E-test. A technique for assessing the vestibulo-ocular reflex.,” *Acta Otolaryngol.*, vol. 103, no. 3–4, pp. 273–9.

[189] D. Vital, S. C. A. Hegemann, D. Straumann, O. Bergamin, C. J. Bockisch, D. Angehrn, K.-U. Schmitt, and R. Probst, “A new dynamic visual acuity test to assess peripheral vestibular function.,” *Arch. Otolaryngol. Head. Neck Surg.*, vol. 136, no. 7, pp. 686–91, Jul. 2010.

[190] J. A. Goebel, N. Tungsiripat, B. Sinks, and J. Carmody, “Gaze stabilization test: a new clinical test of unilateral vestibular dysfunction.,” *Otol. Neurotol.*, vol. 28, no. 1, pp. 68–73, Jan. 2007.

[191] M. R. Pritcher, S. L. Whitney, G. F. Marchetti, and J. M. Furman, “The influence of age and vestibular disorders on gaze stabilization: a pilot study.,” *Otol. Neurotol.*, vol. 29, no. 7, pp. 982–8, Oct. 2008.

[192] S. L. Whitney, G. F. Marchetti, M. Pritcher, and J. M. Furman, “Gaze stabilization and gait performance in vestibular dysfunction.,” *Gait Posture*, vol. 29, no. 2, pp. 194–8, Feb. 2009.

[193] L. B. W. JONGKEES, “VALUE OF THE CALORIC TEST OF THE LABYRINTH,” *Arch. Otolaryngol. - Head Neck Surg.*, vol. 48, no. 4, pp. 402–417, Oct. 1948.

[194] “Committee on Hearing and Equilibrium guidelines for the diagnosis and evaluation of therapy in Menière’s disease. American Academy of Otolaryngology-Head and Neck Foundation, Inc.,” *Otolaryngol. Head. Neck Surg.*, vol. 113, no. 3, pp. 181–5, Sep. 1995.

[195] K. P. Weber, H. G. MacDougall, G. M. Halmagyi, and I. S. Curthoys, “Impulsive testing of semicircular-canal function using video-oculography.,” *Ann. N. Y. Acad. Sci.*, vol. 1164, pp. 486–91, May 2009.

[196] B. N. Segal and A. Katsarkas, “Long-term deficits of goal-directed vestibulo-ocular function following total unilateral loss of peripheral vestibular function.,” *Acta Otolaryngol.*, vol. 106, no. 1–2, pp. 102–10.

[197] M. C. Schubert, C. D. Hall, V. Das, R. J. Tusa, and S. J. Herdman, “Oculomotor strategies and their effect on reducing gaze position error.,” *Otol. Neurotol.*, vol. 31, no. 2, pp. 228–31, Feb. 2010.

[198] J. Tian, B. T. Crane, and J. L. Demer, “Vestibular catch-up saccades in labyrinthine deficiency.,” *Exp. Brain Res.*, vol. 131, no. 4, pp. 448–57, Apr. 2000.

[199] G. P. Jacobson and C. W. Newman, “The development of the Dizziness Handicap Inventory.,” *Arch. Otolaryngol. Head. Neck Surg.*, vol. 116, no. 4, pp. 424–7, Apr. 1990.

[200] R. G. Jacob, S. O. Lilienfeld, J. M. R. Furman, J. D. Durrant, and S. M. Turner, "Panic disorder with vestibular dysfunction: Further clinical observations and description of space and motion phobic stimuli," *J. Anxiety Disord.*, vol. 3, no. 2, pp. 117–130, Jan. 1989.

[201] L. E. Powell and A. M. Myers, "The Activities-specific Balance Confidence (ABC) Scale.," *J. Gerontol. A. Biol. Sci. Med. Sci.*, vol. 50A, no. 1, pp. M28–34, Jan. 1995.

[202] C. Ramaioli, P. Colagiorgio, M. Sağlam, F. Heuser, E. Schneider, S. Ramat, and N. Lehnen, "The Effect of Vestibulo-Ocular Reflex Deficits and Covert Saccades on Dynamic Vision in Opioid-Induced Vestibular Dysfunction.," *PLoS One*, vol. 9, no. 10, p. e110322, Jan. 2014.

[203] W. C. Abraham and A. Robins, "Memory retention--the synaptic stability versus plasticity dilemma.," *Trends Neurosci.*, vol. 28, no. 2, pp. 73–8, Feb. 2005.

[204] J. W. Krakauer, "Motor learning: its relevance to stroke recovery and neurorehabilitation.," *Curr. Opin. Neurol.*, vol. 19, no. 1, pp. 84–90, Feb. 2006.

[205] M. A. Frens and A. J. van Opstal, "Transfer of short-term adaptation in human saccadic eye movements.," *Exp. brain Res.*, vol. 100, no. 2, pp. 293–306, Jan. 1994.

[206] J. E. Schlerf, J. M. Galea, A. J. Bastian, and P. A. Celnik, "Dynamic modulation of cerebellar excitability for abrupt, but not gradual, visuomotor adaptation.," *J. Neurosci.*, vol. 32, no. 34, pp. 11610–7, Aug. 2012.

[207] S. E. Criscimagna-Hemminger, A. J. Bastian, and R. Shadmehr, "Size of error affects cerebellar contributions to motor learning.," *J. Neurophysiol.*, vol. 103, no. 4, pp. 2275–84, Apr. 2010.

[208] A. M. Haith and J. W. Krakauer, "Model-based and model-free mechanisms of human motor learning.," *Adv. Exp. Med. Biol.*, vol. 782, pp. 1–21, Jan. 2013.

[209] D. H. Brainard, "The Psychophysics Toolbox.," *Spat. Vis.*, vol. 10, no. 4, pp. 433–6, Jan. 1997.

[210] D. G. Pelli, "The VideoToolbox software for visual psychophysics: transforming numbers into movies.," *Spat. Vis.*, vol. 10, no. 4, pp. 437–42, Jan. 1997.

[211] A. B. Watson and D. G. Pelli, "QUEST: a Bayesian adaptive psychometric method.," *Percept. Psychophys.*, vol. 33, no. 2, pp. 113–20, Feb. 1983.

[212] T. Haslwanter, "Mathematics of three-dimensional eye rotations.," *Vision Res.*, vol. 35, no. 12, pp. 1727–39, Jun. 1995.